DEFECTS IN GALLIUM ARSENIDE LASERS

Thesis submitted for the degree of

Doctor of Philosophy

by

Martin Jeremy Hill

April 1968

Department of Metallurgy
Imperial College of
Science and Technology,
University of London.

ABSTRACT

Diffused GaAs laser diodes were operated close to liquid nitrogen temperature and the infra - red near - field emission patterns photographed at currents above and below threshold. Optical transmission using photon energies close to the band gap energy revealed inhomogeneous donor distributions in the n - type material of the diodes. This method also revealed an affect of Zn diffusion on the donor distribution ahead of the junction. The behaviour of high concentrations of the donor Te was discussed. Chemical etching revealed some of the donor inhomogeneities and also arrays of "misfit" dislocations in the junction region. The donor density variations were correlated with the emission patterns.

A reliable method was developed for preparing transmission electron microscope specimens from bulk GaAs. Using this method, specimens were prepared from laser diodes. Diffusion induced dislocations and precipitates were found in the p - type material.

The theory of semiconductor lasers was reviewed briefly, and the effect of variations in parameters of the material on the equation for threshold current density was considered. It was concluded that, in large diffused diodes, variations in absorption coefficient associated with the non - uniform donor distributions in the GaAs substrate, were the dominant defects causing non - uniform emission.

CONTENTS

CHAPTER 1

INTRODUCTION

Gallium Arsenide is a compound semiconductor with many properties similar to those of the elemental semiconductors germanium and silicon. The technology of device production for GaAs is less well developed than that of Ge and especially that of Si, which is used commercially wherever possible. However, electroluminescent sources cannot be produced from Si or Ge. Many compound semiconductors have electronic band structures which permit efficient production of electromagnetic radiation at visible or near infra-red wavelengths. Soon after the possibility of Light Amplification by Stimulated Emission of Radiation (LASER action) in semiconductors was proposed, it was achieved by passing a large current across a forward biased p - n junction in GaAs. The history of the semiconductor laser and the theory behind its operation are reviewed in Chapter 2.

GaAs electroluminescent devices emit band-gap radiation in the region of 9000Å at room temperature. This wavelength is absorbed and scattered by the atmosphere, in the same way as visible radiation. This restricts the use of these devices to short range applications. A coherent beam at optical wavelengths is, in principle, capable of modulation at extremely high frequencies and therefore of carrying large quantities of information. Many potential uses of GaAs lasers are based on this fact. These include very fast,

short range links carrying large amounts of data in computers, or in equipment where electrical connections are not possible. GaAs lasers have been used to carry communications in space where their small size compared to other types of laser is an advantage. They have also been used as accurate, low level altimeters for aircraft and are used by the U.S. Army as range finders at distances up to one mile.

When laser action was obtained in GaAs it was found that the radiation was not emitted uniformly from the p - n junction. It was realised that if the emission could be made uniform then the electroluminescent efficiency would be improved. In order to obtain laser action at a p - n junction, certain conditions must be satisfied by the electronic band structure of the semiconductor. These conditions lead to both the n- and p- type materials being heavily doped by semiconductor standards. This introduces crystal defects, and it is these defects which have been studied in this work. It is shown in Chapter 2 that the threshold current density for laser action is strongly dependent on the material parameters. Local variations of these parameters (i.e. inhomogeneities in the GaAs crystal) cause large variations in the threshold current density. The research reported here has entailed using several methods of observation. Diodes were examined during operation, and subsequently the defect content was studied, in an attempt to correlate defects with performance.

The mechanisms involved at the p - n junction are so

complex that a comprehensive investigation to determine the relative importance of all possible variables on laser performance was beyond the scope of this work. Chapter 2 is a survey of the literature, but includes so many separate topics that detailed discussion of each one is not possible. Chapter 5 contains a critical discussion of the most relevant work of other authors, and a comparison with the results to be presented in Chapter 4. Also considered is the effect of crystal defects on the theoretical equation for threshold current density.

CHAPTER 2

BACKGROUND AND REVIEW OF LITERATURE

2. 1. Introduction to Lasers

Stimulated emission of electromagnetic radiation involves electron transition between energy states in a medium. When an electron from one energy level transfers to a lower energy level a photon of energy equal to the energy gap between the levels is emitted. If this photon causes another electron in the higher energy state to transfer to the same lower level then the first photon is said to have stimulated the emission of the second. The second photon has the same wavelength and phase as the first, and travels in the same direction. These two photons are coherent. If, in a medium, there is a sufficient density of electrons in the higher level and there are sufficient empty states in the lower level then a coherent beam of light can be produced in the medium. For amplification of the beam, the rate of production of photons must exceed the rate of loss due to absorption, scattering etc. In a coherent beam the fact that the photons are all in phase means that more available energy is present than in an ordinary beam at optical frequencies. Also the angular spread of the beam is small so that inverse square law losses are reduced.

Einstein used an early form of quantum theory to predict the existence of stimulated emission of radiation as a necessary process for thermodynamic equilibrium. The idea of stimulated emission was not applied successfully until Gordon, Zeiger and Townes (1955) used the energy level scheme of ammonia

to produce a coherent beam at microwave frequencies. The first laser producing visible radiation was operated by Maiman (1960). This was the ruby laser using the energy levels of Cr^{+3} ions in Al_2O_3 Soon after this the possibility of laser action in semiconductors was discussed; see for instance Basov, Krokhin and Popov (1960), and (1961) and Bernard and Duraffourg (1961). Laser action in semiconductors was realised simultaneously by Nathan et al (1962) at I.B.M. and by Hall et al (1962) at G.E. Shortly afterwards it was reported at Lincoln Laboratory by Quist et al (1962) and at Services Electronic Research Laboratory (S.E.R.L.) Baldock by Broom et al (1963). These lasers were all fabricated from GaAs, but since then laser action has been reported in many III - V semiconductor compounds including: In P, In As, In Sb, Ga Sb, $GaAs_xP_{1-x}$, InP_xAs_{1-x}, $In_xGa_{1-x}As$ and many II-VI compounds. A list giving details of authors and the methods of production of the laser action is given in the review article by Nathan (1966).

2. 2. Principles of Laser Action

Before describing the semiconductor laser, the principles of laser action which are applicable to all types of laser are outlined in this section.

Fig 2.1. shows the energy level scheme of a typical four level laser. N_0, N_1 etc. are the numbers of electrons $/cm^3$ in each excited state. The transition between level 2 and level 1 is of interest. If an electron in level 2 drops spontaneously to level 1 it emits a photon of energy $h\nu = E_2 - E_1$. However, the electron in level 2 may be stimulated

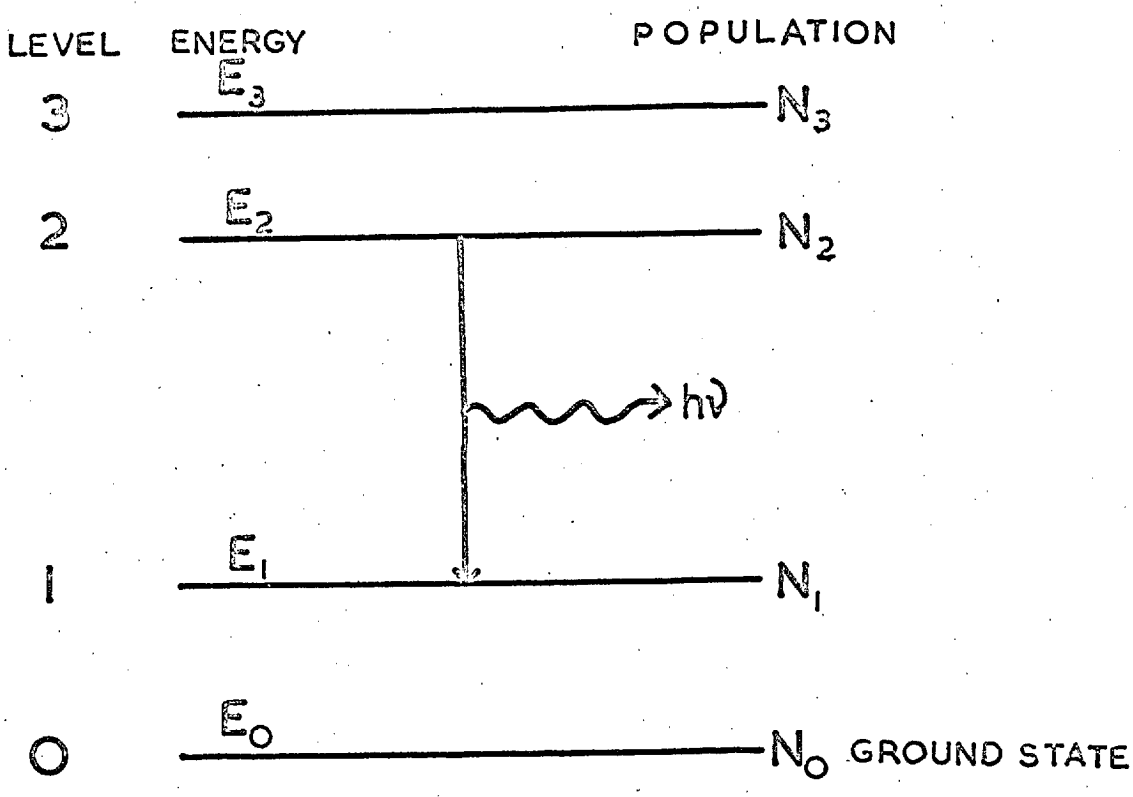

FIG. 2.1 ENERGY LEVEL DIAGRAM OF A FOUR LEVEL LASER.

by another photon of energy $h\nu$ to drop to level 1. For stimulated emission of radiation to predominate over spontaneous emission, N_2 must be greater than N_1, and when this condition is achieved it is called a state of inverted population.

Since an inverted population is thermodynamically unstable, power has to be supplied to maintain the situation. The inverted population may be achieved most easily if electrons in level 2 have a long lifetime and those in level 1 have a short lifetime, so that N_1 may be approximated to zero. Level 3 is usually a broad band with a short lifetime for decay to level 2, and both levels 2 and 1 must be sharp levels. Many lasers use a three level scheme where levels 0 and 1 are the same. This means more power is required to keep the population inverted.

Consider a beam of radiation traversing a region which is active for stimulated emission, i.e. it contains an inverted population of electrons. After travelling a distance x the intensity I is given by

$$I = I_0 \exp(-\alpha x) \qquad (2.1.)$$

where I_0 is the initial intensity, and α is the absorption coefficient due to all loss mechanisms. The absorption coefficient due to transitions between levels 1 and 2 only, is given by

$$\alpha(\nu) = \frac{c^2 \left[N_1(g_2/g_1) - N_2\right] A(\nu)}{8\pi\nu^2 \bar{n}^2 \tau} \qquad (2.2.)$$

where c is the velocity of light in vacuum

g_1 and g_2 are the statistical weights of the two states

ν is the frequency

τ is the radiative lifetime of electrons in the upper level for spontaneous emission.

$\bar{n}$ is the refractive index of the active medium

and $A(\nu)$ is the normalised line shape so that $\int A(\nu)\,d\nu = 1$

A derivation of this equation is given by Lengyel (1962) and in most text books dealing with lasers. When α in equ. (2.1.) is positive the beam is attenuated. However in an active medium with an inverted population the conditions may be such that at frequency ν there is sufficient stimulated emission to amplify the beam as it traverses the medium. $\alpha(\nu)$ is then negative, and is in fact, a gain coefficient $g(\nu)$. Equ. (2.2.) can then be written

$$g(\nu) = \frac{c^2 \left[N_2 - N_1(g_2/g_1) \right] A(\nu)}{8\pi \nu^2 \bar{n}^2 \tau} \qquad (2.3.)$$

Laser action will occur at the frequency at which $g(\nu)$ is a maximum. This is where

$$A(\nu) \longrightarrow A(\nu)_{max} = \frac{1}{\Delta\nu}$$

where $\Delta\nu$ is the spontaneous emission line width.

In an active region for stimulated emission, the spontaneous emission occurs isotropically. This means the stimulated emission also occurs isotropically. To ensure that the stimulated emission builds up in one direction, an accurately parallel pair of semi-reflecting mirrors is placed with one mirror at each end of the active medium. These mirror surfaces cause positive feedback in the direction perpendicular to them, so that the laser beam propagates preferentially in

this direction. The active medium is thus contained in a Fabry-Perot cavity.

In order to obtain laser action, there must not only be stimulated emission, but also sufficient gain g to overcome all the losses. Let R be the reflectivity at the mirror faces so that 1 - R is the fraction of radiation transmitted, and let g_t be the gain at the threshold of laser action. Then in a Fabry-Perot cavity the condition that a light beam just makes a complete traversal of the cavity, including one reflection, without changing in intensity is

$$R \exp\left[(g_t - \alpha)\ell\right] = 1 \qquad (2.4)$$

where ℓ is the length of the cavity.

In all lasers except semiconductor lasers, the energy to excite the inverted population is provided by an indirect means. For instance, in solid state and liquid lasers, light is supplied by powerful lamps, while in gas lasers an electrical discharge is generally used to supply the energy to the atoms. Both of these methods are inefficient compared with the direct conversion of electroluminescence in semiconductors under the proper conditions.

2.3. Semiconductor Lasers

The ideas developed so far apply to all lasers, including semiconductor lasers. In the following sections, these ideas are further developed for the semiconductor p - n junction laser and the properties of real diode lasers are discussed.

2.3.1. The Application of the Principles of Laser Action to Semiconductors

All lasers except semiconductor ones use sharp energy levels associated with localised wave functions, i.e. for amplification there must be a population inversion between two atomic energy levels. In the case of semiconductors the electronic states are represented by a Bloch-type wave function defined throughout the bulk material. This leads to broad bands of states - the conduction and valence bands - with an energy gap between them. In semiconductor lasers the population inversion is obtained between these two bands. Under equilibrium conditions the probability of a state of energy $E(k_w)$ being occupied by an electron is given by the Fermi distribution function

$$f = \frac{1}{1 + \exp\left[(E(k_w) - F)/KT \right]}$$

where F is the Fermi energy, k_w is the wave number, K is Boltzmann's constant, and T is absolute temperature. The probability of a hole occupying the same state is 1 - f

When carriers are injected into semiconducting material of the opposite type (i.e. they become minority carriers) they attempt to reach thermal equilibrium with the majority carriers. If the time in which this occurs is short compared to the recombination lifetime of the minority carriers, then the distribution of minority carriers in the conduction and valence bands can also be described by Fermi functions. The electron distribution in the conduction band of p-type material is given by

$$f_c = \frac{1}{1 + \exp\left[(E(k_j) - F_c)/KT \right]} \qquad (2.5.)$$

Similarly the hole distribution in the valence band of n type material is given by

$$f_v = \frac{1}{1 + \exp (E(k_i) - F_v)/KT} \qquad (2.6.)$$

F_c and F_v are the quasi - Fermi levels for minority carriers in the conduction and valence bands respectively and k_j and k_i are the wave numbers of electron states in the conduction and valence bands.

From considerations of quasi - Fermi levels, Bernard and Duraffourg (1961) derived a necessary condition for stimulated emission of radiation in semiconductors. In the presence of radiation, the number of quanta absorbed per unit time is

$$Q_a = K' \Gamma_{vc} f_v(k_i)\left[1 - f_c(k_j)\right] \qquad (2.7.)$$

and the number emitted per unit time is

$$Q_e = K' \Gamma_{cv}\left[1 - f_v(k_i)\right] f_c(k_j) \qquad (2.8.)$$

K' is a constant and includes the densities of states in the two bands; $\Gamma_{vc} = \Gamma_{cv}$ are the transition probabilities for electrons between the two bands, for upward and downward transitions respectively. The condition for amplification is $Q_e > Q_a$ and taking the photon energy as

$$E(k_j) - E(k_i) \simeq h\nu$$

it then follows using equations (2.5) to (2.8) that

$$F_c - F_v > h\nu \qquad (2.9)$$

where ν is the frequency of the stimulated radiation. This condition in relation to p - n junction lasers is illustrated in the following section.

At this point it is necessary to distinguish between direct and indirect band gap semiconductors. Fig 2.2. shows schematically

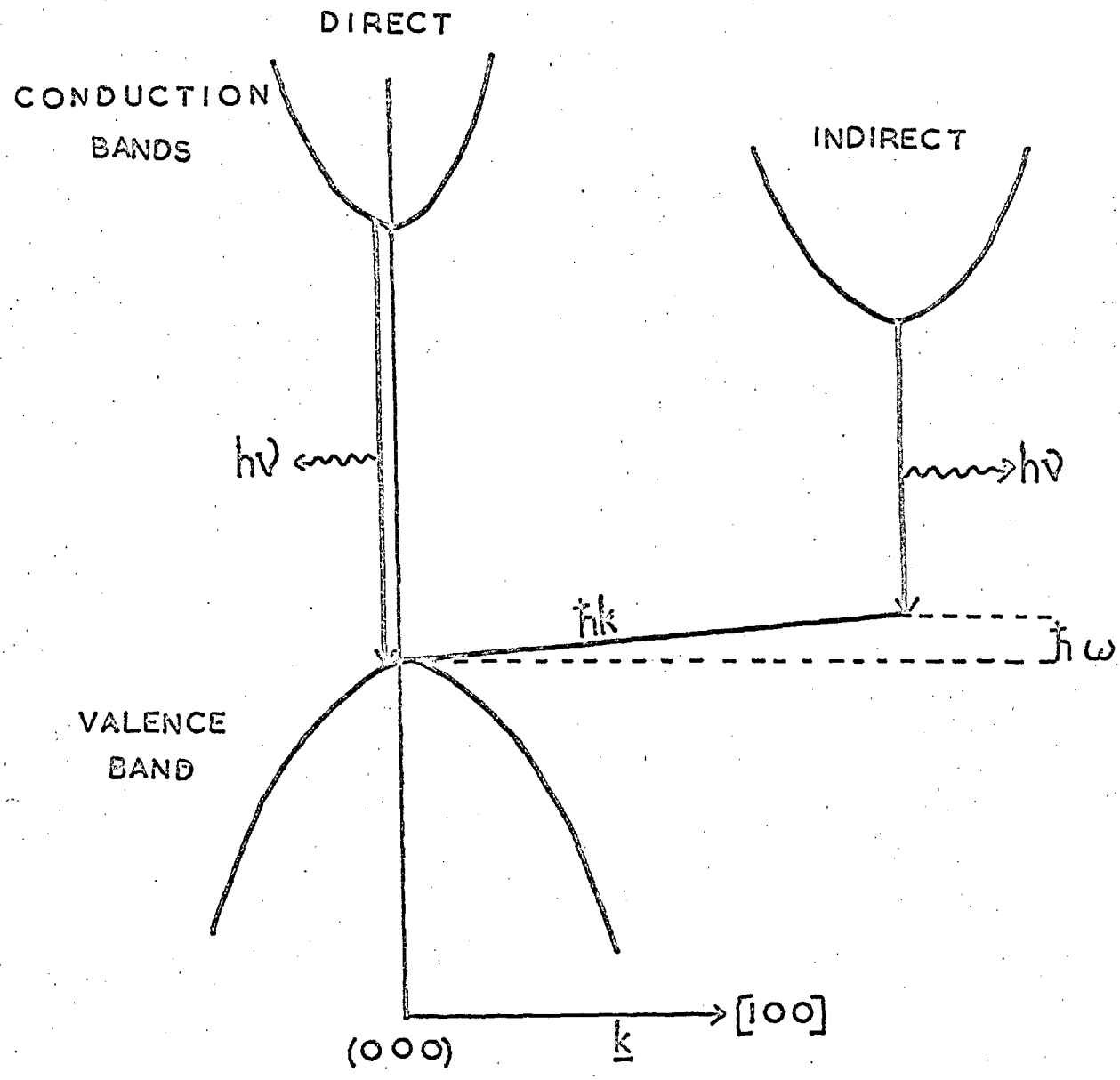

FIG. 2.2 ENERGY VS. WAVE VECTOR DIAGRAM SHOWING DIRECT AND INDIRECT BAND GAPS.

an energy versus wave vector diagram for a direct and an indirect band gap semiconductor. In the indirect case there is a difference in momentum between the minimum of the conduction band and the maximum of the valence band. This means that when an electron transfers from the conduction to the valence band, in addition to emitting a photon, a phonon must be produced to conserve momentum, which is a second order transition. The probability for a second order transition is much less than the probability for the first order transition involved when the conduction band minimum and valence band maximum have the same momentum vector, $\underline{k}$. All of the III - V semiconductors in which laser action has been achieved have a direct band gap. Laser action has not been achieved in Ge or Si which are both indirect band gap materials. Dumke (1962) first showed theoretically that for direct band gap materials like GaAs, the induced transition probability was great enough to overcome the expected losses due to free carrier absorption. The discovery by Keyes and Quist (1962) and Pankove (1962) that a p - n junction in GaAs had a radiative recombination efficiency approaching unity, made workers concentrate on the possibility of obtaining laser action in junction emission rather than from bulk material. Laser action in compound semiconductors has now been produced using at least four methods of excitation, (Nathan (1966)). These are,

(1) High energy electron beam injection

(11) Optical pumping

(111) Avalanche injection (Weiser and Woods (1965))

(1V) Injection across a p - n junction.

Some of these methods have been successful in only a few semiconductors, and the only material in which they have all been observed is GaAs. The work carried out in the research reported here was all on GaAs p - n junction injection lasers. Accordingly the remainder of this review considers only this type of laser.

2.3.2. Population Inversion at a p - n junction

When a GaAs diode is heavily doped with donors ($\gtrsim 5 \times 10^{17}/cm^3$) on the n side and heavily doped with acceptors on the p side ($\gtrsim 10^{19}/cm^3$) the electron and hole states involved in the emission become degenerate. Degeneracy occurs when the Fermi level rises into the conduction band in n - type material or drops into the valence band in p - type material (see fig. 2.3.). Keyes (1963) pointed out that the material must be degenerate on at least one side of the junction for laser action to occur. The quasi - Fermi level difference ΔF cannot be greater than the "built in" potential eV_D (fig. 2.3(a)) and since $\Delta F > h\nu$ for laser action then $eV_D > h\nu$. Since the doping level determines V_D this imposes a lower limit on the doping concentration. Heavy doping is also required on both sides of the junction to provide large carrier densities.

Fig 2.3. shows the band structure at a p - n junction in degenerately doped GaAs. At the doping levels used the impurity levels are broadened into shallow bands which are usually assumed to be merged with the conduction and valence bands. Fig 2.3.(a) shows the junction with no applied bias with eV_D being the height of the "built in" voltage barrier. Notice that under equilibrium

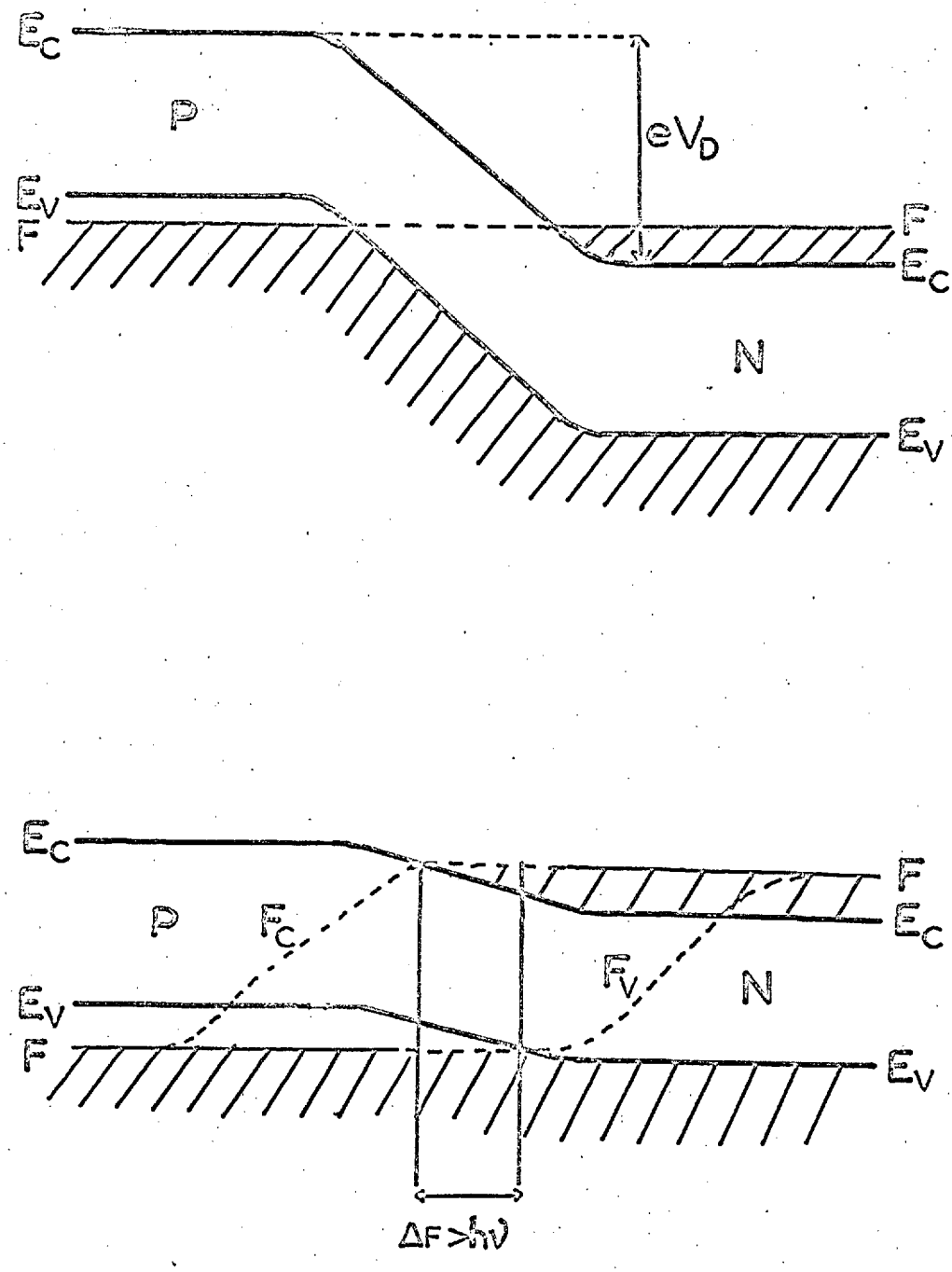

FIG 2.3 ENERGY BAND DIAGRAM OF A DEGENERATE P-N JUNCTION. (a) ZERO APPLIED BIAS. (b) WITH FORWARD BIAS.

$F_c = F_v = F$. Fig 2.3.(b) shows the result of applying a forward bias V_B of approximately $(E_c - E_v)/e$ where $E_c - E_v$ is the band - gap energy. The splitting of the Fermi level into two quasi - Fermi levels in the junction region is indicated. It is clearly shown that $\Delta F > h\nu$ over a certain region at the junction. In this region there are electrons in the conduction band and holes in the valence band simultaneously.

2.3.3. Current Density at Threshold of Laser Action

Equ. (2.3) gave the gain coefficient for light traversing an active region. In a semiconductor, N_1 is taken as zero, since there are plenty of available states in the valence band. Assuming $A(\nu) = \frac{1}{\Delta\nu}$ equ. (2.3) can now be written for a semiconductor as

$$g(\nu) = \frac{c^2 N_2}{8\pi\nu^2 \bar{n}^2 \tau_r \Delta\nu} \qquad (2.10)$$

where τ_r is the radiative lifetime of minority carriers in the inverted population region, and N_2 is now the minority carrier density.

In semiconductors a Fabry-Perot cavity is simple to produce (sect.2.3.4.) and so equ. (2.4.) is applicable. If τ is the overall lifetime of minority carriers and d is the thickness of the active region surrounding the junction, then on forward biasing the p - n junction the current density j flowing across the junction is given by

$$j = \frac{N_2 ed}{\tau} \qquad (2.11)$$

This equation follows directly from the continuity equation. (At this stage no distinction has been made between electrons injected into the p side and holes injected into the n side. This is discussed in the following section.) Eliminating $g(\nu)$ from equs. (2.4.) and (2.10.) and using equ. (2.11.) gives the minimum current density necessary for laser action. This threshold current density is

$$j_t = \frac{8\pi e n^2 \nu^2 \Delta\nu\, d}{\eta c^2}\left[\frac{1}{\ell}\ln\left(\frac{1}{R}\right) + \alpha\right] \qquad (2.12.)$$

$$= \frac{1}{\beta}\left[\frac{1}{\ell}\ln\left(\frac{1}{R}\right) + \alpha\right] \qquad (2.13.)$$

where η is the quantum efficiency and is equal to τ/τ_r. β includes everything in front of the square brackets and is called the gain factor. This relation for j_t was first derived by Lasher (1963).

Equ. (2.10.) applies to sharp energy levels with $N_1 = 0$ but this is only true in semiconductors at $0^{\circ}K$. Thus equs. (2.12.) and (2.13.) are only valid at this temperature. Pilkuhn et al (1964) and others found that β varied strongly with temperature, but that the overall functional form of equ. (2.13) was obeyed for temperatures up to room temperature. They also found α to be weakly temperature dependent.

At the high doping levels used in injection lasers the shape of the energy bands in momentum space is not simple parabolic, but the bottoms of the parabolae merge with the impurity levels. This means that some other form of density of states distribution should be used in theoretical calculations concerning laser characteristics. Lasher and Stern (1964) performed the first

detailed theoretical study of semiconductor laser behaviour. They assumed the bands were still parabolic in spite of any merging with impurity bands, and considered only band to band recombination. Taking a constant momentum matrix element for the radiative transition, they successfully predicted the form of the temperature variation of j_t. The experimental results of Pilkuhn et al (1964) showed that the gain factor varied linearly with current density j, whereas the results of Lasher and Stern gave a definitely non - linear variation. Stern (1966) carried out calculations of the effect of band tails on the stimulated emission. He used a Gaussian distribution for the band tail density of states and a constant momentum matrix element. This predicted a linear variation of gain with current density.

The effect of variations in most of the factors in equ. (2.12.) is considered in detail in the discussion of results in Chapter 5.

2.3.4. The Fabry - Perot Cavity in Diode Lasers

P - n junctions in GaAs may be produced by several techniques (section 2.4.6.). After the junction has been prepared the resonant cavity must be made, in order to feed back a part of the stimulated emission into the active region. In GaAs the resonant cavity is relatively simple to make. The usual structure is a rectangular single crystal wafer of GaAs with the junction plane parallel to the top and bottom surfaces. Fig 2.4. is a schematic drawing of a typical laser diode. Two surfaces, flat and accurately parallel to each other, and also perpendicular to the junction plane, are prepared either by polishing or by cleaving. In the former

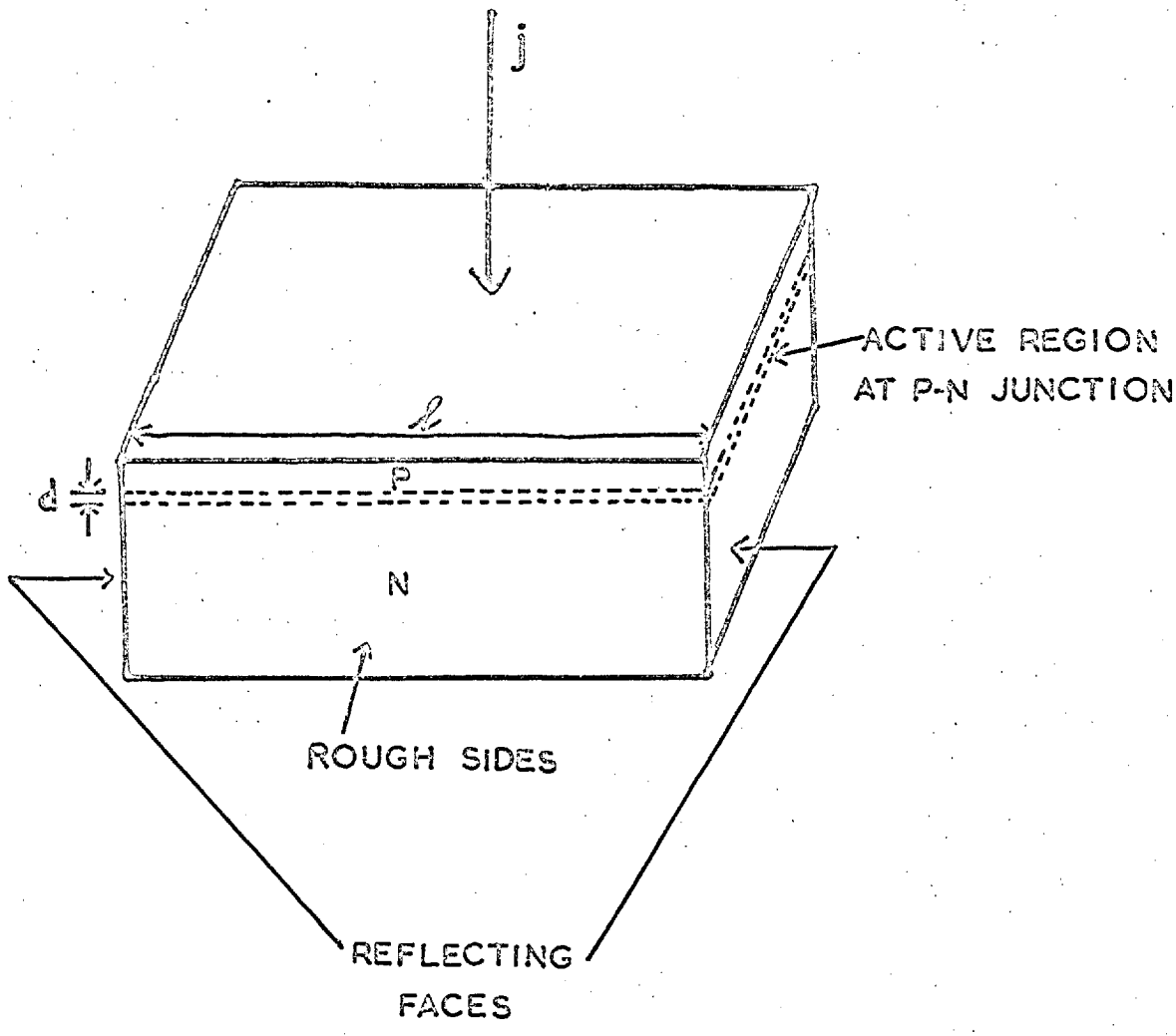

FIG 2.4 SCHEMATIC DRAWING OF A LASER DIODE
ℓ IS THE FABRY-PEROT CAVITY LENGTH.
d IS THE ACTIVE REGION THICKNESS.

case the diode may be made in any crystal orientation, but for cleaved surfaces only the $\{110\}$ cleavage planes of GaAs can be used. The two remaining sides of the diode must be left rough, to prevent laser action occurring perpendicular to these sides. The refractive index $\bar{n}$ of GaAs/air interface is approximately 3·6. This means that the internal reflection, R at normal incidence, which is given by

$$R = \left[\frac{\bar{n} - 1}{\bar{n} + 1}\right]^2$$

is about 32%. Therefore no other form of reflector is necessary. Reflecting films have been applied to one face of many diodes and this reduced the threshold current somewhat. (Burns and Nathan (1964)). Typical diode dimensions range from cubes with 100 μ edges to rectangles with Fabry - Perot cavity lengths, of 2mm or more. d in fig. 2.4. is the thickness of the laser active region and is of the order 1 μ

Removal of the heat generated by resistance heating in the diode is a problem. Heat sinks must be attached to the top and bottom surfaces and the diodes are usually operated at liquid nitrogen or liquid helium temperatures, with current pulses which may be as short as 1 nanosecond. Continuous operation has been achieved at temperatures in excess of 77°K but not as high as room temperature.

For resonance and amplification in a cavity there must be an integral number of half wavelengths in the cavity length, i.e.

$$l = \frac{m \lambda}{\bar{n}\ 2} \qquad (2.14.)$$

where m is an integer. The photon energies emitted are close to the band gap energy and the refractive index at these energies depends critically on the wavelength. Differentiating equ.(2.14) leads to

$$dm = 2\ell\left(\frac{1}{\lambda}\frac{d\bar{n}}{d\lambda} - \frac{\bar{n}}{\lambda^2}\right) d\lambda$$

and letting dm = -1 for adjacent cavity modes gives

$$d\lambda = \frac{\lambda^2}{2\ell}\left(\bar{n} - \frac{d\bar{n}}{d\lambda}\lambda\right)^{-1} \qquad (2.15.)$$

Marple (1964) has obtained $\frac{d\bar{n}}{d\lambda}$ experimentally for GaAs and using typical values of cavity length ℓ gives a wavelength spacing of about 2 Å between cavity modes. Nathan, Fowler and Burns (1963) and Sorokin, Axe and Lankard (1963) observed spectral peaks corresponding to these cavity modes. They occur throughout the width of the broad spontaneous emission line at currents well below threshold. Just below threshold, the spontaneous emission line narrows and at threshold one of the Fabry - Perot modes is selected and laser action sets in at that wavelength.

Much work has been carried out on the emission spectra of GaAs lasers, to determine the mechanisms occurring at the junction. The effect of variations of temperature, current density, doping levels, pressure and application of magnetic fields on emission spectra have been studied. This work was reviewed by Burns and Nathan (1964) and by Thornton (1967). From the observed electroluminescent spectra it appears that the electron and hole distributions are both degenerate, and that at least one of the impurity bands has merged with the respective conduction or valence band, to produce a band - tail into the energy gap.

At high current densities the injection mechanism involved is thought to be electrons tunnelling into the p - side with subsequent radiative recombination with holes. Burns and Nathan pointed out several reasons supporting electron injection into the p - side before recombination, and high magnification near-field emission micrographs appear to confirm that the emission is from the p - side of the chemically defined junction. For example see Michel, Walker and Nathan (1963). From photoluminescence spectra of p - and n - type GaAs, Carr and Biard (1964) found evidence to support p - side emission in junction electroluminescence. Hill (1964) also found support for recombination in the p type material in his spectra of spontaneous junction emission. In no case has emission been reported from the n side of the junction although Hall (1963) stated that it was at the junction.

2.3.5. The Active Region

The active region in which gain occurs is a thin slice of thickness d, contained between two bulk slabs of lossy material. Initial calculations of the internal losses α in the junction region by Lasher (1963) and Hall and Olechna (1963) gave unrealistically large values for α. In order to explain the experimental results for the losses a model was proposed by Lasher (1963) and developed by McWhorter (1963) and Yariv and Leite (1963) among others, in which the real part of the complex dielectric constant, as well as the imaginary part, varied in three different regions near the junction. This model gave a mechanism to confine the radiation to the active region and so reduce the losses. The three regions usually considered are, the bulk p type material,

the active region of width d, and the bulk n type material. The dielectric constant ϵ' is then written as

$$\epsilon_i' = \epsilon_i + \sigma_i/j\omega$$

i = 1,2,3 refers to the three regions and the $\frac{\sigma_i}{j\omega}$ term is due to free carriers. σ is the conductivity and is negative in the active region where there is a population inversion and ω is the angular frequency of the emitted radiation. ϵ_i is the dielectric constant in the absence of free carriers. The radiation confinement described by this model results in a reduction of the predicted threshold current density to values close to those found experimentally. Radiation confinement and losses in the junction region were discussed in detail by Thornton (1967).

The thickness, d, of the active region (fig 2.4.) is uncertain. The diffusion profile results of Cunnell and Gooch (1960) and Pilkuhn and Rupprecht (1964) show that the Zn acceptor concentration in diffused diodes, drops from a value of $>10^{19}$ Zn atoms/cm^3 to below the donor doping level of 2×10^{18}/cm^3 in a distance of only about 5 μ. This means the junction is well defined. According to Hall (1963) the diffusion length of electrons in p type material is $\sim 1\,\mu$ while 2·6 μ was quoted by Anderson (1965) and between 1 and 4 μ by Vilms and Spicer (1965). Aukerman, Millea and McColl (1967) showed that the electron diffusion length in the p side of a Zn diffused diode varied with substrate donor concentration, from 20 μ for lightly doped diodes to 2 μ for donor concentrations $> 10^{18}$/cm^3. Casey et al (1966) considered two components of

the spontaneous emission. One had a wavelength peak, λ_p, which was independent of applied bias and the other had λ_p which shifted with bias. The former component, which gave stimulated emission under the right conditions, had an active region thickness $> 1\mu$ determined by interference observations perpendicular to the junction plane. It is apparent that, at the doping levels used in GaAs injection lasers the diffusion length of electrons into the p-type material is $> 1\mu$ and $< 5\mu$. Distinction should be made between the active region thickness which is controlled by carrier diffusion lengths, and the region into which the radiation is confined by the mechanism described previously. Kazarinov et al (1965) calculated that this latter region was of the order of 10μ and Bagaev et al (1964) found experimentally that some stimulated emission came from regions tens of microns thick.

The small thickness, d, of the active region means that the area over which it intersects the mirror faces of the diodes may be treated in a similar way to light transmission through a single slit. The angular spread, Θ, of light diffracted by a slit is given approximately by

$$\Theta = \lambda/d \qquad (2.16.)$$

where λ is the wavelength. For GaAs diodes, if λ is taken as 8,400 Å and $d = 3\mu$ this gives an angular divergence of about 16°. Beam divergence angles perpendicular to the junction plane of about 15° are common (Jonscher and Boyle (1966) and Pilkuhn and Rupprecht (1967)). The emission pattern usually consists of several lobes of high intensity asymmetrically placed about the

normal to the mirror surface. Anomalous variations in diffracted intensity perpendicular to the junction plane are generally visible in far-field micrographs. In some cases the angle of emergence of the more intense lines can be explained by the mechanism described explicitly by Ludman and Hergenrother (1966). This involved bending of the beam by refractive index changes as in all mode confinement mechanisms, but the bending was such that a beam was caused to oscillate between the p and n sides during one traversal of the cavity. The angle of emergence, Θ, depended on which direction the beam was being bent as it left the diode. The predicted dependence of Θ on the cavity length ℓ was found, assuming refractive index variations of not greater than 2% across the junction.

From equ. (2.16.) with a diode having mirror faces of width 100 μ a value of Θ for the beam divergence in the plane of the junction of less than 1^{o} is predicted. Experimental values of in the plane of the junction are never smaller than 1^{o} even for diodes with large emitting faces. In fact the far-field emission patterns of all diodes contain many lines of increased intensity perpendicular to the junction plane, covering an angle Θ of about 5^{o} either side of the normal. See for instance Fenner and Kingsley (1963) and Jonscher and Boyle (1966). These results show that the junction does not emit uniformly. When injection diode emission is examined in near-field at currents just above threshold it is found that stimulated emission occurs at lower current densities in some areas of the junction than in others.

As a result isolated areas of stimulated emission appear along the line of intersection of the junction plane with the mirror surface. This commonly termed "spotty" emission is always observed to some extent in junction lasers. Usually the current must be increased considerably above the threshold current density, j_t, before the whole junction lases, and even then the intensity is non - uniform (Broom et al (1963). The behaviour of the emission spots is much as expected. Since the near field emission patterns of the two reflecting faces can always be correlated the spots are in the form of filaments running throughout the length of the cavity. Also, on increasing the diode current above j_t the spots always appear in the same positions and at the same values of diode current. There is not generally any coherence between individual spots. Fenner and Kingsley (1963) and Raab, Bachert and Kaiper (1966) found wavelength differences between different spots, and Broom et al found the plane of polarisation of each filament was often different.

Fowler and Walker (1964) showed that by applying a magnetic field parallel to the filaments they could deflect the current carriers in the diodes so that the current density was varied in different parts of the junction. As the field was increased the stimulated emission spots did not move smoothly as expected, but jumped from one position to another along the junction. Fenner (1966) found the same thing when he altered the current distribution by having a divided contact on the p side and varying the current through each part of the contact. Nathan et al (1965) divided

the p side contact by a line parallel to the mirror faces and found a variation of j_t with the ratio of the currents through the two terminals. They found that j_t was raised for non - uniform current distribution and that the cavity mode of maximum gain also depended on the current distribution. Michel and Walker (1964) found that a non-uniform adsorbed dielectric film on the diode surfaces altered the reflectivity of the mirrors in a non-uniform way and caused changes in the intensity distribution along the junction.

Nannichi (1966) pointed out that once a filament was established in part of the junction, then the life-time of electrons would be reduced and hence more would be injected into this region. This would result in depletion of electrons and subsequent suppression of laser action in the volume surrounding the filament. Jonscher and Boyle (1966) also suggested a mechanism which would restrict the light of a filament from spreading. They suggested the confinement was due to the refractive index change caused by the depletion of free carriers in the region of the laser action. These mechanisms would prevent a filament from spreading, but would not explain the considerable differences in threshold current found between different filaments in the same diode. It is probable that the defect content of the GaAs would have to be reduced before these mechanisms became of importance in determining the emission pattern. The high concentrations of impurities necessary for laser action may preclude this level of crystal perfection ever being attained in the junction region.

The above discussion indicates the presence of non-uniformities

in the laser diode material. The literature concerning these inhomogeneities and crystal defects in GaAs is discussed in the remainder of this chapter.

2.4. Material Properties of Gallium Arsenide

2.4.1. Crystal Structure

GaAs, like many of the III - V compound semiconductors crystallises in the sphalerite (Zincblende) structure. This is similar to the diamond structure which consists of two face-centred cubic sub-lattices with their origins at (0,0,0) and $(\frac{1}{4},\frac{1}{4},\frac{1}{4})$, so that the two sub-lattices interpenetrate. In the sphalerite structure one sub-lattice is occupied entirely by Ga atoms and the other entirely by As atoms. Thus every atom has four nearest neighbours of opposite type, arranged at the apices of a regular tetrahedron. The tetrahedral co-ordination of the interatomic bonds is due to the sp^3 hybrid orbitals of the electrons. This configuration is a mixture of one s - type and three p - type orbitals to form orbitals directed to the corners of a regular tetrahedron.

The sphalerite structure has no centre of symmetry and this leads to polarity effects in certain directions. These effects were reviewed by Barber and Heasell (1965). The $\langle 1\ 1\ 1 \rangle$ directions in particular show the effects of polarity. Fig 2.5. is a view of the $(1\ \bar{1}\ 0)$ plane which is perpendicular to the $(1\ 1\ 1)$ plane Two possible ways of separating $\{1\ 1\ 1\}$ planes are shown by lines $\alpha\beta$ and $\gamma\delta$. The former involves breaking one bond per atom and is energetically more favourable than the latter which involves

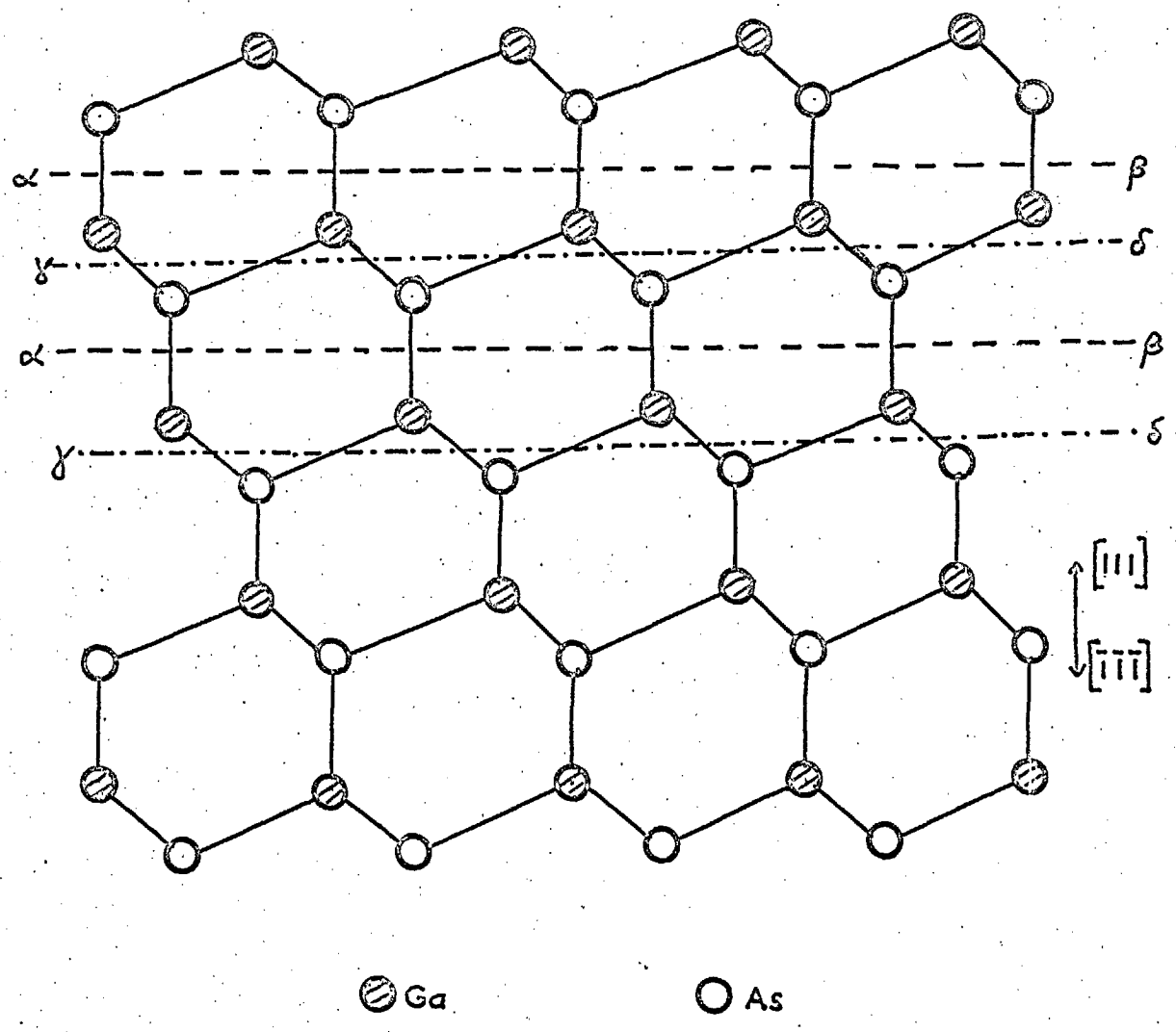

FIG. 2.5. PROJECTION OF GaAs STRUCTURE ON $(1\bar{1}0)$ PLANE. LINES α-β ARE TRACES OF ACTUAL (111) SURFACES.

breaking three bonds per atom. Thus a wafer with $\{1\ 1\ 1\}$ surfaces has one surface containing only Ga atoms (called an A or (1 1 1) surface) and the other containing only As atoms (a B or $(\bar{1}\ \bar{1}\ \bar{1}$) surface). The two opposite (1 1 1) surfaces of GaAs were first shown to have different properties by Schell (1957) who revealed a different etching characteristic for each surface. In $\langle 100 \rangle$ directions the $\{100\}$ planes contain alternatively all Ga and all As atoms , but are equally spaced. Each plane is linked by two bonds per atom to the next, so there are no detectable surface polarity effects. The $\{110\}$ planes are equally spaced and each contains an equal number of Ga and As atoms. The $\{110\}$ plane is the cleavage plane in GaAs. Values of the lattice parameter of GaAs at several impurity concentrations have been determined by Black and Lublin (1964). For undoped material the value found was 5·6534 Å.

2.4.2. Geometry of Dislocations in the Sphalerite Structure

The arrangements of atoms in the cores of dislocations in the sphalerite structure were described by Holt (1962) using the notation of Hornstra (1958). The direction of a dislocation line (a) and it Burgers vector (b) determine the slip plane of the dislocation and the angle between a and b is used to describe the dislocation. For instance, a dislocation with Burgers vector $\underline{b} = \frac{1}{2}[\bar{1}\ 0\ \bar{1}]$ and line direction $\underline{a} = [1\ \bar{1}\ 0]$ is a 60° dislocation and is one of the most common types in the sphalerite structure. There are always dangling bonds in the cores of edge dislocations.

Haasen (1957) pointed out that there are two types of dislocation core for edge dislocations in the sphalerite structure. These occur when (i) the row of atoms at the edge of the extra half plane consists of group III atoms (an α dislocation) and (ii) the row of atoms consists of group V atoms (a β dislocation). α and β dislocations have different chemical properties during etching and different electrical properties.

2.4.3. Electrical Properties of Dislocations

Dislocations in semiconductor crystals produce localised donor or acceptor states, but the mechanisms involved do not appear to be explicable on a simple dangling bond model. Heine (1966) discussed the difficulties of a simple interpretation and suggested that the states arise through variation of the atom density at the cores of the dislocations. The effects of these dislocation - induced impurity states on the electrical properties of semiconductors have been studied in InSb by Lavine, Gatos and Finn (1961), Willoughby (1965) and Bell et al (1965) and in Ge by Broudy (1963). A point, first made by Holt (1960) is that the electrical effect of the dislocation - induced states must depend strongly on the position of the Fermi level. The effect of these states on the recombination radiation of Ge has been studied by Gippius and Vavilov (1963),(1965). They explained their recombination radiation spectra by assuming transitions involving energy levels in the band gap due to the dislocations. In GaAs light emitting diodes, which are always heavily doped, the dislocation donor and acceptor levels may be included in the

broad impurity bands. However, there are no reports of any properties of the emission spectra of GaAs being attributed to dislocation - induced levels.

Logan, Chynoweth and Cohen (1962) reported microplasma breakdown in GaAs p - n junctions having 10^6 dislocations/cm^2. Michel, Nathan and Marinace (1964) found localised emission at visible and infra-red frequencies at points in the junction plane of GaAs diodes, but no correlation was made with any crystal defects. In reverse biased Si diodes Chynoweth and Pearson (1958) found a positive correlation between light emitting spots and dislocations passing through the junction. Thornton (1963) measured the voltage distribution and transient photoconductive response on high resistivity GaAs specimens with known dislocation distributions. Only in specimens grown by one particular technique was any correlation between electrical inhomogeneities and dislocation distribution found, and it was suggested that some form of decoration of the dislocations had occurred in these specimens.

2.4.4. Growth of Gallium Arsenide

The usual methods of growing bulk single crystals of III - V compound semiconductors are, horizontal freezing and Czochralski pulling from the melt. In compound semiconductors having high melting points like GaAs, In P and GaP, the group V element has a high vapour pressure at the melting point. The melting point of GaAs is 1237°C and the partial vapour pressure of arsenic at this temperature is 0·9 atmos. This necessitates modifications of the standard crystal growing techniques before they can be applied to

these materials.

In the application of the gradient freeze technique to GaAs, the constituent elements are put in a graphite boat and sealed into a quartz furnace tube. A small amount of arsenic in excess of the stoichiometric quantity is used. The tube is placed in the furnace and the temperature slowly increased to allow the arsenic to vaporise and dissolve in the liquid gallium. The temperature distribution in the furnace is critical. One end of the tube is held at 605°C to control the vapour pressure of arsenic at 0·9 atmos. The boat containing the melt is in a region of the furnace held at 1240°C and there is a uniform temperature gradient between the boat and the arsenic source. The power supply to the furnace is reduced so that the temperature gradient moves slowly (about 2cms/hr.) along the boat containing the melt. The melt solidifies at one end and the liquid-solid interface moves steadily along the boat. Ingots prepared in this way often grow spontaneously as single crystals, otherwise they contain a few large crystallites of possibly several cm^3 volume. To obtain a particular orientation the melt may be seeded. The horizontal Bridgman technique is similar to the gradient freeze method except that the temperature gradient in the furnace is kept constant and the quartz tube moved slowly with respect to the temperature gradient.

The Czochralski technique is often used for growing ingots of GaAs. A seed crystal is dipped into a boat of liquid GaAs and pulled at about 2cm/hr. from the melt. The ingot is usually rotated at the same time to give some stirring of the melt. Gas-tight movable

lead throughs have to be used. A layer of liquid boric oxide (B_2O_3) can be used to cover the melt surface from which the ingot is being pulled. This prevents the escape of arsenic and also contamination from the atmosphere. Even with highest purity Ga and As starting materials the ingots grown by the methods mentioned above are always contaminated with donors from the crucible, sometimes with impurity concentrations as high as 10^{17} atoms/cm^3. In bulk GaAs, grown by horizontal boat techniques or by Czochralski pulling, the dislocation content is typically of the order of $10^4/cm^2$. Steinemann and Zimmerli (1967) reported that they had grown dislocation-free material using the Czochralski method.

GaAs can be produced by vapour phase epitaxy in purer forms than by the methods described above. The temperature of the material being deposited is well below the melting point and hence contamination is reduced. Using $AsCl_3$ as a supply of arsenic vapour to react with liquid gallium Whitaker and Bolger (1966) produced epitaxial GaAs with donor concentrations as low as 1 X 10^{14} electrons/cm^3 at 77°K.

A common defect in doped crystals of bulk semiconductors is the formation of striations of varying impurity concentration. These are most common at the high impurity levels needed for electroluminescent devices. The striations, which are found in pulled and boat grown material are discussed in the following section.

2.4.5. Striations in Semiconductor Crystals

Striations and cellular segregation in crystals grown from the melt have been a common feature in metal alloys for a long time.

When semiconductor technology demanded extremely homogeneous single crystals, these effects attracted further attention. Burton et al (1953 a & b) and Camp (1954) found variations in impurity concentration in Ge crystals grown by the Czochralski technique. In all cases the striations could be distinguished from those due to the rate of rotation and pulling of the crystal. Gatos et al (1961) found striations in non-rotated, pulled In Sb crystals doped to about 10^{18} Te atoms/cm^3 and Muller and Wilhelm (1964) found similar bands in horizontal boat-grown crystals. Gatos et al suggested the cause was supercooling and subsequent remelting at the interface due to emission of latent heat of fusion. However Morizane, Witt and Gatos (1966) showed that this explanation was incorrect. They put sensitive thermocouples in the melt near the liquid-solid interface and found irregular fluctuations in the temperature gradient. The striations were shown to correspond to the temperature fluctuations.

Hurle (1966) studied these temperature fluctuations in a Ga melt in a horizontal boat. He showed that for low temperature gradients the temperature variation with time at a point in the melt was caused by heat waves passing from end to end of the melt and that the wavelength was equal to the length of the boat.

At steeper temperature gradients the fluctuations at a point in the melt appeared to be random, but on careful spectral analysis Hurle, Gillman and Harp (1966) showed that the fluctuations were composed of several harmonics of the fundamental wavelength. The temperature fluctuations found by Morizane, Witt and Gatos and by Muller and Wilhelm can be explained by the mechanism of Hurle, Gillman and Harp. The temperature fluctuations cause microscopic variations in the growth rate at the crystal face. These variations in the growth rate cause small changes in the impurity segregation coefficient which is known to be dependent on the growth rate. Thus bands of varying impurity concentration are produced in the crystal.

In GaAs, striations have been reported by several workers using various techniques, but they have not been studied during growth. Lemay (1963) found them in Czochralski grown GaAs and suggested they were due to supercooling. Drougard (1966) studied the refractive index changes across striations using a Schlieren technique. Meieran (1965) studied striations in Te doped GaAs by transmission electron microscopy and found the density of precipitates of Te varied across the striations. Precipitates of Te were seen only when $N_{Te} \geq 2 \times 10^{18}$ Te atoms/cm^3 although the striations were visible by chemical etching when N_{Te} was as low as 10^{17}/cm^3. The crystals examined were all Czochralski grown and it is not known whether the striations corresponded to the rotation and pulling rates, or whether they were due to temperature fluctuations. Wittry (1966) found bands of varying Te concentration by electron probe

x-ray fluorescence and scanning electron beam excited recombination radiation (SEBERR). The Te concentration varied by 30% but the free electron concentration by less than 10%. Ziegler and Henkel (1965) observed striations by infra-red transmission in Czochralski grown GaAs and studied their effect on laser action. In this case the striations were due to the pulling and rotation. Casey (1967) also found SEBERR efficiency variations revealed striations in GaAs.

The application of a transverse magnetic field during solidification can be used to remove or reduce the striations in GaAs, as was found in the Ga melt by Hurle (1966) and in InSb by Chedzey and Hurle (1966).

Striations in GaAs have been seen in material doped with Te, Se, Sn and Zn and in material grown by all bulk methods. Thus it is a common feature of the growth of GaAs doped to greater than 10^{17} impurity atoms/cm^3.

2.4.6. Impurity Diffusion in Gallium Arsenide

The first GaAs junction lasers were made by diffusing acceptor impurities (usually Zn) into n - type substrates. Diffusion is still commonly employed, but the use of epitaxial deposition to produce p - n junctions has recently been developed. This method has been found to give diodes of lower threshold current density than diffused diodes for room temperature operation (Pilkuhn and Rupprecht (1967)). However, as the diodes used in the work reported here were all diffused, only diffusion of impurities in GaAs is reviewed here.

Gunnell and Gooch (1960) and Goldstein (1960) did the first systematic work on the diffusion of the acceptor Zn into n - type

GaAs, using the radioactive tracer technique to determine the diffusion profile. Pilkuhn and Rupprecht (1964) determined the Zn profile by incremental sheet conductivity measurements using a four point probe. They assumed complete ionisation of the Zn atoms and converted the conductivity measurements into Zn concentrations. Fig (2.6.) shows typical diffusion profiles obtained by Cunnell and Gooch, and Pilkühn and Rupprecht. There is good agreement between the two methods. The profiles show a much sharper concentration gradient at the diffusion front, than the complementary error function curve predicted by Ficks' Law. This assumes there is only one diffusion coefficient and that it is independent of the Zn concentration. Pilkuhn and Rupprecht explained their profiles by a double stream mechanism, first suggested by Longini (1962) and considered in detail by Weisberg and Blanc (1963). Some of the Zn diffuses slowly via substitutional lattice sites and some rapidly via interstitial sites. There is equilibrium between the Zn on the two types of site. Weisberg and Blanc also showed that the data of Cunnell and Gooch could be explained on this basis. Weiser (1963), assuming a singly ionised interstitial Zn ion has calculated the ratio of the concentrations of interstitial (C_i) to substitutional (C_s) Zn atoms at various temperatures and also the diffusion coefficients for the two types of site. The ratio C_i/C_s was of the order of 10^{-12} at 900°C.

Chang and Pearson (1964) studied the diffusion of radioactive Zn in uniformly Zn doped GaAs. After considering the possible mechanisms of diffusion they concluded that their results were explained by an interstitial-substitutional mechanism, with the

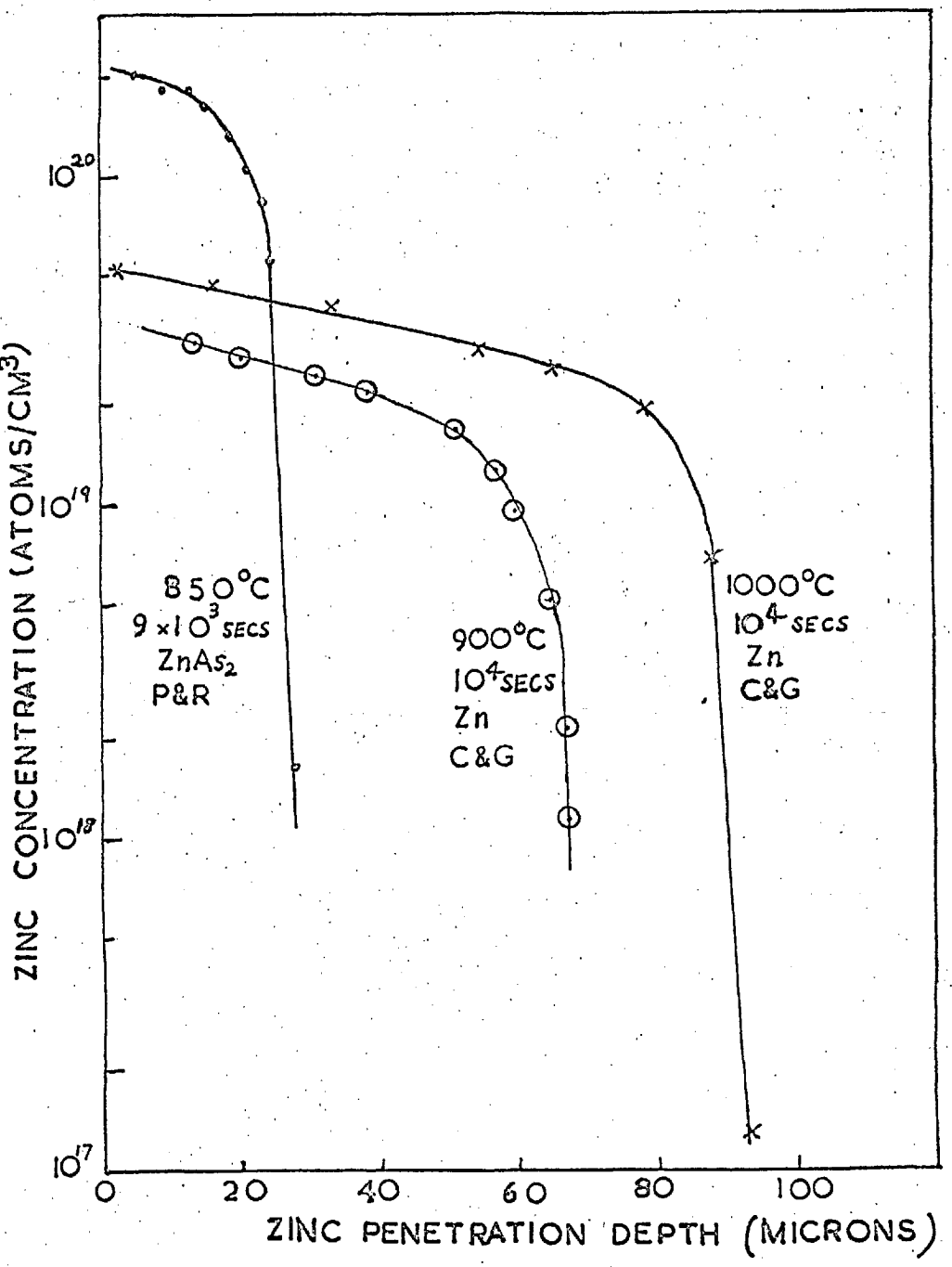

FIG. 2.6 SOME TYPICAL ZINC DIFFUSION PROFILES IN GaAs. TEMPERATURE, TIME & DIFFUSANT ARE SHOWN. CURVES ARE DUE TO CUNNELL & GOOCH (1960) AND PILKUHN & RUPPRECHT (1964).

interstitial playing the dominant role. To obtain this agreement between theory and their experimental results they assumed that the interstitial Zn atoms were doubly charged and substitutional Zn atoms were singly charged or neutral. Frank and Azim (1967) used a spreading resistance technique to determine the Zn profile and using the double stream theory of Weisberg and Blanc explained their results by assuming the interstial Zn to act as singly charged donors and the substitutional Zn to act as acceptors. From the above results it appears that a double stream mechanism involving interstitial and substitutional Zn atoms does explain the diffusion profiles obtained, but that the charge states of the Zn atoms are uncertain.

Peart et al (1966) used radioactive Zn and Mn to study the effect of Zn diffusion into uniformly Mn doped GaAs. They found the Mn concentration had a large minimum behind the diffusion front, which was explained by thermodynamic arguments, and fluctuations of - 40% and + 20% at 4 and 8 μ respectively ahead of the p - n junction. Larrabee and Osborne (1966) studied the effect of Zn diffusion into GaAs substrates uniformly doped with radioactive Cu. They found an order of magnitude decrease in the Cu distribution about 20 μ ahead of the junction, with the Cu concentration only reaching its equilibrium value again at about 80μ ahead of the junction. In the cases of both Mn and Cu the authors suggested that the minimum ahead of the junction was due to donors being swept into the bulk material by the electric field of the diffusion front.

Cu and Mn both show amphoteric doping behaviour in GaAs, probably due to their different electrical properties when they occupy interstitial or substitutional sites in the lattice.

Because of the anomalously large diffusion rate of Zn in GaAs, junction depths of tens of microns can be reached before non-planar effects become intolerable (Marinace (1963)). In order to maintain stoichiometry in the GaAs crystal, $ZnAs_2$ is generally used as the diffusant. Sufficient must be used to produce an As_4 vapour pressure equal to that of GaAs under the same diffusion conditions. Marinace studied the experimental conditions during diffusion and concluded that the optimum conditions for producing plane junctions were, a. $ZnAs_2$ charge of about 1 mg/cm^3 of diffusion tube volume, and diffusion for 3 hours at 850°C. This gave a junction depth of about 40 μ. Junction non-flatness in diffused diodes has been attributed by Pilkuhn and Rupprecht (1964) to, (1) inhomogeneous distribution of donors in the substrate, particularly striations, (11) diffusion down grain boundaries, and (111) clustering of defects. Gunnell and Gooch found junction planarity was not critically dependent on surface preparation and Marinace found that the uniformity of the Zn distribution on the surface during diffusion was not critical.

As mentioned in section 2.3.5. the steep diffusion profile leads to a small active region thickness d, which by equ. (2.12.) reduces the threshold current density j_t.

Defects associated with chemical diffusion in heavily doped GaAs are considered in section 2.6.

2.5. Detection of Defects in GaAs

A wide variety of techniques have been used to investigate defects in GaAs, and several of these are discussed with relevant results in this section. These are all direct methods of observation.

2.5.1. Chemical Etching

Many chemical etches and polishes have been reported for GaAs. A comprehensive list of these was given by Faust (1962). However, these reagents were all restricted in their uses. That is, each of them could be used only for a few particular crystallographic planes. This was due to the polarity effects in the sphalerite structure, already mentioned in sect. 2.4.1. Most of the early work was concerned with the structure of the two types of $\{1\ 1\ 1\}$ surface. Abrahams and Buiocchi (1965) developed an etchant of much more general application, which selectively attacked decorated dislocations on the low index planes of GaAs. These planes included the Ga$\{1\ 1\ 1\}$and As$\{1\ 1\ 1\}$as well as $\{100\}$ and $\{110\}$. When the dislocations were not decorated, the etchant revealed only As (or β) dislocations. The sensitivity of the etch was independent of dislocation orientation with respect to the surface, and even revealed dislocations parallel and close to the surface. It also revealed stacking faults on some crystallographic planes. Abrahams and Buiocchi performed several experiments which showed correlation between the etch patterns produced by their etch, and known dislocation distributions.

Abrahams and Buiocchi (1966) subsequently used their etchant

to reveal interfacial dislocations in the (0 0 1) junction plane of epitaxial laser diodes. The dislocations lay along $[1\ 1\ 0]$ and $[1\ \bar{1}\ 0]$ directions; only dislocations in one of these directions appeared to be decorated. These dislocation networks were found only in the junction region and were attributed to lattice mis-match between heavily doped p - and n - type materials (sect. 2.6.1.). A direct correlation was found between emission spots and the positions of decorated dislocations running perpendicular to the mirror faces.

2.5.2. Infra-Red Transmission

The homogeneity of bulk n - type GaAs can be examined by viewing transmitted light of photon energy less than the band gap energy. The experimental conditions for optical transmission work on GaAs are simpler than for Si and Ge. The band gap energy is larger and wavelengths as short as 9,100 Å are transmitted at room temperature. Ordinary glass lenses can be used and film is available commercially which is sensitive to this wavelength. An image converter tube must be used for visual examination. The optical inhomogeneities which are found correspond to variations in the distribution of impurities grown into the crystal. The absorption coefficient of GaAs is very dependent on impurity concentration at near - band gap energies (see Chapter 5 for further discussion), so that small variations of impurity concentration are detected in transmission.

Irregular distributions of transmitted intensity are often found, and regular bands due to striations may be seen if the specimen orientation is correct. (Ziegler and Henkel (1965))

Drougard (1966) has used the refractive index variations associated with impurity variations, to show up striations in bulk GaAs. He used the Schlieren technique to cut out the direct transmitted beam and imaged the light which had been deviated from the optic axis of the system by refractive index changes.

Dash (1956) decorated edge dislocations in silicon by immersion in copper nitrate solution and subsequent annealing. The copper diffused rapidly into the bulk material and precipitated along edge dislocations. When viewed by infra-red transmission, networks of dislocations were clearly visible. Black and Jungbluth (1967 b) found precipitates and decorated dislocations in GaAs which was Zn doped in the melt and subsequently more heavily Zn diffused, by using infra-red transmission. They correlated their transmission patterns with etch patterns and found convincing evidence for precipitation of Zn on dislocations.

2.5.3. Transmission Electron Microscopy

Transmission electron microscopy has been shown to be a powerful technique in studying Si, but GaAs has received less attention than Si, using this method. Specimen preparation of GaAs for transmission electron microscopy has always been difficult. The X-ray, and hence the electron scattering factors of Ga and As atoms are greater than for Si. It turns out that, for good quality electron micrography, specimens must be about half as thick as in the case of Si. Meieran (1965) produced specimens from bulk GaAs by a combination of chemical and electro-polishing using fine jets of liquid on $\{1\ 1\ 1\}$ and $\{1\ 0\ 0\}$ surfaces. The thin area was detected by visual observation of transmitted light.

Electro-polishing is undesirable when specimens may be of variable resistivity e.g. near p - n junctions. Biedermann and Brack (1966) reported a reagent which gave a good polish on {1 1 1} faces for chemical jet thinning. They employed an apparatus of the type used by Booker and Stickler (1962) for Si. This apparatus used a jet of chemical polish on the underside of a ready mounted specimen. When light from the combined jet and light pipe was detected by an observer viewing from above the polishing was stopped. In the work reported here using the equipment described by Holt, Porter and Unvala (1966) the results were found to be unreliable, mainly due to observer fatigue over the periods of half to one hour taken to thin the specimens. The equipment of Holt, Porter and Unvala was further developed and made automatic as is described in sect. 3.4.2.

Meieran (1965) first reported systematic work on GaAs by transmission electron microscopy. He used Te doped Czochralski pulled crystals and studied the growth striations. He found precipitates of what he assumed were Te only at electron carrier concentrations greater than 2 X $10^{18}/cm^3$. He also found some precipitates looking like stacking faults which he suggested were due to an oxide of Ga or As. By studying slip traces on one specimen, Meieran estimated the foil thickness to be about 4000 Å

Abrahams Buiocchi and Tietjen (1967) used transmission electron microscopy to study Se doped GaAs, and Abrahams and Buiocchi (1967) studied twins and stacking faults in vapour grown material. In

Se doped GaAs there is a marked discrepancy between the Se concentration and the carrier concentration. (Vieland and Kudman (1963) and sect. 2.6.2.). In their Se doped specimens which all had carrier concentrations $\geq 2 \times 10^{18}/cm^3$, Abrahams, Buiocchi and Tietjen found evidence of precipitation. The Moiré fringe spacings observed in electron transmission led them to suggest the presence of Ga_2Se_3 particles, and they showed that these could account for the above discrepancy.

All the materials studied in the works mentioned above had dislocation densities in the bulk, of less than $10^3/cm^2$. This meant that on the electron microscope scale there were insufficient dislocations to enable them to be examined in detail.

2.5.4. Electron Probe Techniques

The term "electron probe" is used here to describe the instrument in which a high energy beam of electrons is scanned over the specimen surface. The interaction of the electrons with the specimen may produce several observable phenomena. A detected signal is used to modulate the beam of a cathode ray display tube which is being scanned in synchronism with the specimen. Thus an image of the specimen is built up with bright regions corresponding to areas of the specimen giving large signals.

The electron probe was originally designed to determine the spatial origin of fluorescent X-rays generated by the electron beam, thus giving the distribution of constituents in a specimen. To analyse the fluorescent X-rays, a crystal spectrometer is included

in the vacuum system and can be set so that any particular wavelength may be singled out to act as the modulating signal. The limit of detection of impurities is about 10^{19} atoms/cm^3, which means this method is applicable only to extremely highly doped semiconductors. The electron probe is however useful for studying local areas of non - stoichiometry. The resolution for detection of small particles and precipitates is about 1μ.

Other signals which can be picked up and used to form an image, include (1) back scattered electrons, (11) secondary electrons, (111) the current passing through the specimen, and (IV) the cathodoluminescent output. Casey and Kaiser (1967) used the spectral distribution of this scanning electron beam excited recombination radiation (SEBERR) to develope a technique for studying carrier concentration variations in n - type GaAs. They found that the spectral shape, and the position of the peak of the emission spectrum, could be used to determine the free electron concentration to within $\pm$ 15% at concentrations in the region of 5 X 10^{17} electrons/cm^3, and $\pm$ 7% at 5 X 10^{18}/cm^3.

If the electron beam is scanned across the junction region of a semiconductor diode, electron - hole pairs are produced which are separated by the junction field. If the p and n sides of the diode are electrically connected by an external circuit a current will flow. This current, when amplified may be used to modulate the intensity of the display on the cathode ray tube and produce an image of the junction region. The numbers of electron - hole pairs created and subsequently collected, depends in a complicated

way on the local crystal perfection, and imperfections like dislocations show up as regions of varying intensity. Holt and Chase (1968) called this mode of operation the SEBECC technique standing for scanning electron beam excited charge collection, and using this method they found decorated dislocations in the junction region of GaAs diodes. Variations in electrical conductivity of bulk semiconductor specimens can also be used to form an image by collecting the current leaking to earth through the specimen, as the primary electron beam scans the specimen surface. Shaw et al (1966) used a form of this in which the specimen was biased, and found spikes due to locally enhanced Zn diffusion down grain boundaries in diffused GaAs diodes.

The magnification range of the electron probe is intermediate between those of optical microscopy and electron microscopy.

2.5.5. X-ray Topography

In transmission of X-rays through single crystals, the intensity reflected from a particular set of crystal planes, may be used to form an image of the material through which the beam has passed. The image can be recorded on a photographic emulsion. A technique of scanning the specimen and photographic plate simultaneously across the X-ray beam to obtain large area images was first developed by Lang (1959) and adapted by Schwuttke (1965). Schwuttke and Rupprecht (1966) used this technique on GaAs with specimens 0.1 mm thick, which is near the maximum specimen thickness suitable for this technique.

Using the Borrmann effect of anomalous X-ray transmission

Jungbluth (1965) studied GaAs slices about 1mm thick. In this method a large diameter monochromatic X-ray beam impinges on the specimen so that the Bragg condition is satisfied for one set of reflecting planes. Both the directly transmitted and diffracted beams are recorded on a photographic plate, each producing an identical image at unit magnification. From the contrast in these images the orientation of many crystal defects can be determined. Using these X-ray techniques, crystal imperfections such as precipitates, dislocations and stacking faults can be resolved. Black and Jungbluth (1967 a & b) used anomalous X-ray transmission to study the diffusion of high concentrations of Zn into GaAs.

The magnification of these X-ray techniques is limited by the grain size of the film emulsion, and by the separation of the K_α lines of the X-ray source. The advantages are, that all the defects in a slice are seen simultaneously (provided the density of defects is not too great), some information on the crystallographic structure of defects can be obtained, and the method is non-destructive.

2.6. Defects in GaAs Laser Material

In the remainder of this Chapter, the results obtained by the techniques just described, on material of the type used for laser diodes, are reviewed and some possible effects on laser action discussed. Further detailed discussion is given in Chapter 5 where the results reported in Chapter 4 are considered.

2.6.1. Misfit Dislocations

When a crystal lattice is heavily doped by an impurity, whether substitutional or interstitial, the lattice is strained

and the average lattice parameter is altered. In diffused GaAs laser diodes both the p and n regions are heavily doped, and hence across the p - n junction there is a sudden change in the mean lattice parameter. Part of this lattice mismatch may be accommodated by strain in the lattice, but in heavily doped junctions much of it is relieved by plastic deformation, resulting in misfit dislocations. In diffused diodes the greatest density of these dislocations should be present in the region of the greatest concentration gradient in the diffusion front.

Holt (1966) has studied the geometry of misfit dislocations in the $\{1\,0\,0\}$, $\{1\,1\,0\}$ and $\{1\,1\,1\}$ planes of the sphalerite structure, by considering models of the interface. This technique assumes an absolutely abrupt transition from material of lattice parameter λ_1 to that of λ_2 which is a closer approximation to an epitaxial junction than a diffused junction. However, in GaAs the diffusion profile is very steep and the region of maximum lattice strain very narrow. The geometry of the dislocations which relieve the lattice strain most easily, must still be the same as in an epitaxial junction. The misfit dislocation networks consist of edge dislocations having their extra half planes of atoms in the material of smaller lattice parameter, with the planes terminating at the interface. For a $\{1\,0\,0\}$ interface between materials of lattice parameters λ_1 and λ_2 the spacing between misfit dislocations was given by Holt as

$$p = \frac{\lambda_1 \lambda_2}{\sqrt{2}\,(\lambda_1 - \lambda_2)} \qquad (2.17)$$

In this orientation the dislocation network is a square grid, with dislocation lines parallel to the two $\langle 1\,1\,0\rangle$ directions. Abrahams and Buiocchi (1966) revealed arrays of dislocations on the (0 0 1) plane of epitaxial laser diodes. These dislocations had the predicted $[1\,1\,0]$ and $[1\,\bar{1}\,0]$ directions. They found order of magnitude agreement between the dislocation spacing determined experimentally and the spacing calculated using the values of λ_1 and λ_2 given by Black and Lublin (1964). Abrahams and Buiocchi found that the dislocations parallel to $[1\,1\,0]$ frequently etched in a different manner to those parallel to $[1\,\bar{1}\,0]$ They attributed this to preferential Zn decoration of the $[1\,1\,0]$ dislocations and proposed an explanation based on the type of dangling bonds present in the dislocation cores. This is discussed further in Chapter 5. They also found that bright emission spots corresponded to etch pits subsequently revealed at the junction on the (1 1 0) diode face. Abrahams and Pankove (1966) later showed that more uniform laser emission was obtained when the emitting faces were perpendicular to the decorated dislocations.

Schwuttke and Rupprecht (1966) found diffusion - induced dislocations having axes along $\langle 1\,1\,0\rangle$ directions in $\{1\,0\,0\}$ planes of diffused GaAs, using scanning X-ray topography on specimens of 0·1 mm thickness. However Black and Jungbluth (1967 a,b) using large area beam, anomalous transmission on specimens of 1·0 mm thickness did not find dislocation networks but a great deal of other damage including probable precipitation of Zn.

In Si there appears to be a difference between the diffusion - induced dislocation densities found by X-ray topography and by transmission electron microscopy. Washburn, Thomas and Queisser (1964) found dislocation densities of about 10^8 lines/cm^2 while by X-ray topography Schwuttke and Queisser (1962) found 10^6lines/cm^2 or below. X-ray topography cannot resolve densities as high as 10^8 lines/cm^2 and at densities as low as 10^6/cm^2 in transmission electron microscopy the field of view is so small that few, if any, dislocations would be seen. The X-ray topographs of Schwuttke and Rupprecht in GaAs revealed similar low density networks but the authors pointed out that this did not exclude the possibility of higher density networks being present.

Misfit dislocations and crystal damage due to impurity concentration gradients in GaAs have been detected by etching and by X-ray techniques. There are no reports yet of transmission electron microscopy studies of diffusion - induced defects in GaAs. Preliminary work on this is reported in Chapters 4 and 5.

2.6.2. Precipitation in GaAs

GaAs laser diodes are almost always prepared from n - type material having $\gtrsim 10^{18}$ donors/cm^3. The acceptor which may be either diffused in, or epitaxially deposited, is therefore present in larger concentrations, usually $\sim 10^{20}$ atoms/cm^3. The usual acceptor is Zn, although Cd has been used. The behaviour of Zn, Te and Se present in large concentrations in GaAs are considered in this section.

Precipitation during Zn diffusion into GaAs has been studied extensively by Black and Jungbluth (1967 a,b). They diffused Zn through Ga $\{1\ 1\ 1\}$ surfaces using a standard diffusion time of 2 hours, at temperatures from 700°C to 1100°C. The three methods of examination used were, anomalous X-ray transmission, infra-red transmission and chemical etching. They found that for diffusion temperatures above 750°C the layers were opaque to X-rays, and in conjunction with the etching and infra-red transmission results, they concluded that submicroscopic precipitates were present. They found precipitation was unavoidable when using pure Zn as the source, but could be avoided when diffusing for short times with $ZnAs_2$. Panish and Casey (1967) studied the solubility of Zn in GaAs at 1000°C and obtained agreement between their calculated solid solubility isotherm and experimental results. Previous calculations had had to assume an unionised form of Zn, which did not agree with the experimental fact that the total Zn concentration equalled the carrier concentration up to 7×10^{19} Zn atoms/cm^3. By considering the formation of an impurity band in the electronic band structure and the position of the Fermi level, Panish and Casey were able to predict the solid solubility isotherm without assuming an unionised form of Zn. However, this agreement between Zn concentration and hole concentration is only accurate to within $\pm$ 30% (Black and Jungbluth (1967 a)), which means that sufficient Zn atoms/cm^3 may be in an unionised state as precipitates.

Black and Jungbluth were not able to determine the nature of their precipitates, but suggested they were probably Zn rich.

Black (1967) subsequently used the electron probe to study the precipitates, and distinguished microscopic and submicroscopic ones. He identified the large visible precipitates as Zn rich by fluorescent X-ray microanalysis in the probe. An area surrounding each of these large precipitates was found to be denuded of submicroscopic precipitates and from this Black concluded that these were also Zn rich. Black and Jungbluth showed that the precipitation only occurred as a result of the Zn diffusion by examining substrates that had been heated under diffusion conditions without any Zn present. They found no crystal damage.

The behaviour of Se in GaAs has been studied by Vieland and Kudman (1963) and Schottky (1966). They both found that above 4×10^{17} atoms/cm^3 the free electron concentration was considerably less than the Se concentration and that the electron carrier concentration increased as the cube root of the Se concentration. To explain these results Vieland and Kudman suggested a complex, consisting of a Ga vacancy surrounded by three Se atoms, and Schottky considered a chemical structure of $Ga_2V_{Ga}Se_3$. Abrahams, Buiocchi and Tietjen (1967) found some evidence by transmission electron microscopy for precipitation of Ga_2Se_3 in GaAs doped to 2×10^{18} Se atoms/cm^3 and higher. Since the structure of Ga_2Se_3 is sphalerite with every third Ga site vacant, the structures of Vieland and Kudman and of Schottky may be very small precipitates of Ga_2Se_3.

Meieran (1965) used transmission electron microscopy to study

precipitates in striated bulk Te doped GaAs grown by the Czochralski technique. He found precipitates of what he assumed was Te in the striations, but not in regions between them. Meieran concluded that Te precipitated out when the solubility limit of about 5 X 10^{18} Te atoms/cm^3 was exceeded. Casey (1967) used the SEBERR technique on the electron probe to study the distribution of Te in bulk doped GaAs. Using the method developed by Casey and Kaiser (1967) he found no detectable variation of free electron concentration across striations, whereas the Te concentration was known to vary with striations. Casey concluded that precipitation, in the striations, of a Te - rich phase with a crystal structure different from GaAs was probably the best explanation of his results. Similarly he suggested precipitation at dislocations to explain the cathodoluminescence results at dislocations.

The behaviour of large amounts of donor and acceptor impurities in GaAs has not been studied extensively. There are only two reports of the use of the most direct method of investigation — transmission electron microscopy — to study donor precipitation and none of its use to study diffusion processes. The behaviour of Se and Te are very different in GaAs. Se has an unionised form at electron concentrations as low as 4 X $10^{17}/cm^3$ and Te probably precipitates at about 5 X 10^{18} electrons/cm^3. Zn has a higher solid solubility than either of these.

2.6.3. Striations

Striations have been found in most heavily doped semiconductors grown in bulk. Their effect on the luminescent

properties of III - V semiconductors has been studied only to a limited extent in GaAs and GaP.

Wittry (1966) used X-ray microanalysis and the SEBERR technique simultaneously on a GaAs specimen having mean carrier concentration of $5{\cdot}2 \times 10^{18}/cm^3$. In order to separate the Te fluorescent X-ray signal from noise in the detector he had to average the signal over periods of several hours. He was able to find a correlation between the cathodoluminescent efficiency and Te concentration, as the beam scanned across several striations. The efficiency η_c decreased with increase in Te concentration, and the Te concentration appeared to be about 50 p.p.m. greater than the free electron concentration. Wittry was unable to detect the expected emission spectrum shape changes (Casey and Kaiser (1967)) between the spectra of the bright and dark bands. This indicated that the free electron concentration, n_o was not varying by more than 10% across the striations. However the X-ray results showed a Te concentration variation of about 30%. These facts show that some Te must be present in an unionised form. Since Hall measurements showed that at these concentrations conductivity was independent of temperature (Nasledov (1961)), all Te atoms on As lattice sites must be fully ionised, and the unionised Te is probably present as precipitates. At Te concentrations $\gtrsim 5 \times 10^{18}/cm^3$ precipitation was found by Meieran (1965). Because of this a reduction of quantum efficiency η_c is not unreasonable. Casey (1967) also saw variations of η_c using the SEBERR technique. He suggested this reduction of η_c above

5 X 10^{18} Te atoms/cm^3 may be partly explained by a shift of the absorption edge to shorter wavelengths when the Fermi level moves into the conduction band (a Burstein shift).

The effect of striations on laser emission spectra has been studied by Raab, Bachert and Kaiper (1966). They showed that the emitted photon energy altered by up to 15 meV for donor concentration variations of 3 X 10^{17} to 5 X $10^{18}/cm^3$, and in a single laser by up to 10 meV from one emission spot to another.

Ziegler and Henkel (1965) assumed absorption was due to charge carriers only. This led them to obtain values of carrier concentration n_o of 2·3 X $10^{18}/cm^3$ for bands of good transparency and 3·7 X $10^{18}/cm^3$ for bands of poorer transparency. They did not state the wavelength used but these results appear to disagree with the results of Turner and Reese (1964) who found that absorption coefficient, α, decreased as n_o increased for photon energies near the absorption edge. Ziegler and Henkel also studied the influence of striations on the threshold current density for laser action, j_t. Diodes were made with the plane of the striations (a) parallel to the junction plane, (b) parallel to the filament direction and perpendicular to the junction and (c) parallel to the mirror faces. In case (c) the laser filament passed alternately through layers of different doping level and the average j_t was two to three times higher than that of the first spot in cases (a) and (b). In case (b) the first active filament could occur in the most favourably doped striation, while in case (a) j_t depended on which layer contained the junction. These experiments showed that laser threshold

current does depend on doping but the mechanism by which this occurs was not considered. Ziegler and Henkel did not find any clear correlation between striations and positions of the first active filaments. Salow and Benz (1965) found striations in boat grown material and showed these were at least partly the cause of inhomogeneous emission. They pointed out that such inhomogeneities in the electrical and optical properties of GaAs starting material, inevitably limit the size of diode from which homogeneous emission can be expected.

CHAPTER 3

EXPERIMENTAL WORK

This chapter describes the equipment and techniques used in this investigation of the laser diodes during operation, and the subsequent examination of crystal defects.

3.1. Experimental Procedure Applied to Each Diode

Before describing the apparatus and experimental procedures in detail, the sequence of techniques applied to each specimen is given.

The diodes, received from S.E.R.L. with terminals attached, were X-rayed using the back-reflected Laué method to determine their orientation, and mounted on the cold finger of the cryostat (sect. 3.2.2.). Each laser diode was operated in the cryostat at liquid nitrogen temperature ($77^{\circ}K$) and the emission pattern on each mirror face (near field pattern) photographed in detail at currents above and below laser threshold (sect. 3.2.7.). Each diode was also photographed by reflected light and by infra-red light transmitted through the GaAs. After the photography, the terminals were removed from the GaAs crystals and they were prepared for chemical etching (sect.3.3.). The final technique was transmission electron microscopy. (sect.3.4.). A chemical jet thinning technique was developed for this.

3.2. Laser Operation

3.2.1. General Description of Laser Equipment

Fig 3.1.(a) shows a schematic drawing of the apparatus used

for optical examination of the lasers, and fig. 3.1.(b) is a photograph of the actual equipment. These figures show the relative positions on the optical bench of the cryostat (V), microscope (M), silicon solar cell (S) and image converter (I, fig. 3.1.(a))or camera (A, fig.3.1.(b)). The pulsed power supply to the laser is also outlined. The cryostat had two windows so that opposite faces of the diodes could be examined simultaneously. M. was a simple metallographic microscope mounted horizontally and had a Burch reflecting objective (B). This gave a working distance of 2·4 cm. from its front surface, but had a Numerical Aperture of only 0·28. The image converter was contained in a housing which fitted over the eyepiece of the microscope. For photography the image converter was replaced by the camera (A). The solar cell was used to check the output intensity of the laser during operation, but for infra-red transmission photography it was replaced by a microscope illuminator at a distance of 30 cm.

3.2.2. Diode Construction and Mounting

The diodes were produced at S.E.R.L., Baldock. However, their construction is described here as it is relevant to the interpretation of results. The bulk material was grown by the horizontal Bridgman technique and was doped with either Te,Se or Si to free carrier concentrations of $2(\pm 1) \times 10^{18}/cm^3$. The ingots were polycrystalline, having crystallites of several cm^3 volume, so that although each diode was single crystal the

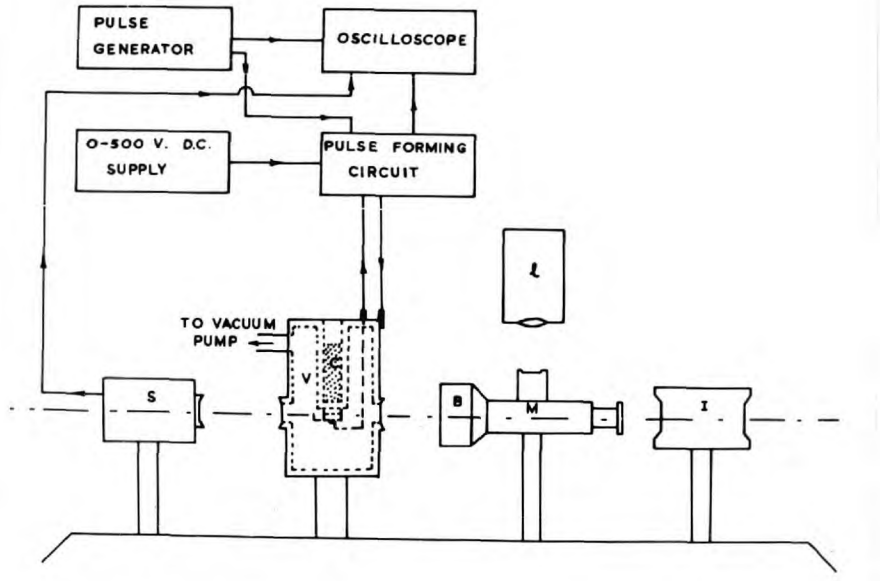

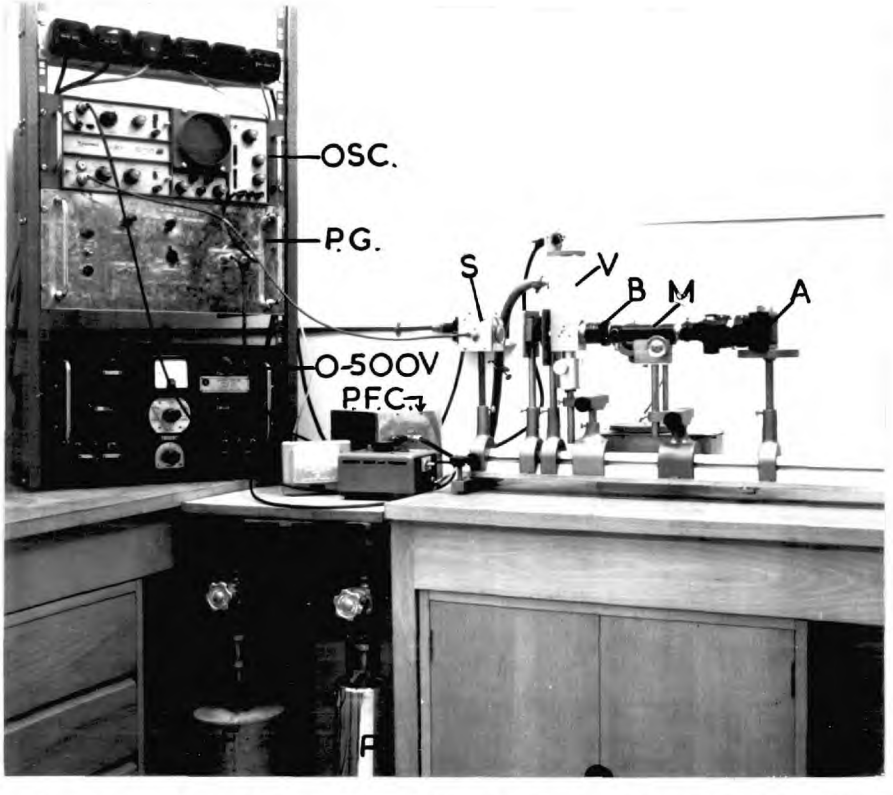

Fig.3.1. Equipment used for investigation of the optical properties of laser diodes. The vacuum cryostat (V), microscope (M), reflecting objective (B), solar cell (S), illuminator (ℓ), image converter(I)and camera (A) are shown. P.F.C. is the pulse forming circuit and P.G. the pulse generator. P is a sorption pump and F the pump bake-out furnace.

orientations of the diodes were not the same. Slices of GaAs were cut from the ingots and mechanically polished on a pitch plate with 2000 grit alumina powder. The slices were then put in a quartz diffusion tube with a carefully controlled amount of Zn and in some cases $ZnAs_2$. The diffusion conditions were either, 15 minutes at 1100°C with no As, or 4 hours at 850°C with As. This treatment produced p - n junctions on both sides of the slice at a depth of 70 - 80 μ. One of the junctions was polished off and a gold film evaporated on to the other diffused surface. The slice was then cut into strips of 2 mm width. The two long faces of the strips, which were perpendicular to the junction were highly polished and accurately parallel to each other and thus formed the Fabry - Perot cavity. The strips were then cut up into rectangular parallelipipeds to give diodes having junction position and dimensions as shown in fig.3.2.(a). The sides were left rough to prevent unwanted modes of laser action occurring. The orientations shown for the diode surfaces applied to only some of the diodes examined. In most cases the junction plane was (100). The junction area of 2 X 1 mm is large by semiconductor laser standards, but was used here to simplify handling, especially for transmission electron microscopy. A molybdenum block coated in a gold-zinc alloy was thermally bonded to the p - side of each diode and a similar Mo block coated in a gold-tin alloy bonded to the n - side. These Mo blocks acted as heat sinks and electrical contacts. Mo was used because it has a similar coefficient of thermal expansion

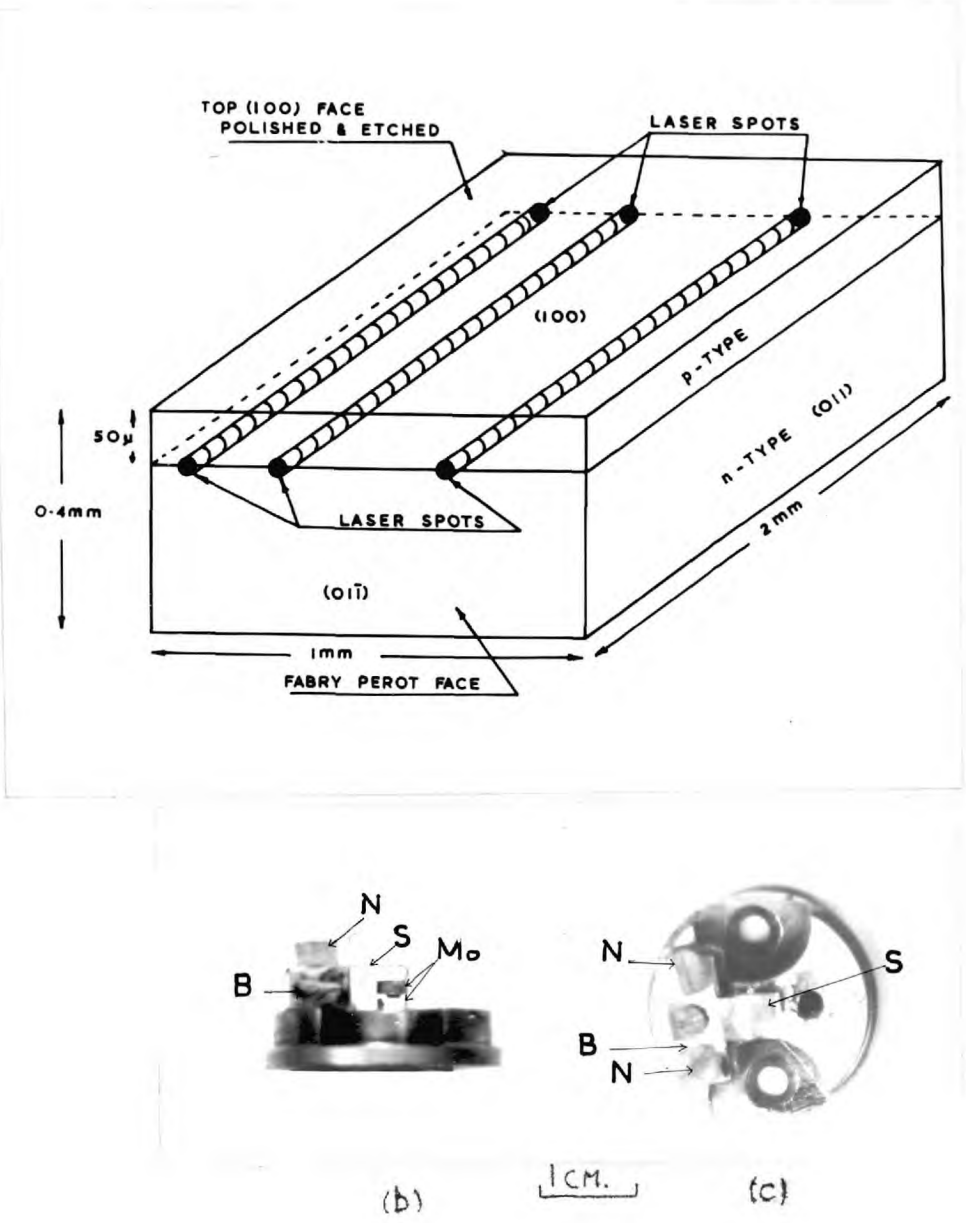

Fig. 3.2. (a) Drawing showing the dimensions of the GaAs diodes used in this work. (b) side view and (c) top view of a diode mounted on the copper disc for the cryostat. The GaAs is between the terminals marked (Mo), (S) is a copper spring contact, (B) a brass block insulated from the disc and (N) are nylon screws. Electrical contact is made to the brass block after the copper disc is attached to the cold finger.

to GaAs.

The completed diodes were received from S.E.R.L., then mounted as shown in fig 3.2.(b) for operation in the cryostat. The p side terminal was attached to the centre of the copper disc using indium, and electrical contact to the n - side was made by the copper spring, through the insulated brass terminal block. The copper disc had screw holes in it for attaching to the cold finger in the cryostat.

3.2.3. The Cryostat

Throughout this work, all the diodes were operated at the same temperature. A cryostat consisting of a liquid nitrogen cooled finger in a vacuum chamber, which was designed at S.E.R.L., was built for this purpose. It is shown schematically in fig. 3.3. The body was made from duralumin and was of square external cross-section. It had windows of 1" diameter optically polished glass discs in two opposite sides, and an outlet to the vacuum pump. The cold finger was a stainless steel cylinder having ·01" thick walls. The thin stainless steel was to reduce thermal conduction from the liquid nitrogen. A circular copper plug was brazed into the bottom of the thin walled cylinder and the diode on its copper disc was attached to the plug by screws. Thus the diode was in good thermal contact with the nitrogen. The temperature of the diodes was not determined, but Broom et al (1963) used a similar cryostat and found the diode temperature was about 100°K. The top of the stainless steel tube was brazed into a square brass plate which made an o - ring vacuum seal to the body of the cryostat.

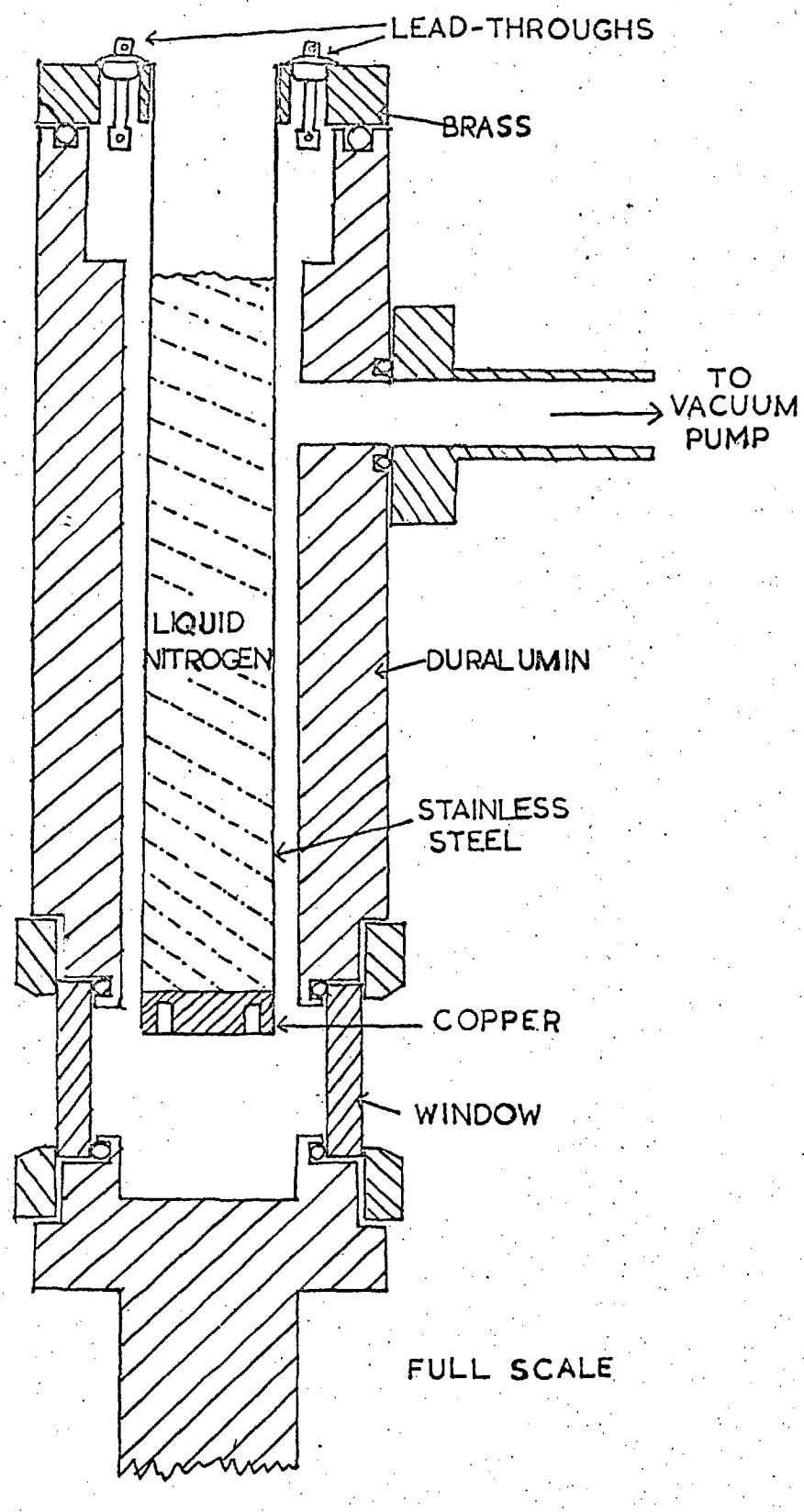

FIG. 3.3 THE VACUUM CRYOSTAT.

The brass plate contained glass-to-metal sealed lead-throughs for the power supplies.

To prevent condensation on the diode, the cryostat was kept at a pressure of ·01 torr. This was initially achieved by an oil rotary pump and liquid nitrogen trap, but oil vapour tended to condense on the specimens. The rotary pump was replaced by two small Mullard sorption pumps. By always having one of the pumps cooled by nitrogen while the other was being baked out, the system was kept at a pressure of ·01 torr for as long as necessary. The pressure was kept constant for all diodes so that the temperature was assumed to be constant in all cases.

3.2.4. Power Supply for the Laser Diodes

In order to reduce the Joule heating in the diodes, the lasers were operated under pulsed conditions. Since the diodes were of large junction area (2 X 1 mm) and the current density at laser threshold is of the order of 3000 amps/cm^2, current pulses of up to 250 amps were required. Equipment was built to designs supplied by S.E.R.L. to supply square current pulses of up to 250 amps of 5 μsec duration at repetition rates of 10 - 1000 pulses/sec.

As shown in fig 3.1.(a) a pulse generator was used to trigger the pulse forming line, with the power being supplied by a 0 - 500 v, D.C. supply. The pulse generator also triggered the oscilloscope which monitored the pulse to the laser. A Telequipment D43R double beam oscilloscope was used to detect the voltage across a 0·1 ohm resistor in series with the diode.

The circuit diagrams of the pulse generator and pulse forming line are given in figs. A1 and A2 respectively of the Appendix where some detail of the construction is also given.

The 0·1 ohm resistor for monitoring the laser current was included in the pulse forming circuit immediately before the output. To preserve the pulse shape the current pulses were led to the cryostat using the two outer sheaths of a short length of double co-axial cable. At pulse currents below about 100 amps the pulse shape was typically as shown in fig 3.4.(a) but at very high currents ($\sim$ 200 amps) it deteriorated to a shape similar to that of fig 3.4.(b). This may be explicable by changes in the diode characteristics due to heating effects at high current densities.

3.2.5. The Photocell

For routine monitoring of the light output of the diodes, a Ferranti MS 11 BE silicon photovoltaic cell was used. The light pulses from the laser produced a current pulse from the Si p - n junction which was short circuited by a calibrated 1 ohm resistor. The voltage pulses developed across this resistor were displayed on the second beam of the oscilloscope. The cell was positioned on the optical bench at a standard distance of 14 cm. from the cryostat window, with a neutral density filter number N D 1 placed between the cell and the window. This was necessary to reduce the light intensity incident on the cell to a level such that the output voltage did not exceed 0·1 volt. The photo- voltage developed by the cell was only guaranteed to be proportional to

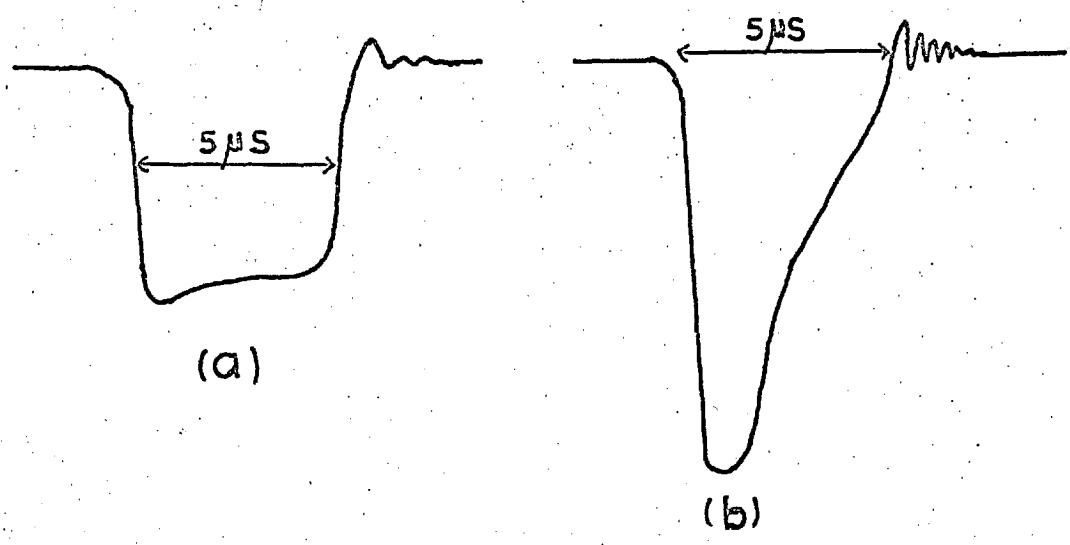

FIG. 3.4 SHAPES OF CURRENT PULSES THROUGH LASER DIODES AT (a) ≤100 AMPS (b) ~200 AMPS.

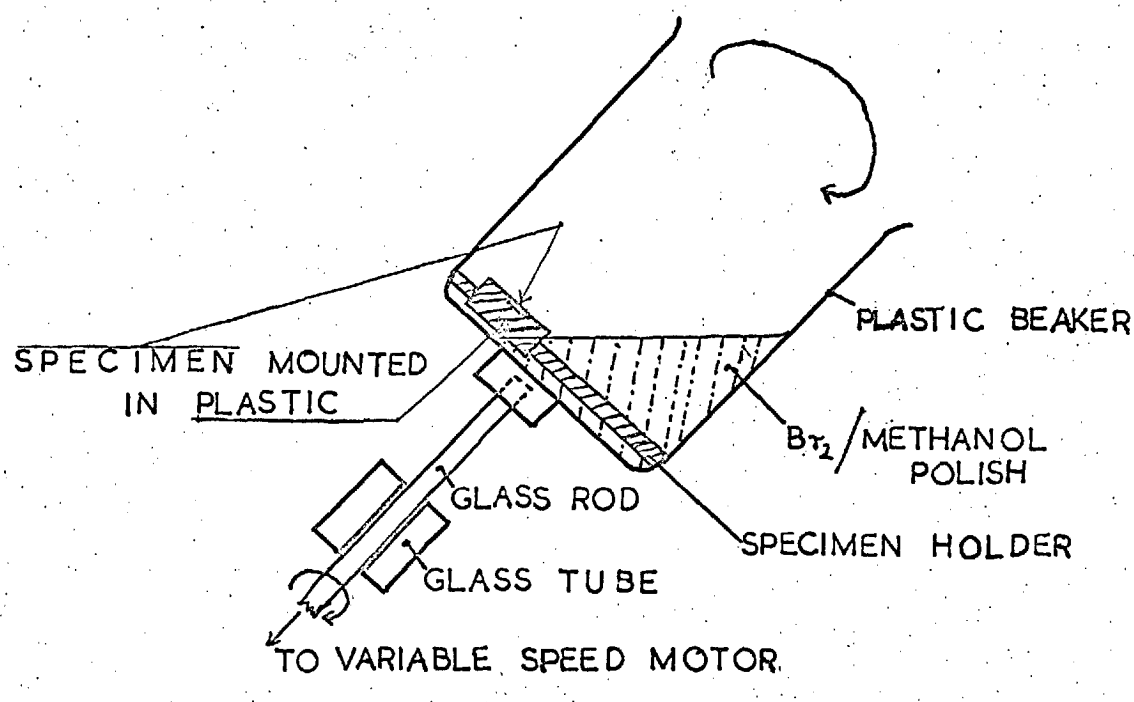

FIG. 3.5 DIAGRAM OF ROTATING BEAKER POLISHING APPARATUS.

light intensity below this value.

A characteristic curve of photovoltage versus diode current was plotted for both faces of every laser, before examination began, and the output was checked frequently during operation.

3.2.6. The Infra-Red Image Converter

Throughout the investigation of the optical properties of the laser diodes, an image converter tube was used to align the optical equipment and to observe the emission and transmission patterns. The tube used was a Mullard type 6929 with a caesium on oxidised silver photocathode. This gave a good spectral response for wavelengths between 6000 Å and 12,000 Å with a peak response at 8,000 Å. The emission wavelength of GaAs at 77°K is 8400 Å. A potential of between 9 and 12 kv was necessary to accelerate the electrons emitted by the photocathode on to a phosphor screen 4 cm away. In this way a visible image of the infra-red pattern incident on the photocathode was obtained. The maximum current drawn by the tube was quoted as 0·2 μA, so a small battery - operated H.T. supply was built to an S.E.R.L. design to provide 10 Kv at this low power. The circuit is shown in fig A3 of the Appendix and is briefly described there.

The image converter was contained in a cylindrical brass housing, one end of which slid over the eyepiece of the microscope, and had a viewing port at the other end. This arrangement could be used easily on any microscope under normal room lighting. When not in use a light - tight cap was used to protect the

photocathode from ambient light.

3.2.7. Photography of Lasers During Operation

In fig. 3.1. the microscope (M) had a light input stage for reflection from the diode surface. The diode was aligned by rotating the cold finger until the reflected light intensity was a maximum and the whole front face of the diode was in focus. For transmission through the GaAs diode the solar cell was removed and a microscope illumination lamp having a tungsten filament bulb, was placed about 30 cm. from the cryostat window opposite the microscope. This gave parallel incident light on the back surface of the diode. To prevent stray reflections from the diode mounting entering the microscope, an iris was placed close to the window through which the light entered, and an adjustable opaque screen was placed between the exit window and the microscope objective. The positioning of this screen was critical in cutting out reflections from the gold plated terminals of the diodes, while still allowing direct transmission.

Three different cameras were tried for microphotographing the diodes in the cryostat. A quarter plate bellows camera with no lenses was used for many micrographs, but the time involved in taking a series of exposures was excessive. Since the numerical aperture of the reflecting objective was 0·28 the resolving power of the microscope was only 2 μ and the large magnifications obtainable using the plate camera were unnecessary.

It was found that sufficient definition was obtained using a 35 mm microscope camera (A in fig 3.1.(b)) mounted horizontally, and this was used for the majority of micrographs presented here. The film used was Kodak 1R - 135 which was commercially available in convenient strips of 20 exposures. All photography was carried out in subdued background lighting. The third camera used was a Watson Photomicro Camera with Polaroid Land Back designed for use on most upright microscopes. It was mounted horizontally on rigid supports on the optical bench. However difficulty was experienced in aligning it and good definition micrographs were not obtained. The cost of Polaroid type 413 film for the large numbers of micrographs required for each diode would have been excessive. Type 413 film has a sensitivity to wavelengths as long as 9,200 Å whereas other commercially available infra-red films are sensitive only to wavelengths shorter than 8,800 Å. The absorption edge, and emission wavelength of GaAs at 77°K are about 8,400 Å, but increase to about 9,200 Å at room temperature. Because of this the transmission photography was carried out at liquid nitrogen temperature.

Before mounting for the cryostat, the orientation of each diode was determined using the back reflection Laué X-ray technique. Provided the diodes were mounted accurately in the X-ray beam and a small collimator was used, the spot pattern due to the GaAs crystal could be separated from the ring patterns due to the diode terminals. Each diode was then mounted and inserted in the cryostat. If the sorption pumps had been precooled with liquid

nitrogen for at least half an hour, the cryostat reached a pressure of ·01 torr in about one minute. After aligning the diode by reflection, the light output versus diode current characteristics were taken for emission from both faces. During these measurements the image converter was used to view the distribution of stimulated emission along the line of intersection of the junction plane and mirror face. This near field emission pattern consisted of a nearly uniform line of spontaneous emission across the whole diode face, with bright regions showing the presence of laser action. The near field emission patterns at values of diode current just below and many values above threshold were photographed. Each of the diode faces was photographed by reflected and transmitted light and composite pictures in emission and transmission, and emission and reflection also taken. In many diodes it was found that detail seen in transmission was improved by adjusting the illuminator so that the incident illumination was a few degrees off the normal to the diode face.

3.3. Etching and Polishing Techniques

Chemical etching was used to study the crystalline imperfections in the region of the p - n junction. After removal of the diode terminals, the laser crystal was alternately chemically polished and etched through the p - type material in planes parallel to the junction, until the junction region was reached. In this way the bulk crystal structure was studied. In this section the procedure applied to each diode is described.

Removing the diode terminals without damaging the GaAs presented some difficulty. The method used was to mount the whole diode in metallurgical mounting plastic with one terminal exposed. After mechanical polishing on SiC paper until about half of the terminal was removed, the whole specimen was immersed in hot aqua regia to dissolve the remaining Mo. After about 10 minutes the remains of the Mo was removed by tweezers and the gold alloy coating peeled off the GaAs without causing any damage. The diode was dissolved out of the plastic by immersion in acetone and the process repeated for the other terminal.

When both terminals were removed the GaAs was remounted in plastic with the p - type surface exposed. The plastic mount was cylindrical of $\frac{1}{2}$ inch diameter and $\frac{1}{4}$ inch thickness as shown in fig 3.5. After a light polish on 600 grit SiC paper followed by 7 μ then 1 μ diamond polishes, the specimen was ready for chemical sectioning. For removing layers of material of known thickness by chemical polishing the rotating beaker technique was used. Fig. 3.5. is a drawing of the apparatus. The beaker was at an angle of 45° to the vertical and rotated at about 50 r.p.m. The specimen was secured to the base of the beaker and chemical polish added until the base of the beaker was half covered. The polish was a dilute solution of bromine in methanol, first reported by Fuller and Allison (1962). In order to determine the rate of polishing of this method Levene (1966) carried out some systematic work. {100} specimens of GaAs were set in mounting

plastic and half the exposed surface masked off with lacquer. The specimens were polished in the rotating beaker with various concentrations of bromine in methanol. After washing in deionised water the lacquer was removed to reveal a step in the surface. The height of this step was measured on a Talysurf instrument, to give the rate of removal of the specimen surface. Fig. 3.6. shows the variation of attack rate with bromine concentration obtained by Levene. The more dilute the solution, the better was the polished surface.

The chemical etch used throughout this work was that of Abrahams and Buiocchi (1965). This consisted of

2cc water H_2O

8mg silver nitrate $AgNO_3$

1gm chromium trioxide CrO_3

1cc hydrofluoric acid HF

The components were added in the order given to ensure that the $AgNO_3$ all dissolved. Etching was carried out at room temperature in a P.T.F.E. beaker continuously agitated by hand. Etching times were varied from 10 secs. to 4 mins. using about 5cc of etchant. All specimen washing was done in deionised water. From the results of Levene and of Abrahams and Buiocchi, the depth of material removed by polishing and etching was known to within 10 μ. Etching and polishing was stopped either just before the junction, at the junction, or just after it, depending on which region was required for transmission electron microscopy. This was made easier by

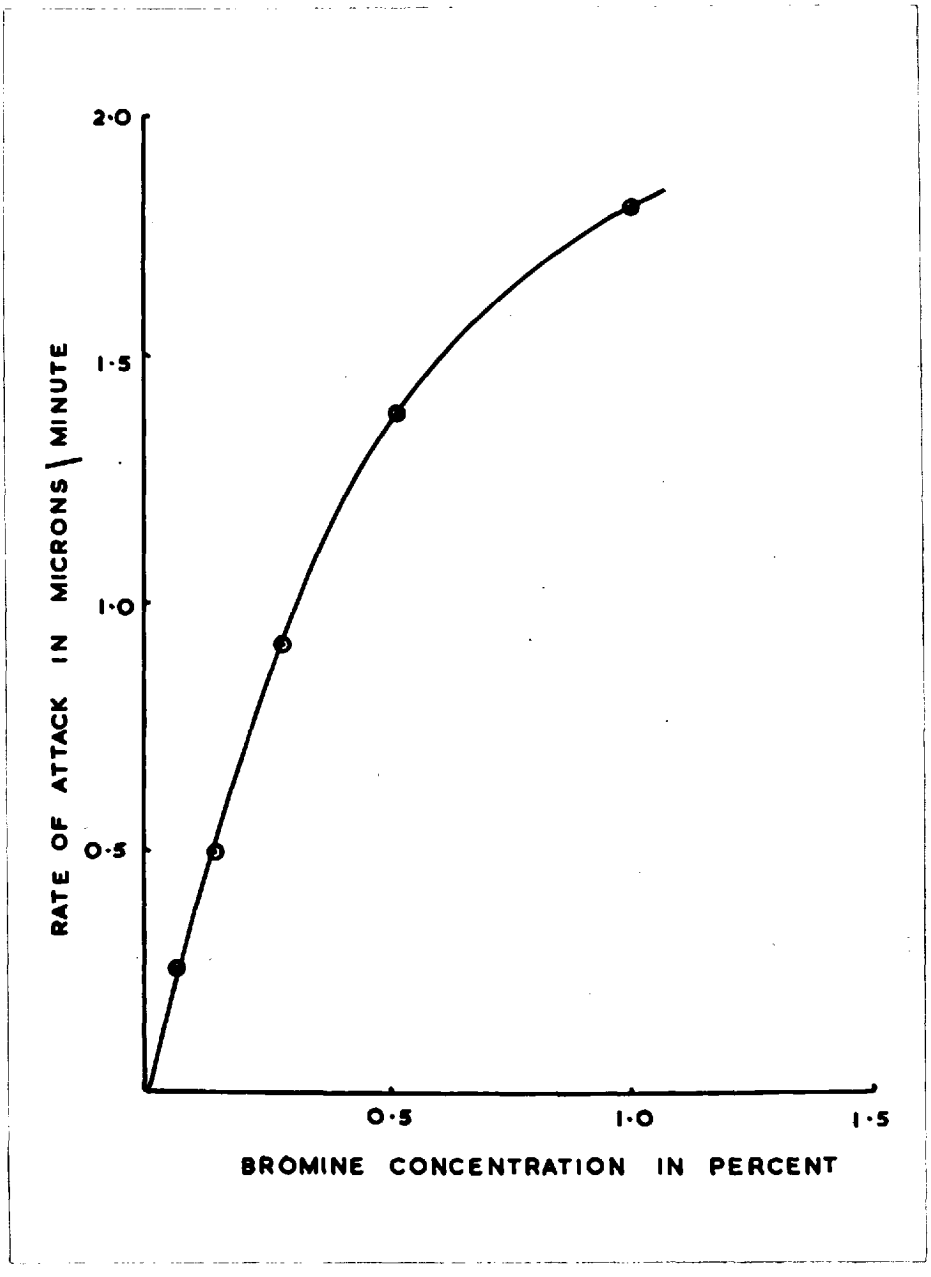

Fig 3.6. Rate of attack of Bromine/Methanol polish on GaAs versus Bromine concentration, for the rotating beaker apparatus. (S.H. Levene (1966))

the difference in etching characteristics between the p and n sides of the junction as shown in chapter 4. Some diodes were also mounted end-on for etching studies of planes parallel to the reflecting mirrors.

After etching, the diodes were demounted by dissolving the plastic in acetone, and prepared for transmission electron microscopy.

3.4. Specimen Preparation for Transmission Electron Microscopy

3.4.1. Difficulties of Specimen Preparation

For transmission electron microscopy, specimens of GaAs must be less than about 5,000 Å thick, at which thickness they are extremely brittle. In this work, thin areas were prepared in bulk GaAs specimens by chemical jet thinning so that handling was simplified. The jet thinning was based on the method of Holt, Porter and Unvala (1966). They used a low pressure jet of chemical polish which impinged on the underside of the specimen and etched a dimple in it. When a region of the material was of the right thickness for electron transmission it also transmitted light from an illuminator under the jet. The top surface was observed by a low power microscope until a pinpoint of light was seen in transmission. This method was unreliable when applied to GaAs, because the thinning time was about half an hour and fatigue usually caused the observer to miss the moment when the light appeared. The initial chemical polish used was sodium hypochlorite NaOCl containing 2% W/W available chlorine, but the surface was

so poor on the electron microscope scale that no details could be seen. Subsequently the polish reported by Biedermann and Brack (1966) was used. This consisted of

40 parts HCl

4 parts H_2O_2 (20 vol)

1 part H_2O,

parts by volume, and gave satisfactory results.

Electropolishing was not used because of the variations in electrical properties of the specimens in the p - n junction region where examination was required.

3.4.2. Automatic Specimen Thinning Apparatus

In order to eliminate the human factor in the technique of Holt, Porter and Unvala, a photomultiplier was used to detect the transmitted light. The output from the photomultiplier was amplified and made to trigger a silicon controlled rectifier (S.C.R.) which energised an electromagnet. The electromagnet moved the specimen from the chemical jet to a washing jet of deionised water. The apparatus is shown schematically in fig 3.7.(a) and a photograph is shown in fig 3.7.(b). A microscope illuminator was mounted vertically under the combined perspex light pipe and jet. The jet was made from perspex rod 13cm long and tapered from 12mm to 4mm diameter over a length of 10cm. A $^1/_{64th}$inch drill was used to drill out the jet, and the chemical polish entered through the side of the light pipe. The specimen in its opaque mount (sect. 3.4.3) was held in tweezers with the specimen surface 1mm above the jet nozzle. The unobstructed liquid jet height was

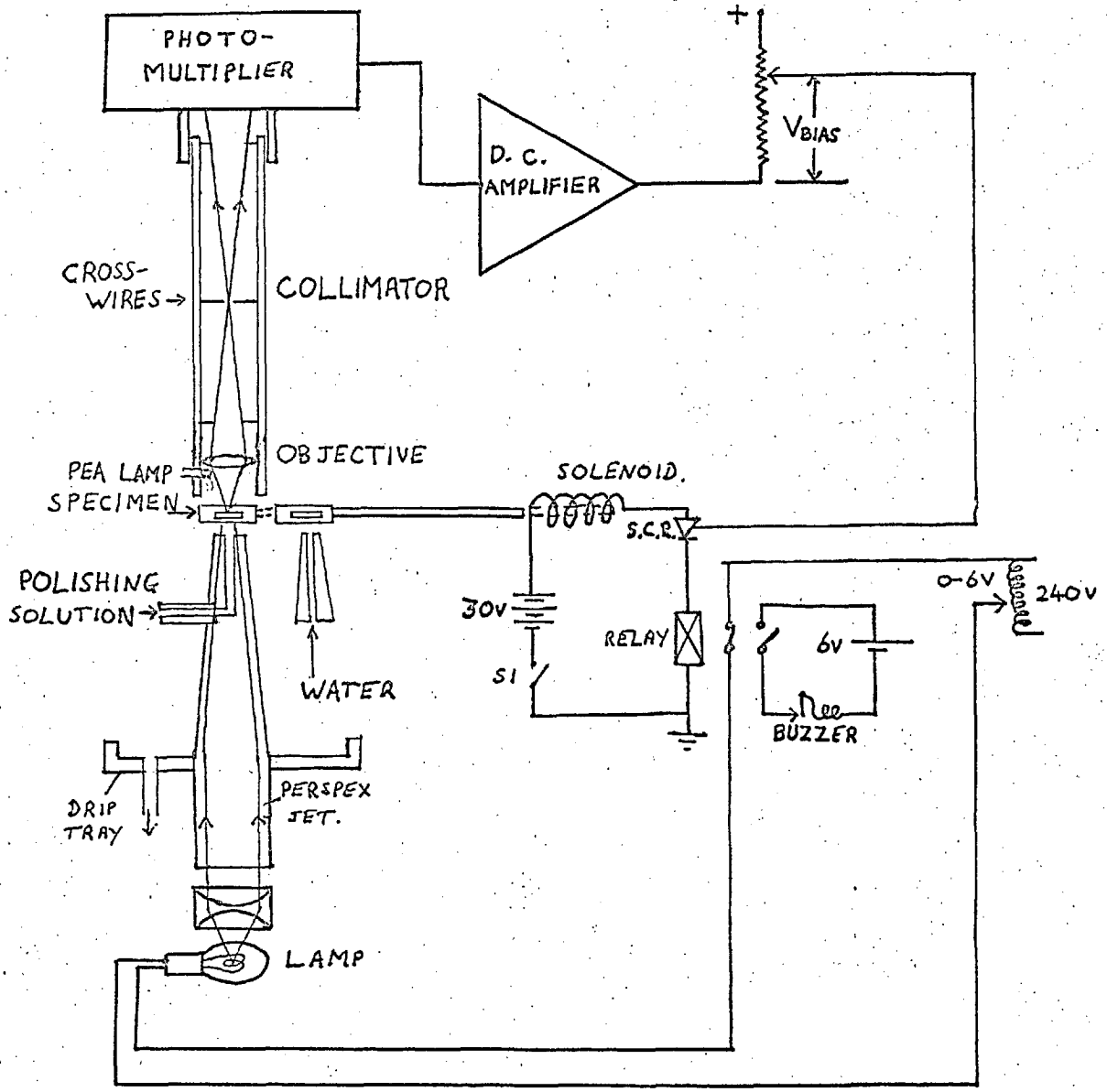

FIG 3.7(a) DRAWING OF JET THINNING APPARATUS

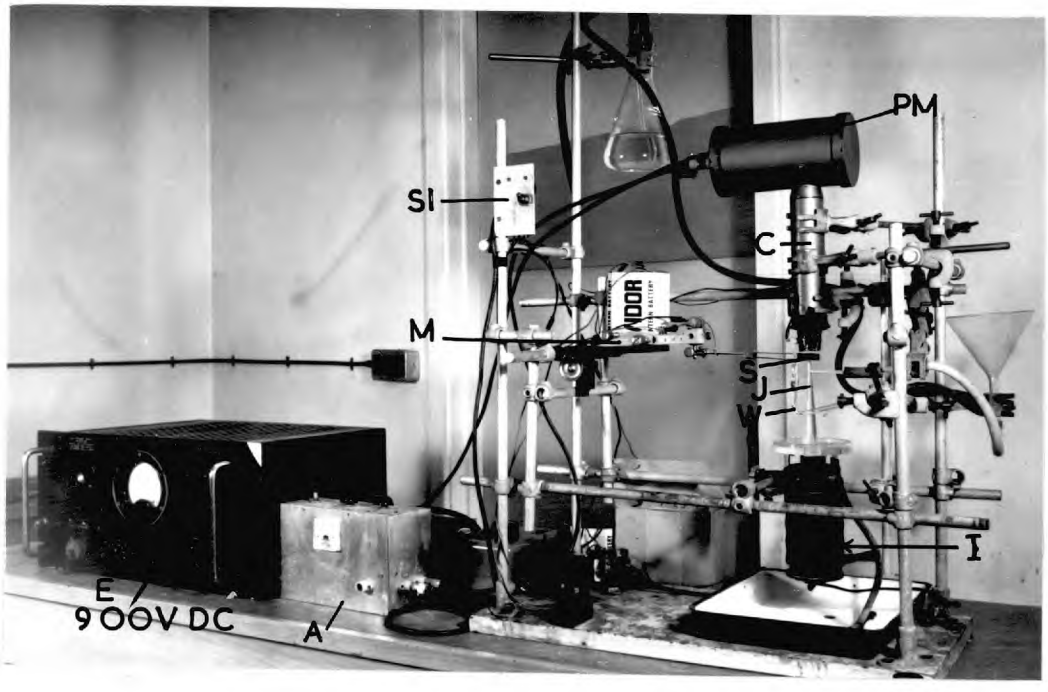

Fig 3.7.(b) Photograph of jet thinning apparatus. PM is the photomultiplier, C collimator, S specimen, J combined jet and light-pipe, I illuminator, W water jet, M micromanipulator, A amplifier and E photomultiplier power supply.

about 2mm.

The microscope tube was made of brass, with apertures positioned as shown to cut out background light. The photomultiplier screwed into the top of the collimator tube. For alignment there were crosswires in the top aperture, which were viewed by an eyeglass placed in the top of the tube. The focal length of the objective was about 25 mm and produced an image of the jet nozzle in the plane of the crosswires. The jet was aligned on the crosswires, then the specimen inserted and the area of interest aligned. The solenoid and tweezers holding the specimen were both mounted on a micromanipulator so that specimen positioning to better than 100μ was possible. After alignment, the eyepiece was replaced by the photomultiplier which was an E.M.I.no.9664B operated at 900 volts. It had an S10 photocathode sensitive to wavelengths up to 8,000 $\mathring{A}$. This was the cheapest photomultiplier available commercially, and had sufficient sensitivity while being robust. The collimation in the microscope tube allowed the apparatus to be operated under normal ambient lighting conditions, provided these were constant. However this meant that a small pea lamp had to be used to view the specimen by reflection during alignment.

The photomultiplier output was fed to a D.C. amplifier and the output from this went to an S.C.R. capable of carrying at least 2 amps. The switch S1 (fig.3.7.(a)) was kept open until the specimen was aligned and the photomultiplier in position. When

the amplifier output had been set at 0·4 volt, S1 was closed. Initially the illuminator intensity and amplifier setting which controlled the required final specimen thickness were determined by a few trial runs and subsequently kept constant. Finally the chemical jet and the washing jet were started. The only attention needed was a periodic check that background light intensity changes had not altered the amplifier output voltage. The drift of the amplifier itself was not greater than 0·2 volts in an hour.

When the amplifier output voltage rose above 1·0 volt the S.C.R. was triggered and energised the solenoid, which moved the tweezers so that the specimen was then positioned over the water jet. A relay (fig. 3.7.(a)) was included in series with the S.C.R. and solenoid to operate a warning buzzer and switch off the illuminator. This prevented direct illumination reaching the photomultiplier when the specimen was removed.

The amplifier circuit was based on the double long-tailed pair amplifier analysed by Grigson (1964). The circuit is given in fig. A4 of the Appendix and briefly described there.

3.4.3. Specimen Mounting for the Thinning Apparatus

The method just described for thinning GaAs was developed for laser-sized crystals and has been applied to specimens smaller than 1mm X 1mm. Handling these small specimens was simplified by mounting them on 0·5mm thick tantalum discs of 3mm diameter, with a hole in the centre. 3mm was the diameter of the electron microscope specimen holder. Fig 3.8. shows the method used to

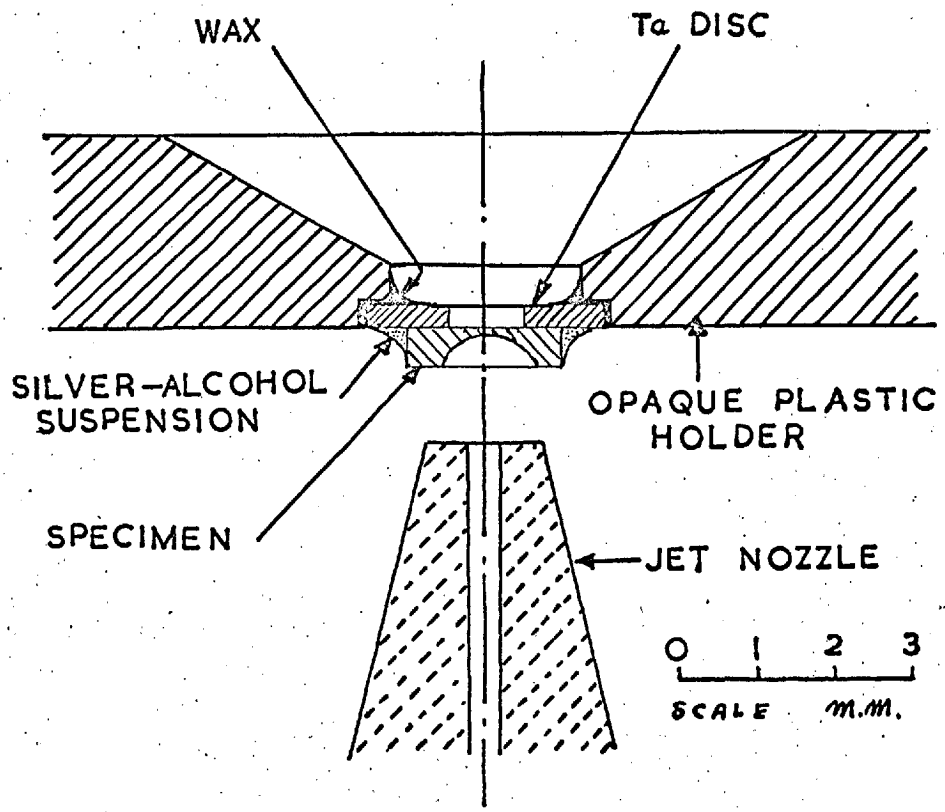

FIG.3·8 METHOD OF MOUNTING SPECIMENS FOR JET THINNING.

mount the GaAs specimens for jet thinning. After preparation by chemical polishing, the specimen was attached to the Ta disc by painting a colloidal suspension of silver in alcohol round the edges and baking for several hours at 100°C under a lamp. This gave a liquid-tight seal between the GaAs and Ta, and was resistant to the chemical polish. The specimen surface which was to be examined, faced through the hole in the disc. The specimen on the Ta disc was mounted in the opaque plastic holder using vacuum wax as shown in fig. 3.8. Slight warming of the wax was found to be useful in making a liquid-tight seal. Any traces of wax left on the Ta after removal from the plastic holder did no harm in the electron microscope. In order to ensure that the chemical polish flowed smoothly and produced a good dimple on the underside of the specimen it was essential that nothing projected below the level of the GaAs, and that the nozzle-to-specimen distance was between 0·5 and 1·5 mm. After removing the thinned specimen from the washing jet, no further washing was necessary, provided the specimen was dried quickly in a clean atmosphere.

This technique thinned through to one surface of the specimen, but in this work the area of interest was always previously revealed on this surface by chemical polishing. The mounting method was time-consuming but with the jet thinning apparatus a specimen suitable for examination was assured every time and no specimens were lost in handling.

The jet thinning technique developed here is applicable in principle to any semiconductor having an absorption edge in the

near infra-red or visible regions of the spectrum. Filters must be used to cut out the wavelengths transmitted by the bulk material to which the photomultiplier is sensitive. This was not necessary for GaAs as the S10 photocathode was sensitive only to wavelengths shorter than 8,000 Å, and the absorption edge of GaAs was about 9,000 Å.

An account of this technique has been published by Hill, Holt and Unvala (1968).

3.5. Work on Particular Specimens

The reflectivity of the mirror faces of two laser diodes was measured, to determine whether slight variations of reflectivity were present which might have correlated with the emission and transmission patterns. The apparatus used was that of Drs. J.M. Jones and G.M. Murchison of the Department of Geochemistry, University of Newcastle-upon-Tyne. The main features of this equipment were a photomultiplier mounted on the eyepiece of a Zeiss microscope, with apertures and a viewing eyepiece arranged so that reflected light from the precise area viewed was detected. The photomultiplier output was recorded on a chart as the field of view was moved across the specimen in steps. The wavelength used was 7090 Å, because the photomultiplier was not sensitive to infra-red wavelengths. The apparatus could detect reflectivity variations of less than one per cent at the reflectivity of GaAs which is about 32%.

The electron probe microanalyser was used to determine the Zn

concentration of two specimens from the fluorescent X-ray emission. An attempt was also made to detect the Te concentration, but this was below the limit of sensitivity of the instrument. The junctions of the same two diodes were examined using the SEBECC technique, but no features were found which corresponded with defects revealed by other methods.

CHAPTER 4

Experimental Results

In this chapter the results are presented and described in the order in which they were obtained for each diode, as outlined in sect. 3.1. Sect. 4.2. describes the optical microscopy of the diodes in the cryostat, sect.4.3. the etching results, and sect. 4.4. the transmission electron microscopy results. Other results are mentioned where appropriate.

The two opposite mirror faces of the diodes are referred to as faces A and B. There is no connection between this notation and the notation for the opposite $\{111\}$ crystal planes in the sphalerite structure.

4.1. The Diodes

Table 4.1. gives the relevant information supplied with each diode by S.E.R.L. and also the orientations and threshold currents. The diode serial numbers are those used at S.E.R.L. and all diodes having the same four figure number (column 1) were prepared from the same substrate and same diffusion run. The diodes were oriented by Laüé X-ray diffraction and the orientations are given in columns II and III. The junction planes were all within 3^{o} of (001) except for diode numbers 2640/1 and 5 whose junctions were oriented close to an(011) plane. The orientation of the Fabry-Perot faces was not selected in any way at S.E.R.L., except for diode 3434/5 which had $\{110\}$ cleaved mirror faces. All the substrate crystals were doped to average electron concentrations of

DIODE NO.	ORIENTATION		DONOR	CRYSTAL GROWTH METHOD	DIFFUSION CONDITIONS			j_t Amps	T.E.M. N or P
	MIRROR FACE	JCT. PLANE			TEMP	TIME	DIFFUSANT		
I	II	III	IV	V	VI	VII	VIII	IX	X
2659/4	110	001	Te	Horizontal Bridgman	1100°C	15m	Zn	60	-
2659/5	110	001	Te	"	1100	15	Zn	52·5	n
2659/6	110	001	Te	"	1100	15	Zn	108	n
2659/7	110	001	Te	"	1100	15	Zn	75	p
2613/6	210	001	Si	"	1100	15	Zn	35	p
2613/7	210	001	Si	"	1100	15	Zn	51	n
2839/6	310	001	Se	"	850	4h	$ZnAs_2$	65	n
2640/1	510	011*	Si	Static Freeze	1100	15m	Zn	-	p
2640/5	510	011*	Si	"	1100	15	Zn	-	-
3434/5	110**	001	Te	Czochralski	850	$7\frac{1}{2}$h	$ZnAs_2$	-	-

Table 4.1. Details of the diodes examined. Column IX gives the threshold current for the onset of stimulated emission, and Column X gives the side of the junction which was examined by transmission electron microscopy.

* approximately 8° off this orientation

** This diode had cleaved mirror faces.

2 ($\pm$1) X $10^{18}/cm^3$ with the donors shown in column IV. The threshold current given in column IX is the diode current at which the first intense spot appeared on the image converter screen. Column X shows which side of the p - n junction was examined by transmission electron microscopy.

4.2. Optical Microscopy in the Cryostat

Systematic emission and transmission results are presented for three diodes, each of which was prepared from a different substrate crystal. The diode numbers were 2613/7, 2659/7 and 2839/6. Results from other diodes are given where they illustrate particular points.

4.2.1. Emission

In fig. 4.1. the light output versus diode current curves are given for each of the above three diodes. The ordinate in each case is the voltage developed by the Si solar cell as described in section 3.2.5., and was proportional to the light output of the diode. The onset of stimulated emission as viewed on the image converter is marked by an arrow on each curve. Above threshold the light output varied approximately linearly with diode current. A series of near-field emission micrographs for each of the same three diodes is given in figs. 4.2., 4.5. and 4.8. These show how the emission varied with current density from just below threshold for the first spot of stimulated emission up to values of 200 amps. Diodes 2613/6 and 2839/6 showed marked "spots" of stimulated emission while 2659/7 showed a rather diffuse area which increased in size as

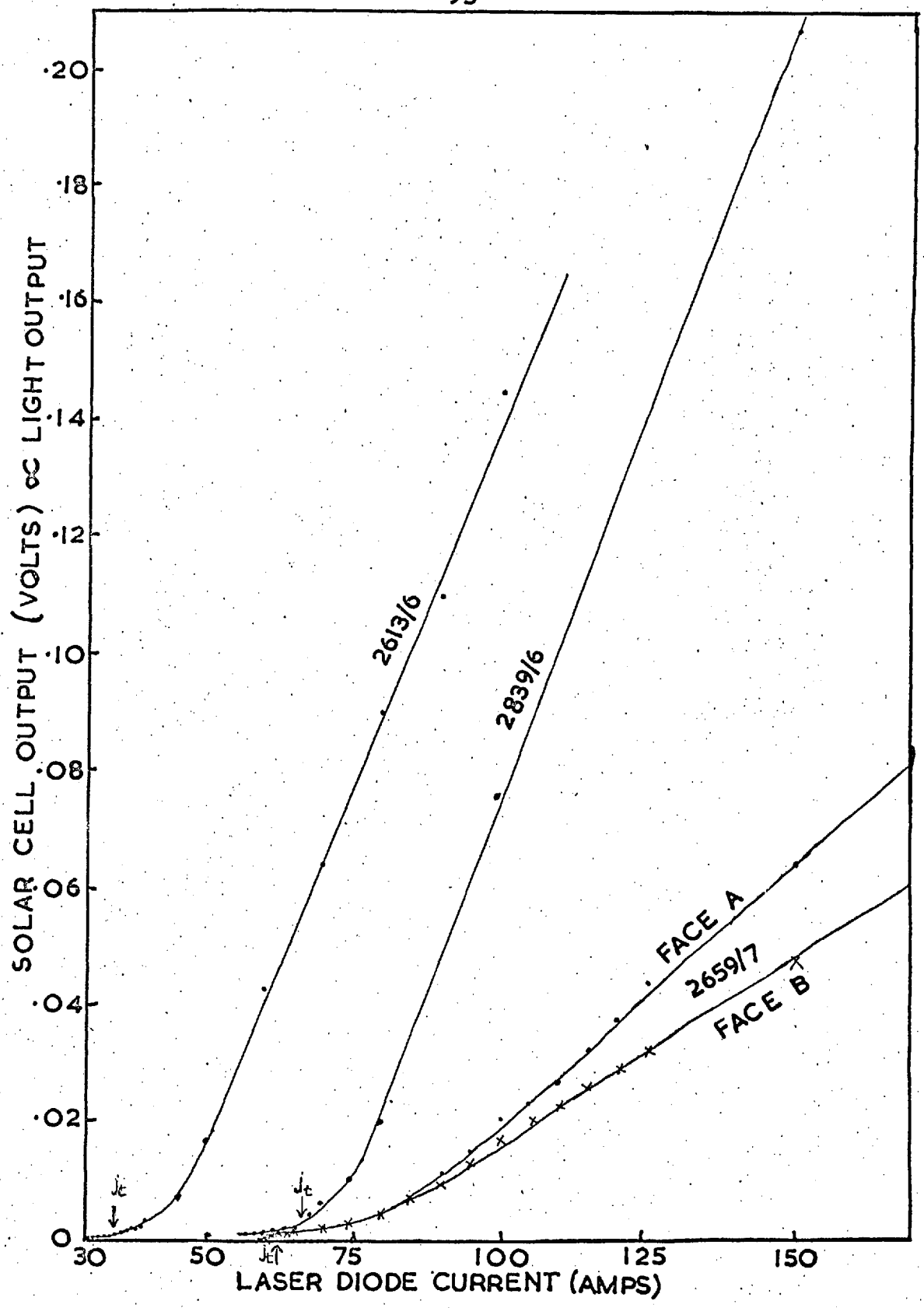

FIG. 4.1 LIGHT OUTPUT VS. DIODE CURRENT FOR THREE LASER DIODES

the current increased. In each diode there was agreement between the current at which the first spot of stimulated emission appeared and the current at which the sharp increase in solar cell output occurred. Because the diodes were rotated through 180° between photographing each face, the emission patterns from the opposite faces are mirror images of each other. Fig 4.3. (c) is a near field emission pattern from diode number 2659/5 taken well above threshold, and shows two areas of stimulated emission. The threshold for the second area was nearly twice that for the first. In fig. 4.3.(a) and (b) the emission patterns of the opposite faces of the diode are shown just above threshold. These were taken using long exposures and show that considerable scattering into the n side of the junction occurred. The striations are more clearly visible than those in 2659/7 fig 4.6. Fig 4.3.(a) was printed in reverse to show the correspondence between the ends of the diode, as indicated in the adjacent drawing. The striations therefore ran through the crystal as parallel planes perpendicular to the mirror faces. These striations were found in all diodes numbered 2659.

4.2.2. Reflection

Reflection micrographs of diode 2613/6 taken in the cryostat are shown in fig 4.2.(h), and fig. 4.6.(a) and (c) show the two faces of diode 2659/7 taken using Nomarski interference contrast. In all the polished diodes these interference contrast micrographs showed considerable damage due to polishing. Most of the scratches were not visible by ordinary reflection microscopy, but a few of the larger scratches were. In no case was any correlation

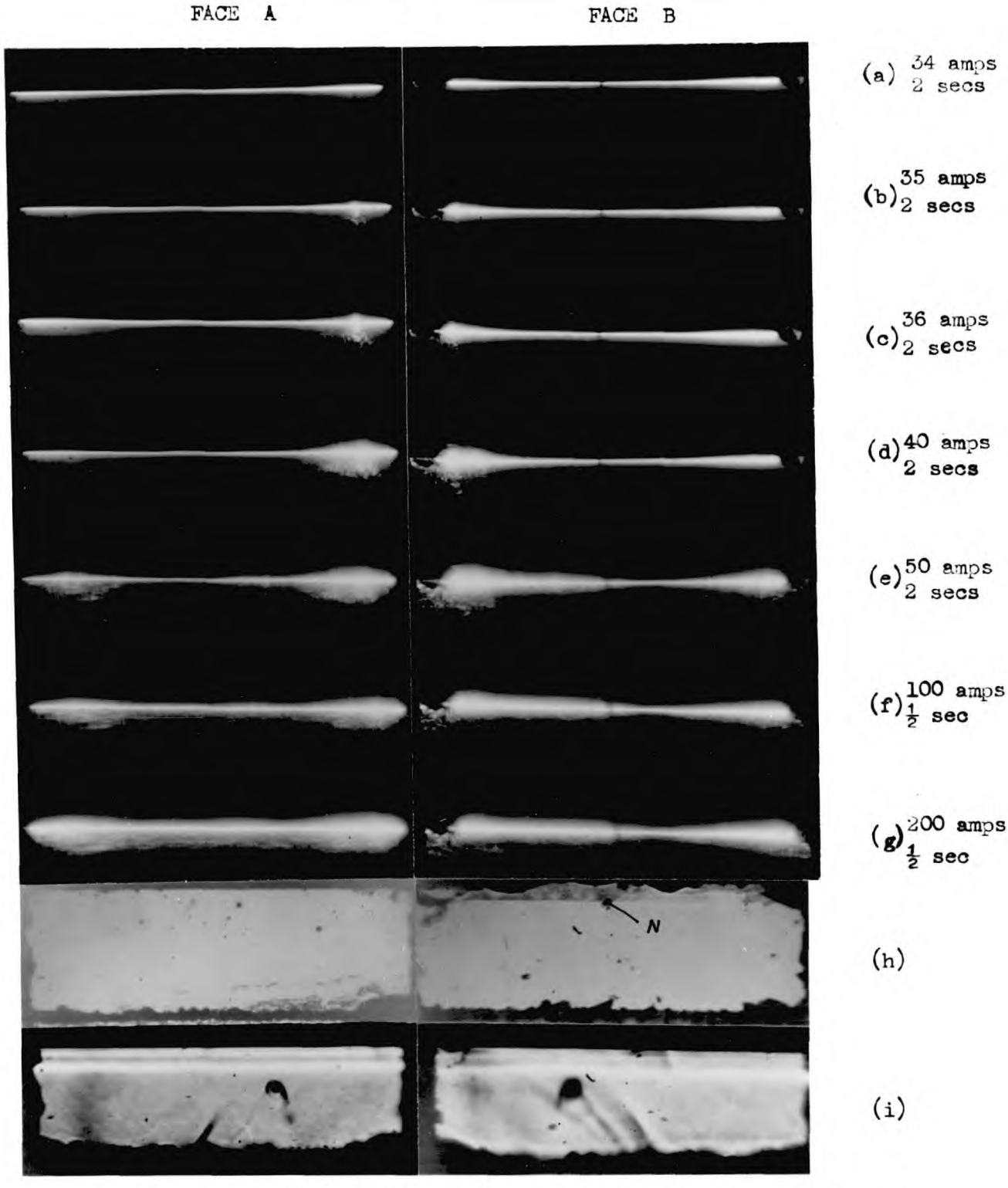

Fig 4.2. Diode No. 2613/6. (a) - (g) Near - field emission micrographs of each mirror face, taken with values of diode current and exposure times as shown, at 14 current pulses/sec. The corresponding reflection micrographs (h) and optical transmission micrographs (i) are shown. N is a surface defect which reduced the emitted intensity.

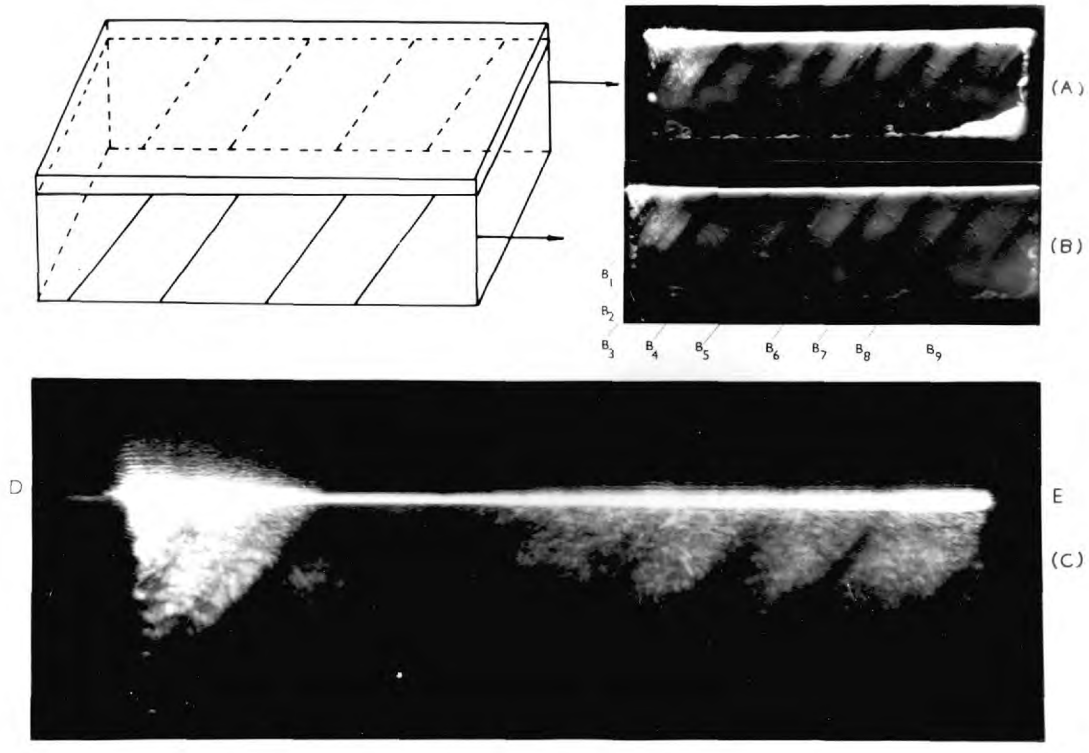

Fig. 4.3. Diode No. 2659/5 Near field emission patterns with 54 amps flowing (A) & (B) and 80 amps flowing (C). (A) and (B) show the two opposite diode faces with (A) printed in reverse to show the correspondence between the emission patterns at the two faces. The adjacent drawing shows that the striations pass through the whole length of the diode and are perpendicular to the mirror faces. Fig. 4.4.(a) gives the infra-red transmission pattern of this diode.

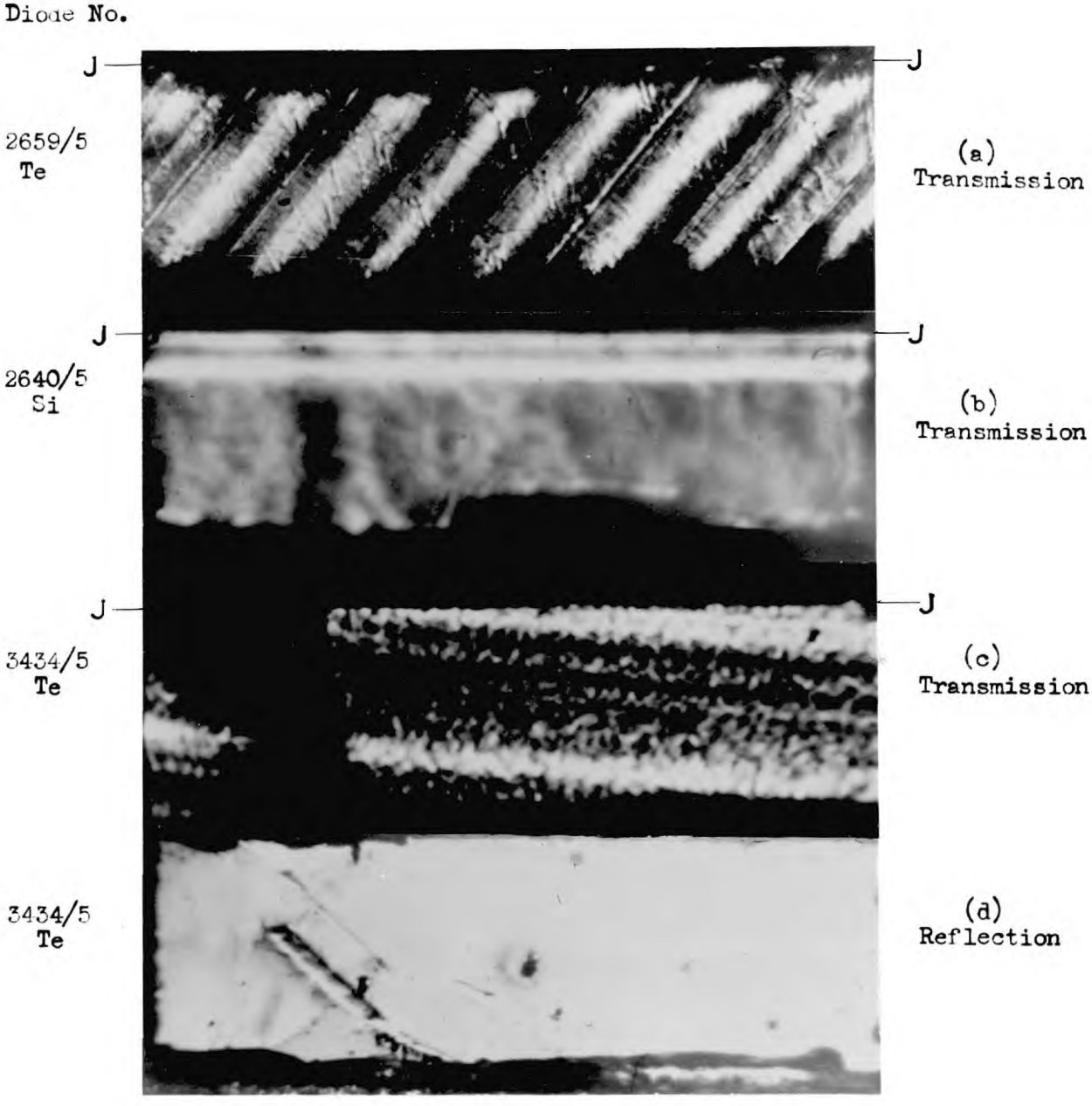

Fig. 4.4. (a) and (b) Diode Nos. 2659/5 (Te doped) and 2640/5 (Si doped) viewed by transmission. (c) and (d) show diode No. 3434/5 (Czochralski, Te doped) viewed by transmission and reflection. Lines J - J mark the p - n junction positions.

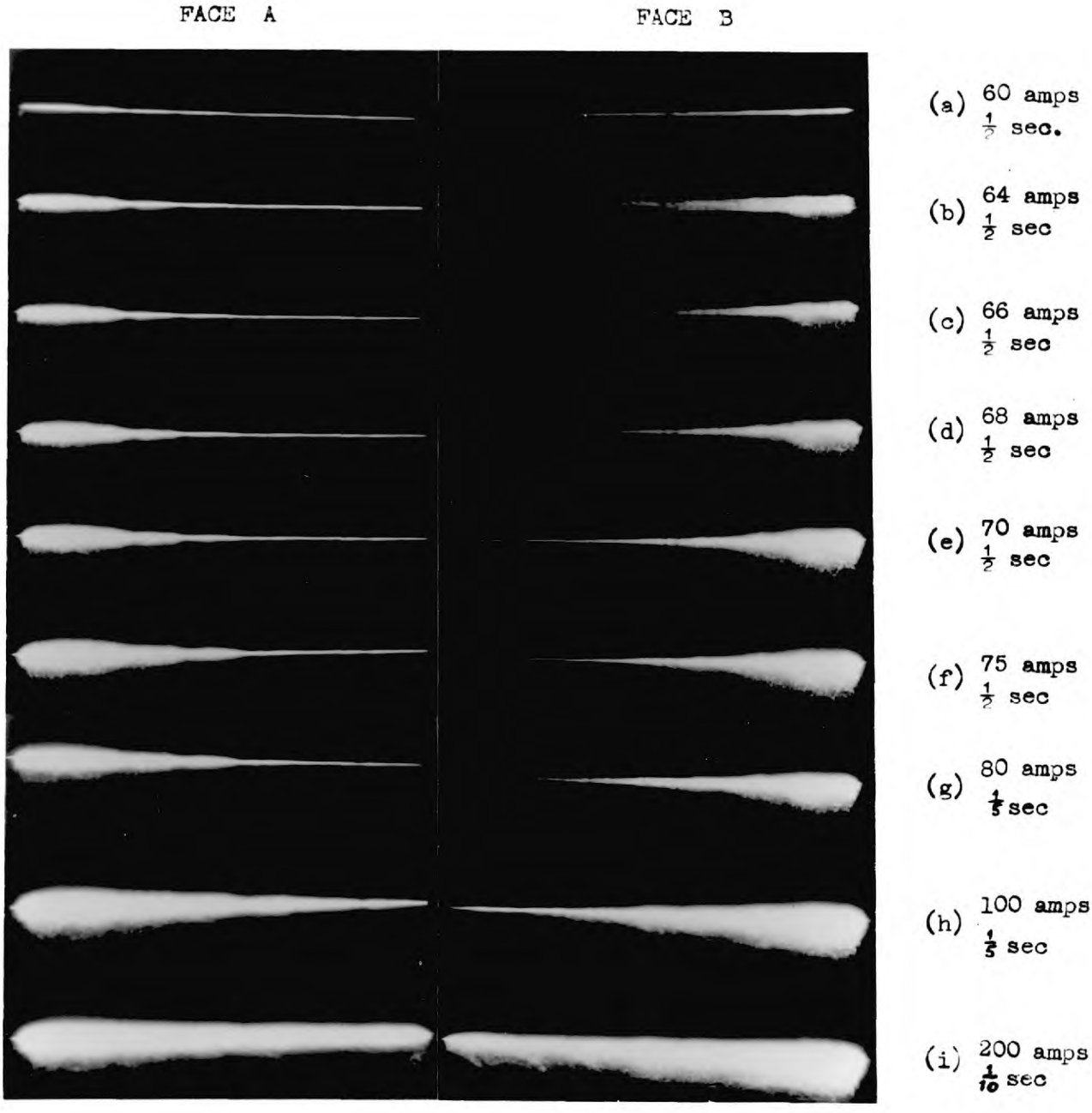

Fig 4.5. Diode No. 2659/7. Near field emission micrographs of each mirror face, taken with values of diode current and exposure times as shown. Pulse repetition rate was 20/sec.

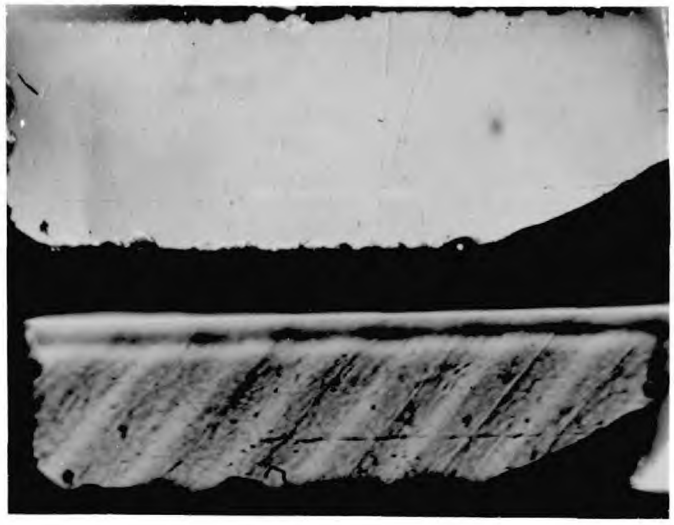

(a) Reflection

FACE A

(b) Transmission & Emission 57 amps

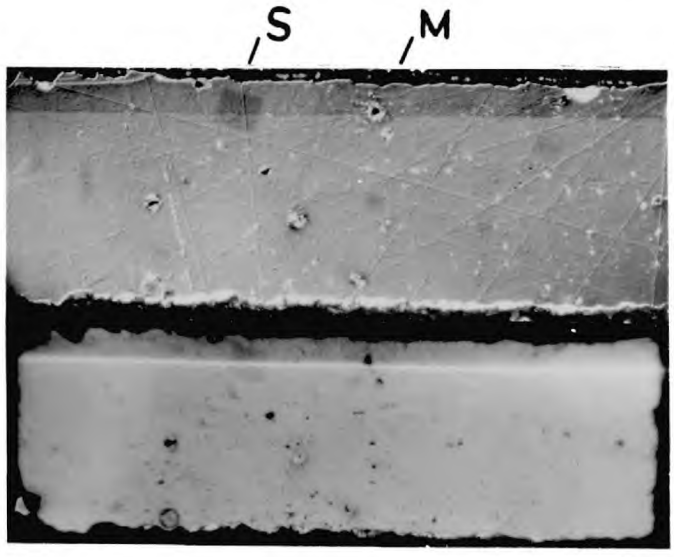

(c) Reflection

FACE B

(d) Reflection & Emission 66 amps

Fig 4.6. Diode No. 2659/7 (a) and (c) are Nomarski interference contrast micrographs of the two diode faces. (b) shows transmission and emission together, and (d) shows reflection and emission together. S is an area previously examined in the electron probe and is an area of carbon contamination. M is a hole in the surface.

found between scratches and junction emission intensity, but the surface damage mark M. in fig. 4.6.(c) caused a slight decrease in the emitted intensity. The effect of a surface defect is shown more clearly at the point marked N in diode 2613/6, fig. 4.2. In figs. 4.2.(h) and 4.6. (c) a film can be seen covering the p-type surface of one of the Fabry-Perot mirrors. These films were present in some diodes when they were received from S.E.R.L., but never on both faces of a diode. The chemical properties of the heavily Zn doped p - type material may have been sufficiently different from the n - type material to allow a film of possibly an oxide, to grow preferentially over the p - region. However the presence of this film on only one of the mirror faces could not be due to different surface properties of the opposite faces, since they were chemically identical. Differences in the treatment of the two faces during diode preparation may have occurred. The film clearly delineated the p - n junction in figs. 4.6.(c) and (d). The dark square mark S in these two figures was carbon contamination resulting from examination in the electron probe. The emission series of fig. 4.5. were taken before this contamination was caused, but when the diode was operated again afterwards there was no apparent difference in the emission due to the carbon film. The reflectivity measurements made at Newcastle University showed no correlation between striations and surface reflectivity. Any reflectivity fluctuations in the n side were less than 1%, and the variations across the p - n junction in fig 4.6. (c) was only 4%.

4.2.3. Infra-Red Transmission

Optical transmission micrographs taken in the laser cryostat are shown for several diodes in the figures listed below

Diode Number	Donor	Figure Number
2613/6	Si	4.2.(h)
2613/7	Si	4.12
2640/5	Si	4.4.(b)
2659/5	Te	4.4.(a)
2659/7	Te	4.6.(b)
2839/6	Se	4.8.(i)
3434/5	Te	4.4.(c)

All these transmission micrographs were taken with the microscope focused on the front face of the diode. Diodes 2613/6 and 7 both showed considerable irregular internal structure. The striations seen in diodes 2659/5 and 7 (and in 2659/4 and 6 - not shown) were of a regular nature and were found to lie along planes almost perpendicular to the polished faces. In the case of 2659/5 (fig. 4.4.(a)) the striations were accurately perpendicular to the Fabry-Perot faces, and with careful alignment of the illumination the striations were shown to consist of many closely spaced parallel planes. Also visible were many irregular lines, whose detail was lost on focussing a short distance inside the crystal.

Infra-red transmission through diodes 2839/6 and 10 showed much less internal detail. Fig. 4.8.(i) shows that in 2839/6 there was one defect (D) near face A, whose effect could just be seen as an area of decreased intensity (D^1) at the opposite face.

In all the transmission micrographs of diodes 2613/6,7, 2640/5, 2659/4,5,6 and 7 there was a dark band parallel to the

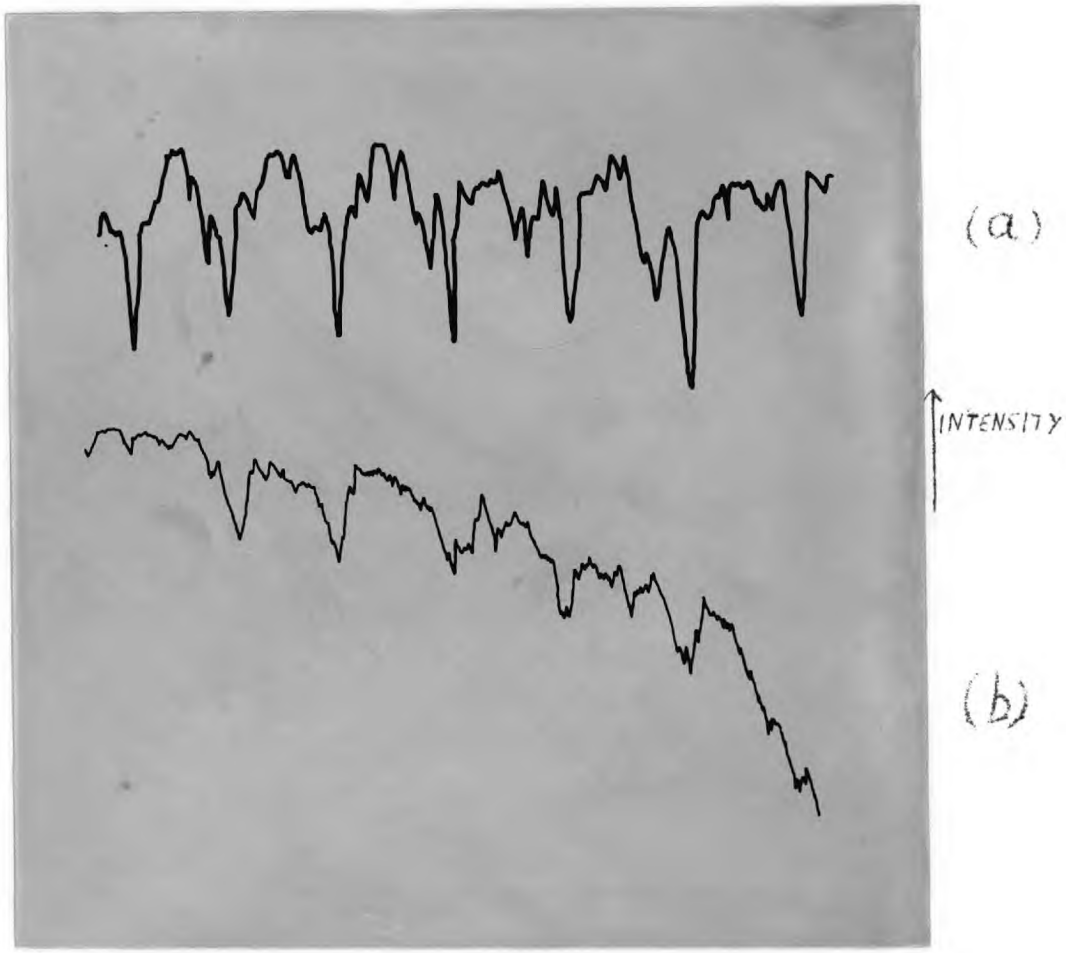

Fig. 4.7. Diode No. 2659/7. Microdensitometer traces taken parallel to the p - n junction on the negatives of (a) a transmission infra-red micrograph and (b) a near-field emission micrograph. Intensity increases upwards, and the left hand side of (b) was an area of stimulated emission.

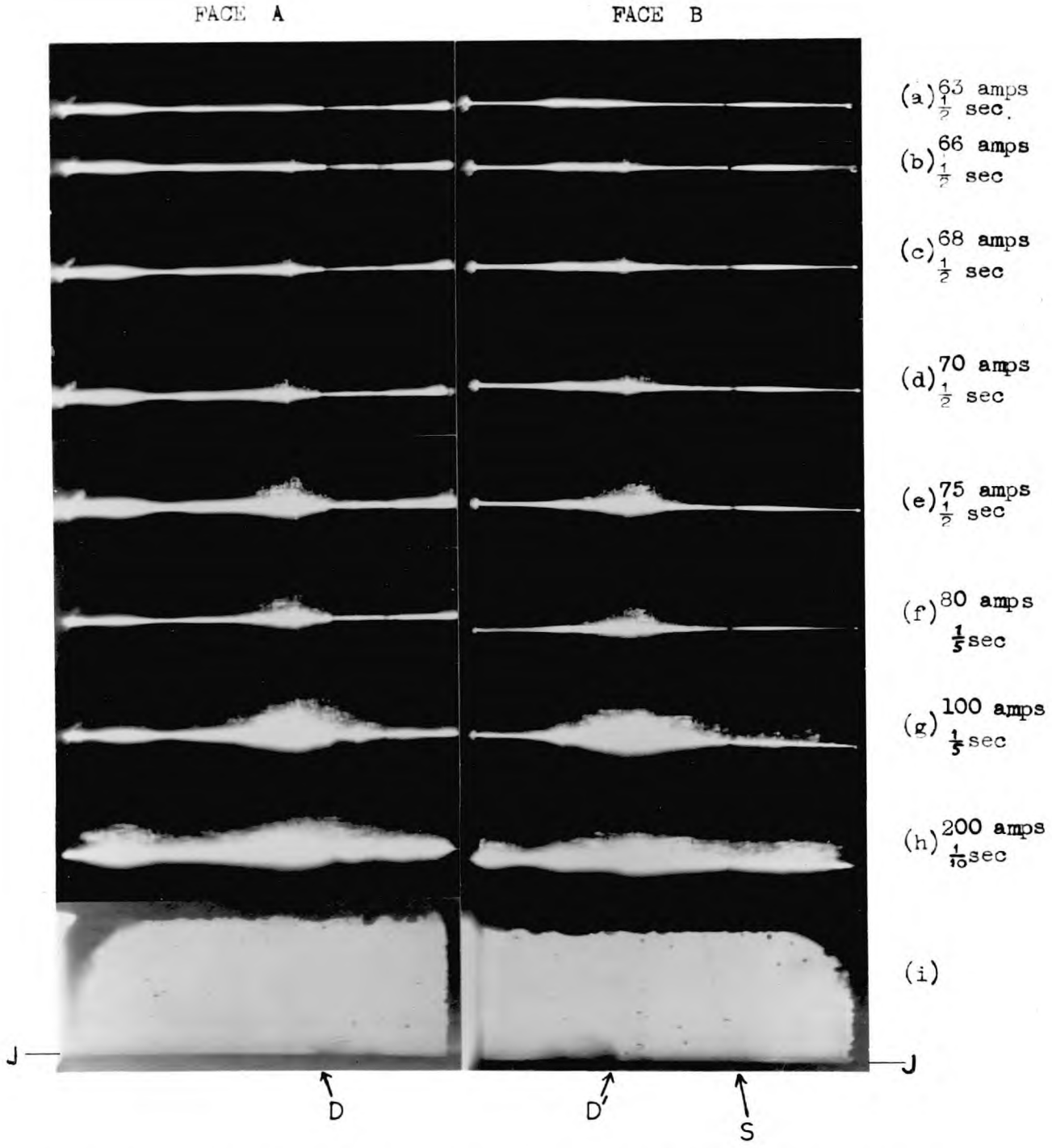

Fig 4.8. Diode No. 2839/6. (a) - (h) Near - field emission micrographs of each diode face, taken with values of diode current and exposure times as shown, at 20 current pulses/sec. (i) are the corresponding transmission micrographs. D and D' mark an internal defect close to face A, and S is a surface scratch.

junction and close to it, on the n side, and a bright band further into the n side. These bands should not be confused with the regular striations seen in some diodes. In diode 2613/7 (fig. 4.12.) the bright band followed the line of some of the internal structure. In the 2659 diodes the intensity of the bright band was affected by the striations. The possibility of stray reflections causing the bands was eliminated by varying the illumination conditions. The bands must be due to an internal effect in the GaAs.

The dark and bright bands were not detected in diodes 2839/6,10 and 3434/5, although in this last case they could have been masked by the striations. These diodes which did not show the effect were all diffused at 850°C in the presence of excess As vapour. 3434/5 was a Czochralski grown, Te doped diode, and clearly showed impurity striations lying at a small angle to the junction plane. A large opaque internal defect was present, which was associated with the irregular cleavage of the front face as seen in fig. 4.4.(d). This defect also probably caused the diode to have very low electrical resistance in both directions which prohibited laser action.

In the 2659 diodes, which all had regular striations, there was a direct correlation between the emitted light intensity and the transmitted intensity. Fig. 4.7. shows microdensitometer traces of micrograph negatives of (a) the transmission and (b) the emission patterns, with the slit scanned along the line of

the junction. The dark striations in the transmitted pattern clearly correspond to regions of decreased electroluminescence. At the left hand end of the junction there was an area of stimulated emission, with the effect of the striations still being evident. In fig. 4.3.(c) this periodic variation of emitted intensity can be seen by looking along the length of the emission line DE. Fig. 4.12. shows that the first emission spot in diode 2613/7 was in the region of least internal detail seen by transmission.

4.3. Chemical Etching

Fig. 4.9.(a) shows the (0 0 1) surface of diode 2659/5 after polishing and etching down to the junction region. The etching of this diode was carried out by Levene (1966). The etch revealed dark bands B_3 to B_8 which corresponded to the striations seen in the adjacent emission micrograph, and by transmission in fig. 4.4.(a). Apart from the striations there were continuous etched lines of a different nature some of which are marked G, and also rows of etch pits marked R, lying along the $[1\ 1\ 0]$ and $[1\ \bar{1}\ 0]$ directions respectively in the (0 0 1) plane. The designation of these two directions was arbitrary, but the directions were chosen as shown in fig. 4.9. to agree with those used by Abrahams and Buiocchi (1966). The spacing between the parallel lines G and between the rows R was of the order of 10 μ or greater. Fig. 4.9.(b) shows an area of (a) at high magnification where parts of the lines showed definite periodic etching, while in other parts

(a)

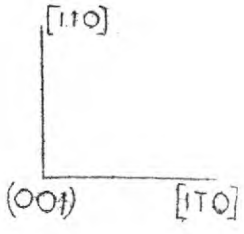

(b)

20μ

Fig. 4.9. Diode No. 2659/5. Micrographs of the (001) surface after polishing down to the junction and etching. (a) shows the whole diode with an emission micrograph to indicate the correspondence between the striations and the etched bands B. Lines of etch pits are marked R and some continuously etched grooves G. (b) is a high magnification micrograph of part of (a).

the etch pits were joined to give continuous lines.

Etched surfaces of diode 2659/6 are shown in fig. 4.10. (a) and (b) show a (1 1 0) mirror face etched for 10 secs. at low and high magnifications respectively. The junction was flat to within 2 μ over the whole 1mm width of the face, but at high magnification slight irregularities (e.g. X in fig. 4.10(b)) were visible. Many dislocations or precipitates were revealed along the line of the junction. The three distinct lines produced by the etch are characteristic of diffused junctions revealed in this way in GaAs, for instance by Marinace (1963). Schwuttke and Rupprecht (1966) also found three lines by chemical etching and by X-ray topography, and they associated the line furthest into the n - type region with the limit of elastic strain ahead of the diffusion front. They suggested the middle line was the chemical junction, and the one furthest into the p side was the knee in the diffusion profile where the Zn concentration began to decrease sharply. The same interpretation may be applied in this case. Lines 1 and 2 in fig 4.10 (b) are at the region of steepest concentration gradient and hence of greatest lattice strain. Therefore the greatest density of "misfit" dislocations is expected close to lines 1 and 2 as is shown in fig 4.10.(b). If these etch pits corresponded to the only dislocations present in the junction region, then the thickness of the region in which they were present was only about 2 μ The whole surface in fig.4.9.(a) could not possibly be sufficiently

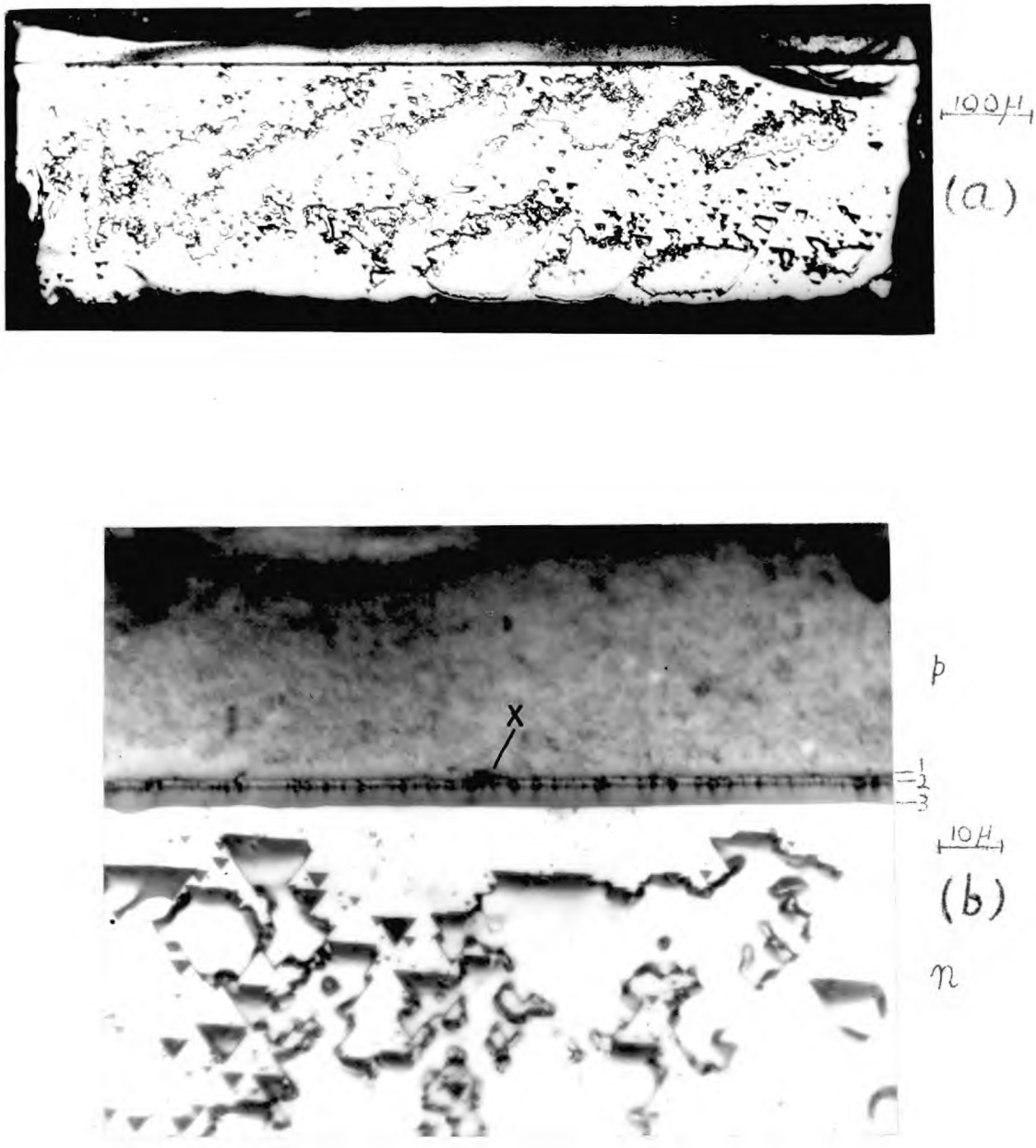

Fig. 4.10. Diode No. 2659/6 (a) a mirror face etched for 10 seconds. (b) Part of (a) at higher magnification. Three lines revealed in the junction region are indicated. X is an irregularity in the junction.

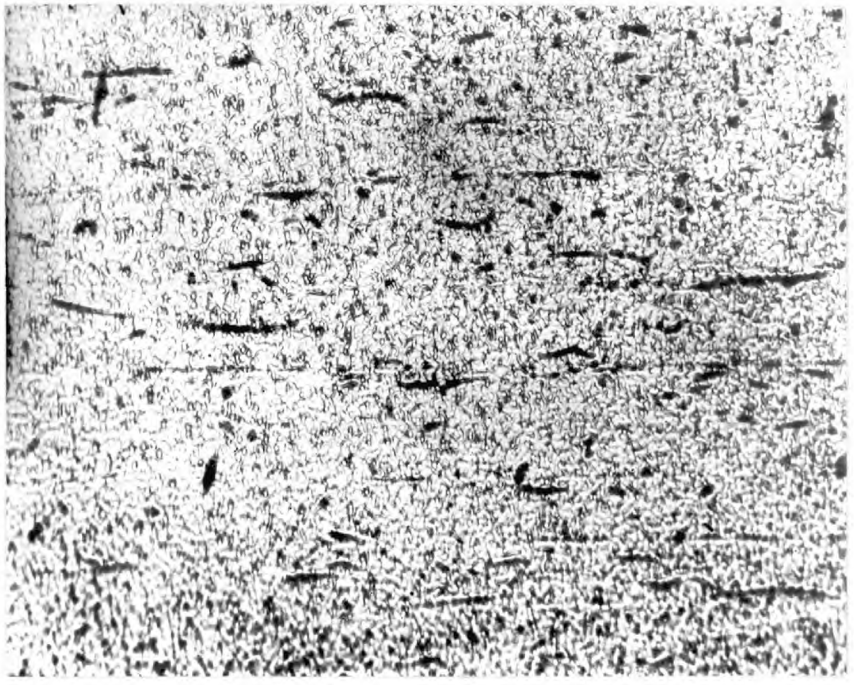

Fig. 4.10. (Continued) Diode No. 2659/6. (C) micrograph of the (001) etched surface in the p side, parallel to the p - n junction plane and within 10μ of it. The microscope was slightly defocused to improve the visibility of the etched lines. (d) is a high magnification micrograph of part of (C)

flat and parallel to the junction plane, to contain this thick layer over the whole junction region. This explains the presence of the majority of the linear defects in the upper half of the micrograph. Fig. 4.10.(c) and (d) show the etched (0 0 1) surface in the p - type material a few microns from the p - n junction. In (c) the microscope was slightly defocused to distinguish the linear etching features from the mottled background.

There appears to be a difference in the etching characteristics of the lines in $[1\ 1\ 0]$ and $[1\ \bar{1}\ 0]$ directions. In fig. 4.9.(a) there are long continuously etched grooves (G) in the $[1\ 1\ 0]$ direction, while in the $[1\ \bar{1}\ 0]$ direction there are only very short sections of such lines, and also rows of etch pits (R) having an etch pit spacing of about 10 μ. Fig. 4.10. (d) confirms this for the p side etching of diode 2659/6 where the only continuously etched lines are in the $[1\ 1\ 0]$ direction. Similar etching behaviour was found to some extent in the junction region of all the diodes examined. If it is assumed that misfit dislocations at the junction are being revealed by the etch, then they would be expected to lie along both $\langle 1\ 1\ 0 \rangle$ directions in the (0 0 1) plane. The fact that $[1\ 1\ 0]$ dislocations etched as continuous lines, and $[1\ \bar{1}\ 0]$ dislocations did not, may be due to a difference in the density of precipitates decorating the two types of dislocation. This is discussed further in section 5.1.4.

Fig. 4.10.(c) clearly shows the striations revealed by the etch in the p side of diode 2659/6. They were curved with a radius

of curvature of 5 ($\pm$1) cm. and also far from perpendicular to the mirror faces. In diode 2659/5 they were straight and perpendicular to the mirror faces which may explain why more detail was seen in the infra-red transmission micrographs of 2659/5 than in those of the other striated diodes. It is also the reason why the illumination had to be at an angle to the optical bench to get any detail at all in the transmission micrographs of 2659/6 and 7. The spacing of the fine striations in fig.4.4.(c) was about 10 μ and the diode length was 2 mm. This meant that for maximum visibility of the striations they had to be oriented to within $0^{o}.3$ of the optic axis of the viewing system, otherwise overlapping of the closely spaced planes occurred. The condition for observation was not so critical as this, since the depth of focus of the microscope was much less than the diode length, and the effect due to defects at the further end of the diode was lost. In many diodes the defect density was so great that on focussing just inside the diode all detail was lost.

Etched surfaces in the p - type material were always mottled (e.g.fig.4.10.(c),(d) and 4.11.), which meant that only defects that etched as continuous lines could be detected in the p side. This mottled texture is shown in detail in fig.4.11.(b) where diode 2659/7 was etched down to the junction region . In one area the p - type material was all removed. The line L in this figure is a striation revealed in the n - type material. Fig. 4.11.(a) shows the whole diode at an earlier stage of etching.

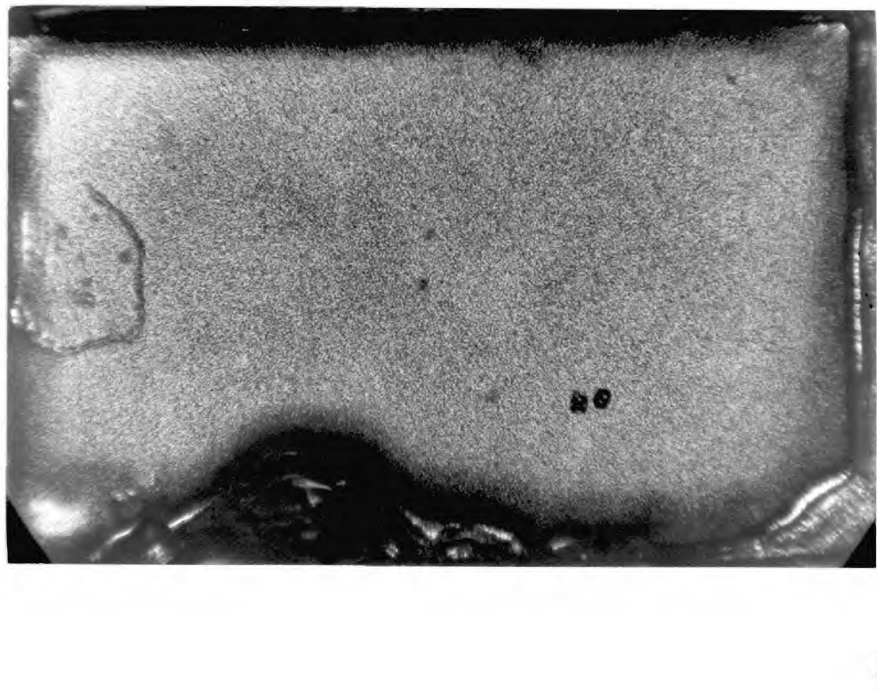

Fig. 4.11. Diode No 2659/7. (a) etched surface parallel to the junction plane in the p side of the junction. (b) $\frac{1}{2}$ min. etch in the junction region at an angle of several degrees to the junction plane, showing mottled p - type and smoother n - type surfaces. L is a striation revealed in the n side.

The striations are barely visible but could be seen by slightly defocusing the microscope. This mottling was probably due to precip - itation in the heavily Zn-doped p side and is discussed further in section 5.1.3.

Fig. 4.12 shows an etched surface in the n-type material of diode 2613/7 parallel to the junction plane, with transmission and emission micrographs of each face. The inhomogeneities seen in transmission in the n side were revealed as regions of uneven chemical attack.

4.4. Transmission Electron Microscopy

Fig 4.13. illustrates the type of chemical polish obtained on the electron microscope scale using (a) NaOCl and (b) the HCl, H_2O_2 polish of Biedermann and Brack (1966). In (a) the surface was so rough that detail in the specimen was lost. (b) is a low magnification micrograph taken at 1000 X, showing the extent of a typical electron transparent area obtained with the jet thinning apparatus. The contrast is due almost entirely to thickness contours. The straight lines running across the specimen show damage which was induced during mechanical polishing at S.E.R.L. This specimen was thinned after about 1μ had been removed by chemical polishing. When a specimen was examined directly after mechanical polishing, the damage was so dense that little could be distinguished in the electron microscope. Fig. 4.14.(a) shows an area of fig. 4.13.(b) taken at a higher magnification. The lines of damage caused by the abrasive particles rolling across the surface are surrounded by dislocation half-loops which relieve

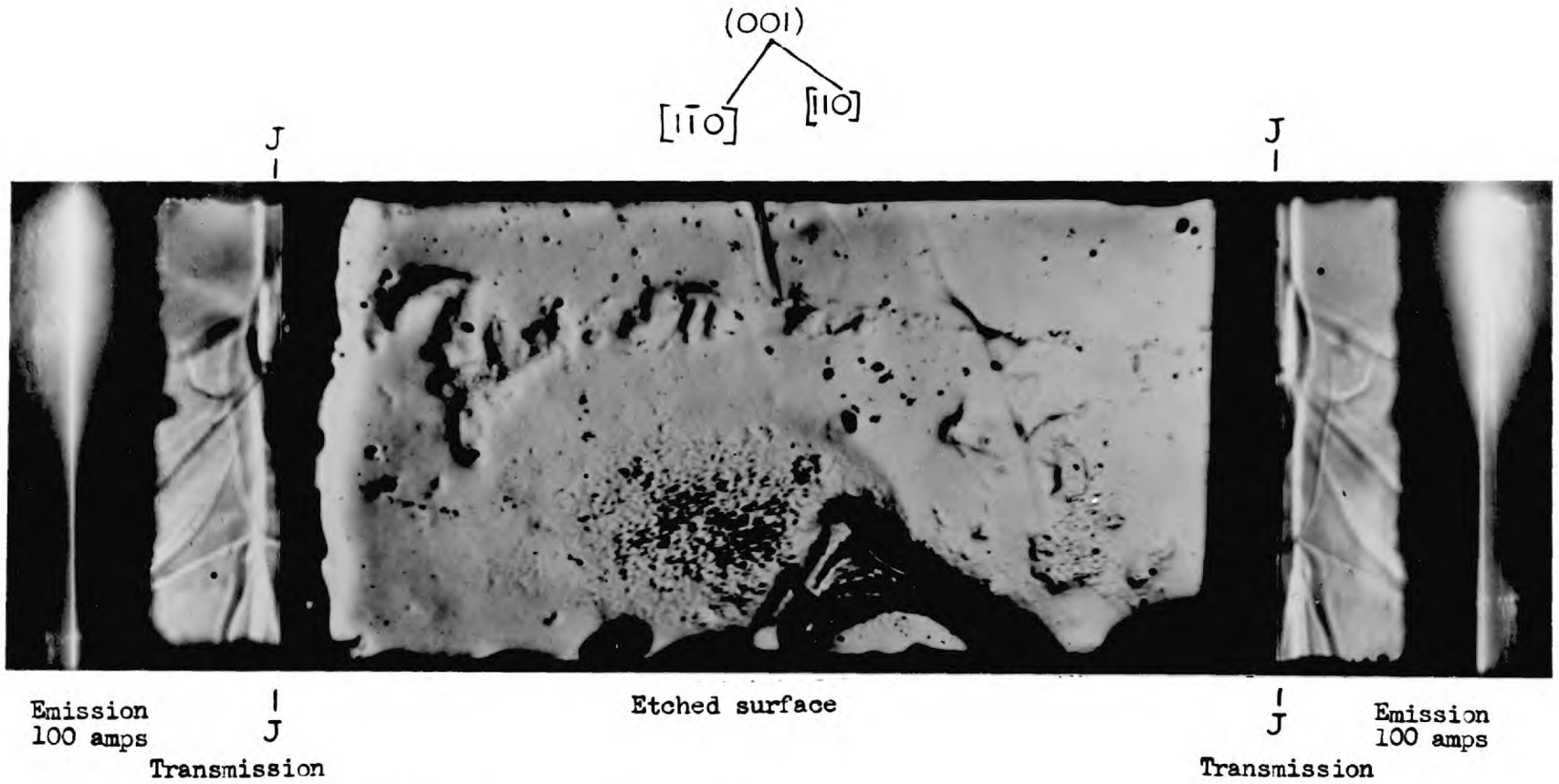

Fig 4.12. Diode No. 2613/7 Composite figure showing an etched surface in n - type material about 20μ from the p - n junction, along with transmission and emission micrographs for each diode face. Lines J - J mark the junction position on the transmission micrographs. The diode length was 2 mm.

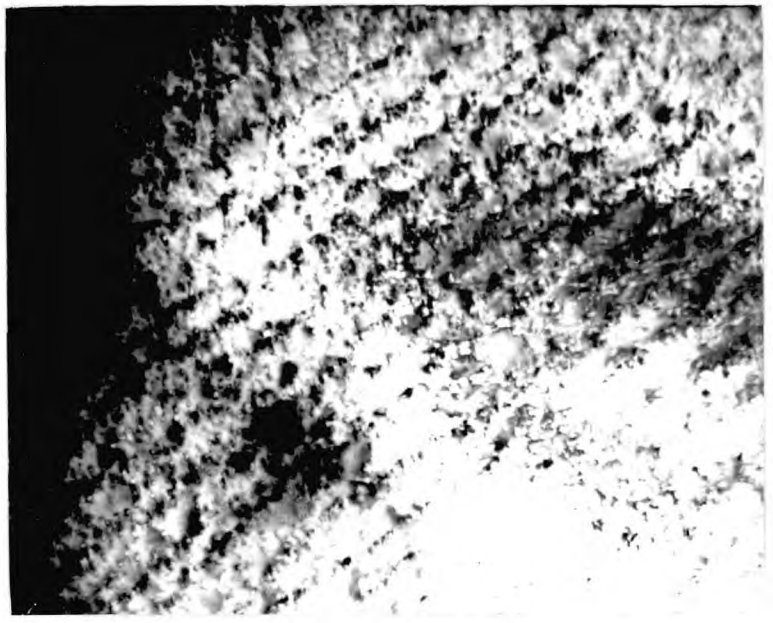

(a)

1 μ

(b)

10 μ

Fig. 4.13. Transmissi on electron micrographs of GaAs specimens thinned with (a) NaOCl. (b) 40HCl: $4H_2O_2$: $1H_2O$. In (b) the area transparent to electrons was greater than 80 μ in diameter.

(a)

1μ

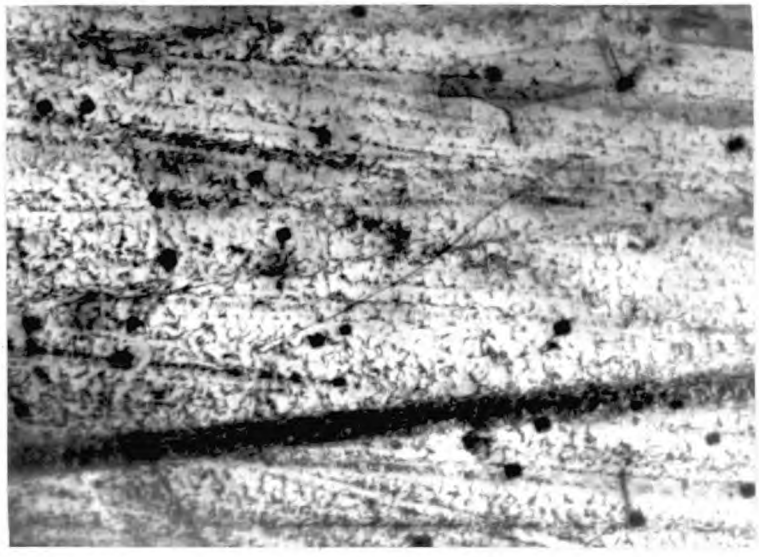

(b)

0·5μ

Fig. 4.14. Damage in GaAs revealed by transmission electron microscopy (a) Damage due to mechanical polishing, remaining after about 1μ had been removed from the surface by chemical polishing. (b) Damage caused by wiping a lens tissue across the specimen surface immediately before thinning. The black dots are precipitates and are not connected with the damage.

the resulting stresses in the crystal. Fig. 4.14.(b) shows the damage caused to GaAs by wiping the surface with a lens tissue immediately before jet thinning. The entire surface is covered with short range damage.

Figs. 4.15. and 4.16. show low magnification electron micrographs of thinned areas in the n sides of striated diodes 2659/6 and 5 respectively. In each case the thinned area crossed a striation which was in the [1 1 0] direction. A typical GaAs {1 0 0} diffraction pattern is shown for diode 2659/6. In this diode there was no sign of precipitation, but the form of the thickness contours shows the chemical polishing may not have been very uniform. In 2659/5 (fig.4.16) this was certainly true. In this specimen it was not possible to produce a perfectly smooth polish on one surface before thinning from the other side. When examined in the electron microscope, elongated dark areas were seen parallel to the striation direction. Dirt seen in this micrograph resulted from the specimen mounting technique which was still being perfected. The dark elongated areas were probably inhomogeneities which caused non-uniform chemical polishing.

Transmission electron micrographs of the p side of diodes 2640/1 and 2659/7 are shown in figs. 4.17 and 4.18 respectively. All the diodes whose p - type regions were examined by transmission electron microscopy contained precipitates and dislocations. In no cases were similar precipitates or dislocations found in the

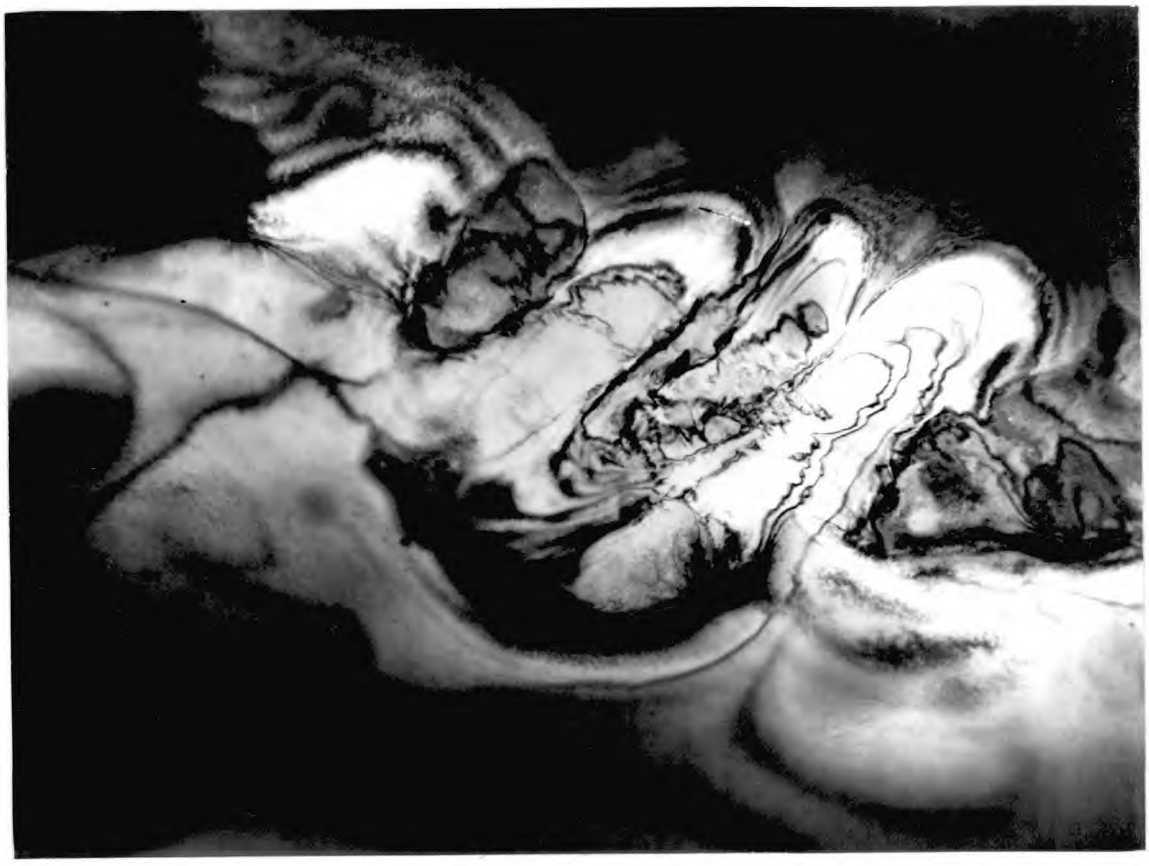

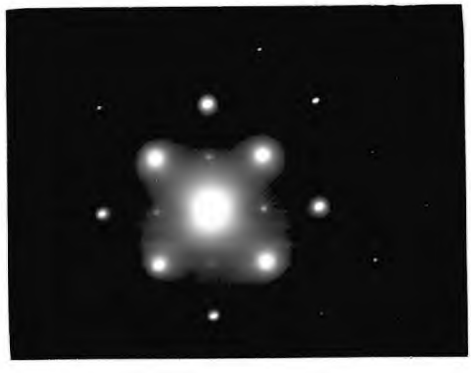

Fig. 4.15. Diode No. 2659/6. Transmission electron micrograph of an area crossing a striation in the n side. The striation direction is along [1 1 0]. The diffraction pattern from the micrograph is shown.

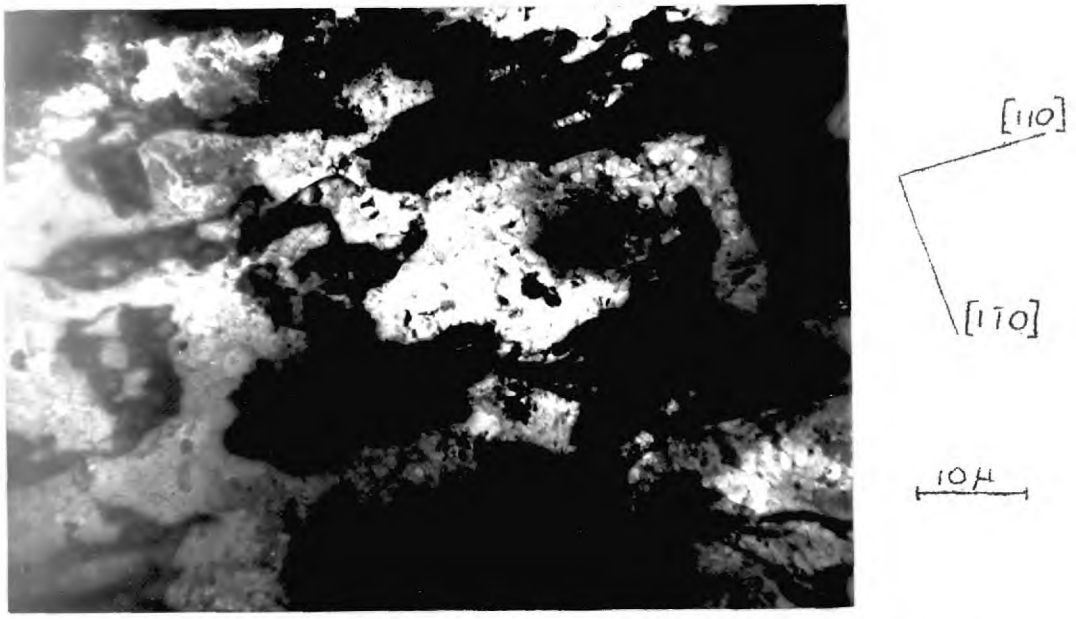

Fig. 4.16. Diode No. 2659/5. Transmission electron micrograph of an area including a striation in the n side. The striation direction is [1 1 0].

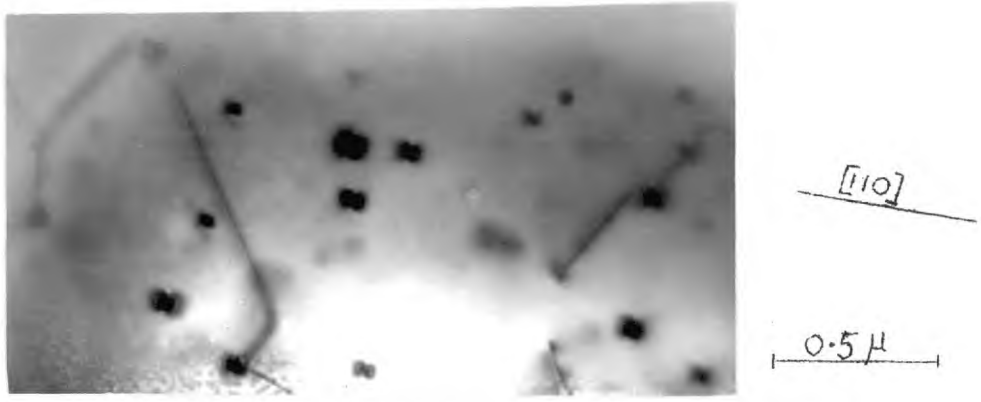

Fig. 4.17. Diode No. 2640/1 Precipitates and dislocations in the p side, seen by transmission electron microscopy. The double lobe contrast due to strain round the precipitates is clearly visible.

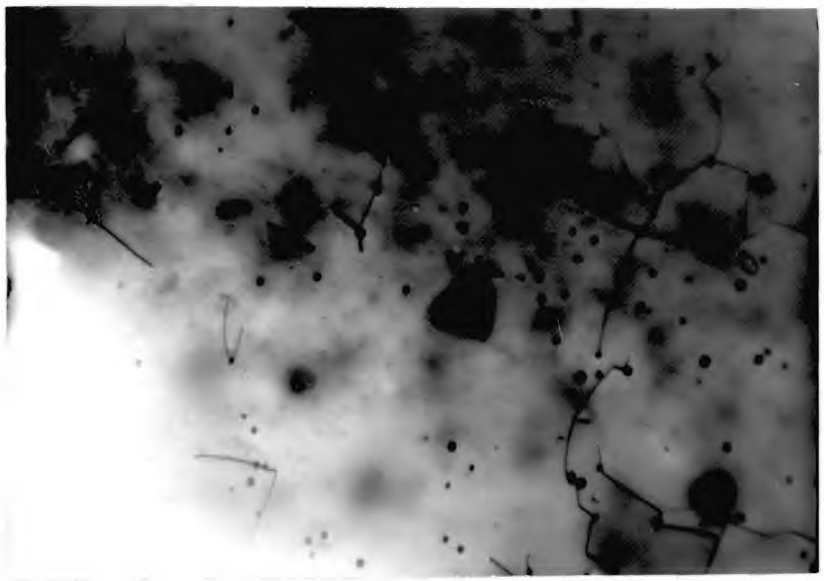

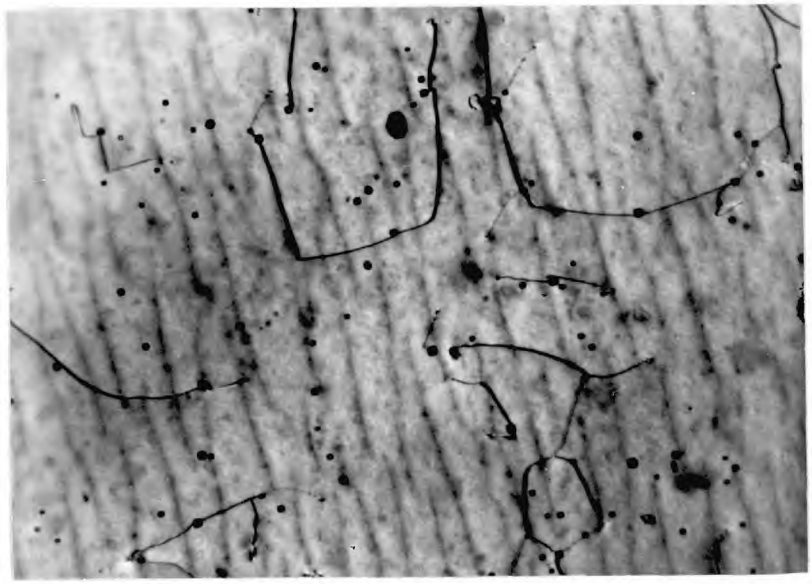

Fig. 4.18 Diode No. 2659/7. Transmission electron micrographs in the p side about 10 μ from the p - n junction, showing precipitates and dislocations. The two micrographs are from different portions of the same diode (see text).

n - type regions, even in diodes prepared under identical conditions at S.E.R.L. In fig. 4.17 the presence of strain contrast round the precipitates is clearly visible as dark loops. In this case the micrograph was taken under approximately two beam conditions. In the multiple beam case of fig. 4.18. no such contrast was seen, although the precipitate and dislocation densities were similar. The two micrographs of fig. 4.18. were of two different specimens from the same diode. Before jet thinning, the diode was cleaved into two pieces of approximately equal size and each of these thinned separately. In fig. 4.18. (b) there is a background of lines which covered the whole transparent area, while no sign of this was found in (a). This effect was found in two other specimens of the same orientation. It is thought that for certain heights of the specimen above the jet, and for certain flow rates of the chemical polish, the motion of the liquid over the specimen surface caused rippling similar to that caused by waves on the sea-bed.

Fig. 4.19. is a transmission electron micrograph of an area about 5μ below the surface of a slice of GaAs that was heavily Zn diffused in a similar manner to the diodes. The density of precipitates was much greater, and their size much smaller than in the other cases. No dislocations were seen in this specimen. The double lobe contrast characteristic of lattice strain is visible at many of the larger precipitates.

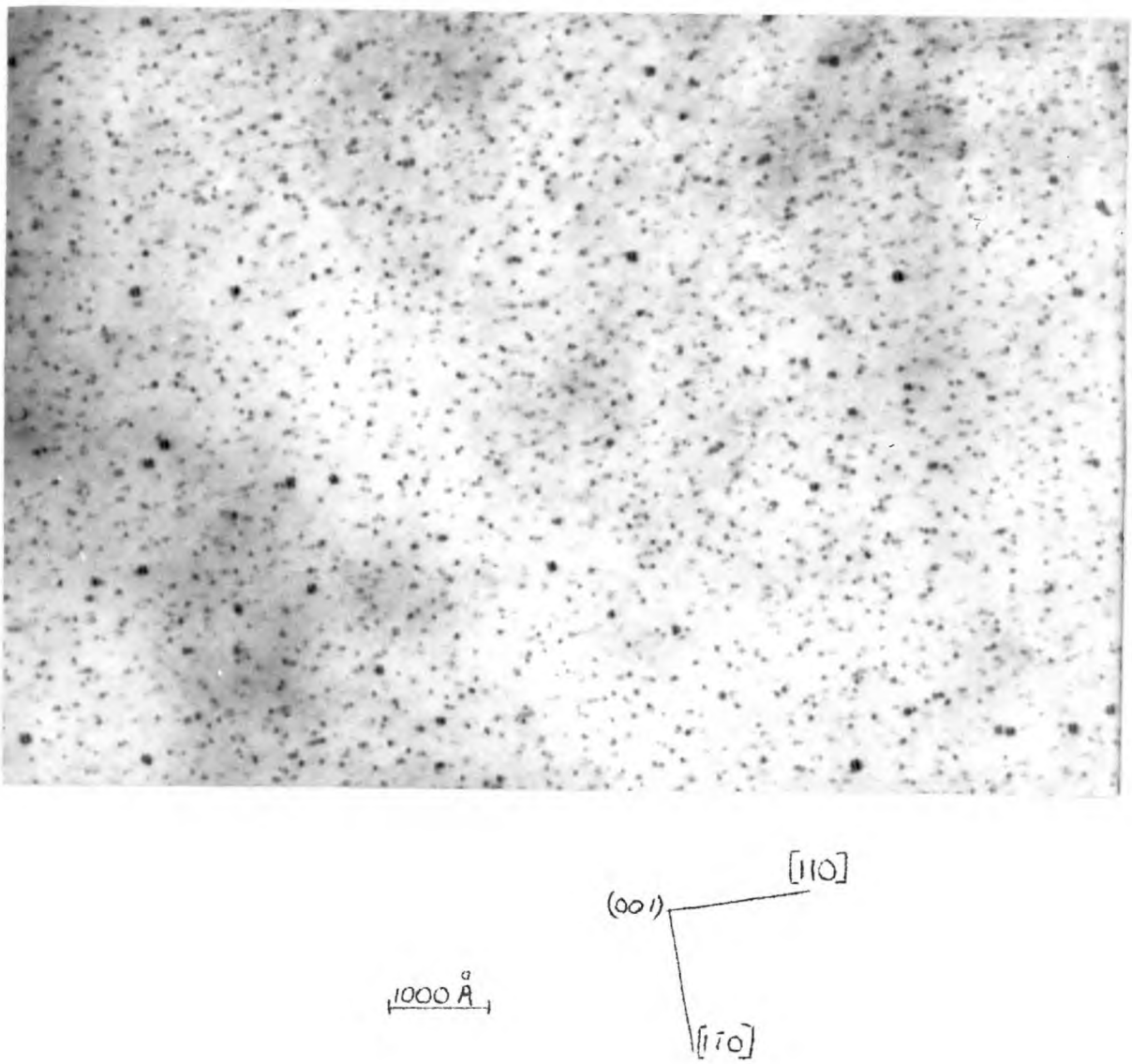

Fig. 4.19 Transmission electron micrograph of an area 5 μ below the diffusion surface of a slice of GaAs, which had been Zn doped in a similar manner to the diodes.

CHAPTER 5

Discussion of Results

The results which were presented in the previous chapter are discussed under two main headings. Defects revealed in heavily doped GaAs are considered in section 5.1, and in section 5.2 the effects of these defects on laser action are discussed.

5.1. Homogeneity of Heavily Doped GaAs

5.1.1. N - type GaAs

All the Te - doped diodes having the number 2659 were prepared from the same ingot, and all contained regular striations which were revealed by optical transmission and by etching. Striations were also found in a Czochralski grown Te - doped diode (3434/5). These striations were Te concentration variations of the type commonly found in bulk-doped semiconductor crystals. These are due to temperature fluctuations in the melt during growth and were discussed in section 2.4.5. In order to obtain further details of these Te fluctuations, the absorption results of Turner and Reese (1964) and of Hill (1964) at 77°K were plotted together in fig.5.1. The authors originally presented these results as curves of absorption coefficient α versus photon energy $h\nu$ for several different values of free electron concentration n_o. In fig. 5.1. they have been replotted as α versus n_o curves for several values of $h\nu$. At all the photon energies between 1·42eV (8,800Å) and 1·53eV (8,120Å), α decreases with increasing n_o when n_o is below about 4×10^{18} electrons/cm^3 and increases again rapidly above this value. These results were for Te doped samples except where

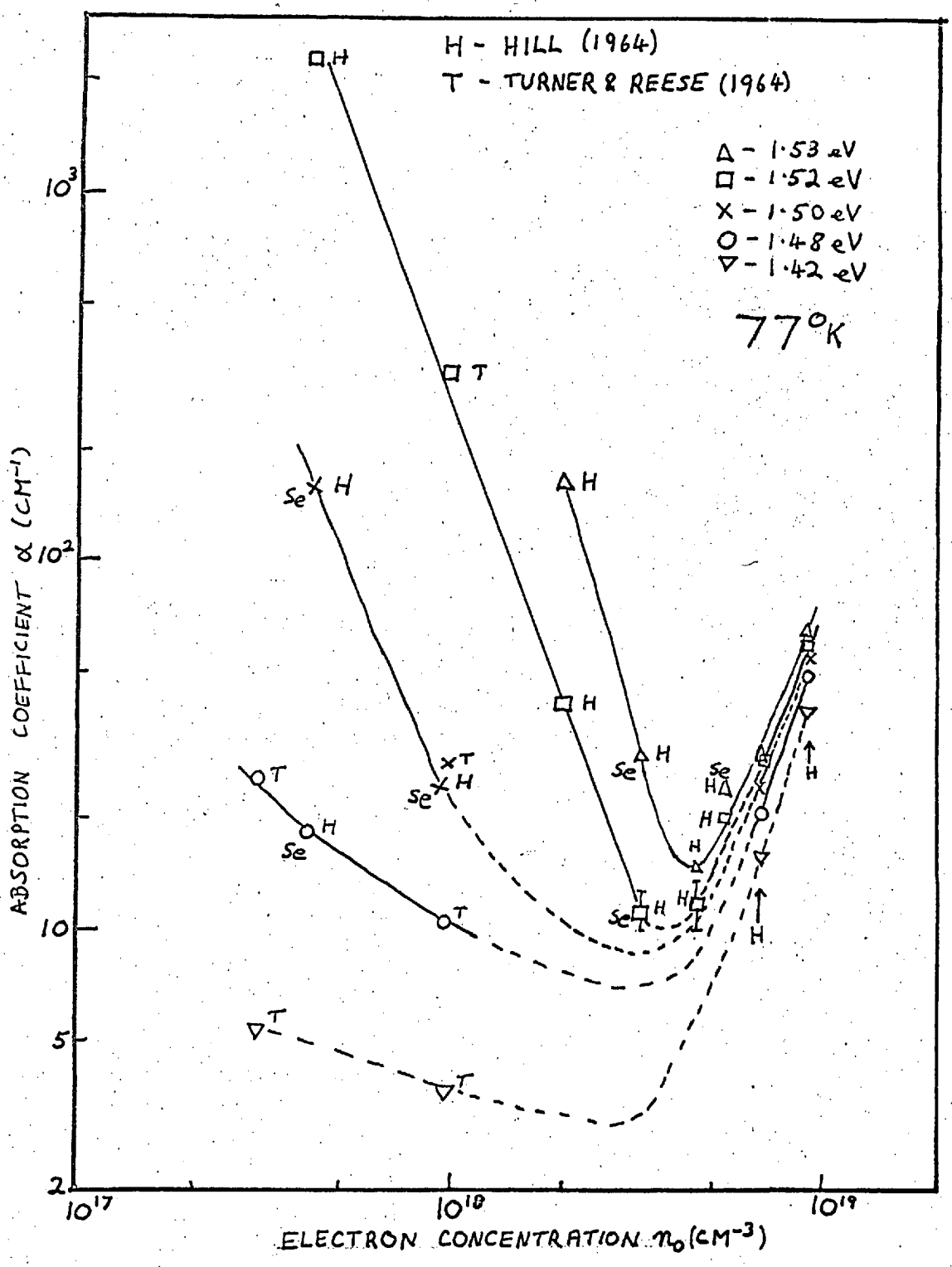

FIG 5.1 ABSORPTION COEFFICIENT α VERSUS ELECTRON CONCENTRATION, n_0 FOR SEVERAL VALUES OF PHOTON ENERGY $h\nu$ AT 77°K. THE POINTS ARE PLOTTED FROM THE RESULTS OF HILL (1964) AND TURNER & REESE (1964).

Diode No.	Donor	Diffusion Temperature	Excess As	Bright and Dark Bands	Fig.No.	Inhomogeneities in the n side
2613/6	Si	1100°C	No	Yes	4.2(i)	Some
2613/7	Si	1100	No	Yes	4.12	Gross
2640/5	Si	1100	No	Yes	4.4(b)	Mottled
2659/5	Te	1100	No	Yes	4.4(a)	Striations and segregation
2659/6	Te	1100	No	Yes	-	ditto
2659/7	Te	1100	No	Yes	-	ditto
2839/6	Se	850	Yes	No	4.8(i)	One small defect
2839/10	Se	850	Yes	No	-	None
3434/5	Te	850	Yes	No	4.4(c)	Striations

Table 5.1. Summary of the optical transmission results. Columns IV and V refer respectively to the presence of excess As during diffusion, and the presence of the bright and dark bands parallel to the junction. Column VII summarises the other details seen in the n - type material.

shown otherwise. In these curves the region shown dotted is only an indication of the form the curve might take if sufficient experimental points were available. It is clear that a great deal more information, at many more values of n_o is needed before the complex behaviour of α at near - absorption - edge wavelengths can be fully understood. Fig. 5.1. shows why the region of 2 X 10^{18} electrons/cm^3 has been found to be the optimum doping level for the n side of junction lasers and lamps at 77°K. Absorption is a minimum and the doping level is high enough to satisfy the conditions mentioned by Keyes (1963) for an inverted population (section 2.3.2.). The optical transmission micrographs of Chapter 4 were all recorded on film which was sensitive only to wavelengths shorter than 8,800Å (1·42eV). Hence only photon energies between 1·42eV and the absorption edge at about 1·52eV were recorded. This range includes the laser emission wavelength at 100°K which is about 1·46eV.

The average donor doping level of all the diodes examined here was given as 2 ($\pm$1) X 10^{18} electrons/cm^3. Fig. 5.1 shows that throughout the n_o range of 1 to 3 X 10^{18}electrons/cm^3 the absorption coefficient α decreases rapidly as n_o increases, for all the wavelengths considered. The rate of decrease of α with increase of n_o is greatest at photon energies $\geq$ 1·50eV, i.e. in the absorption edge. This is illustrated in the 1·52eV curve where $\pm$ 25% variation in n_o gives a nearly fourfold variation in α.

Although the variation is less steep at the lower photon energies of the range, it appears to be sufficient to explain the striated contrast seen in the micrographs of the Te - doped diodes.

Precipitation of Te is thought to start at concentrations of about 5 X 10^{18} electrons/cm^3 (Meieran (1965)) and is the probable cause of the sharp rise in α at n_o values very close to this (fig. 5.1.).

At this point a discussion of the cathodoluminescence efficiency η_c of Te doped GaAs is relevant. Cusano (1964) found that η_c at 77°K and 300°K increased with n_o up to a value of 2 X 10^{18} electrons/cm^3, and dropped rapidly on increase of n_o above about 5 X $10^{18}/cm^3$. Casey (1967) found the same effect at 300°K. Cusano suggested this was due to the onset of precipitation, which caused non - radiative recombination at associated defects. Wittry (1966) found evidence of the presence of Te in an unionised form at room temperature in a specimen having an average free electron concentration of 5·2 X $10^{18}/cm^3$. He found by X - ray microanalysis that Te concentration varied by 30% across the striations but found no spectral shape change of the recombination radiation. From this he concluded that any free electron concentration variations were $< 10\%$. He also found that cathodoluminescence increased in the bands of lower Te concentration, which confirmed that n_o was above the concentration of the peak value of η_c. Thus in Wittry's sample the cause of striation contrast was probably Te precipitation in the dark bands. Fig. 5.2 summarises the behaviour of Te in GaAs with increasing concentration, and also the way in which η_c and α vary. The values at which the various changes occur are not well defined and

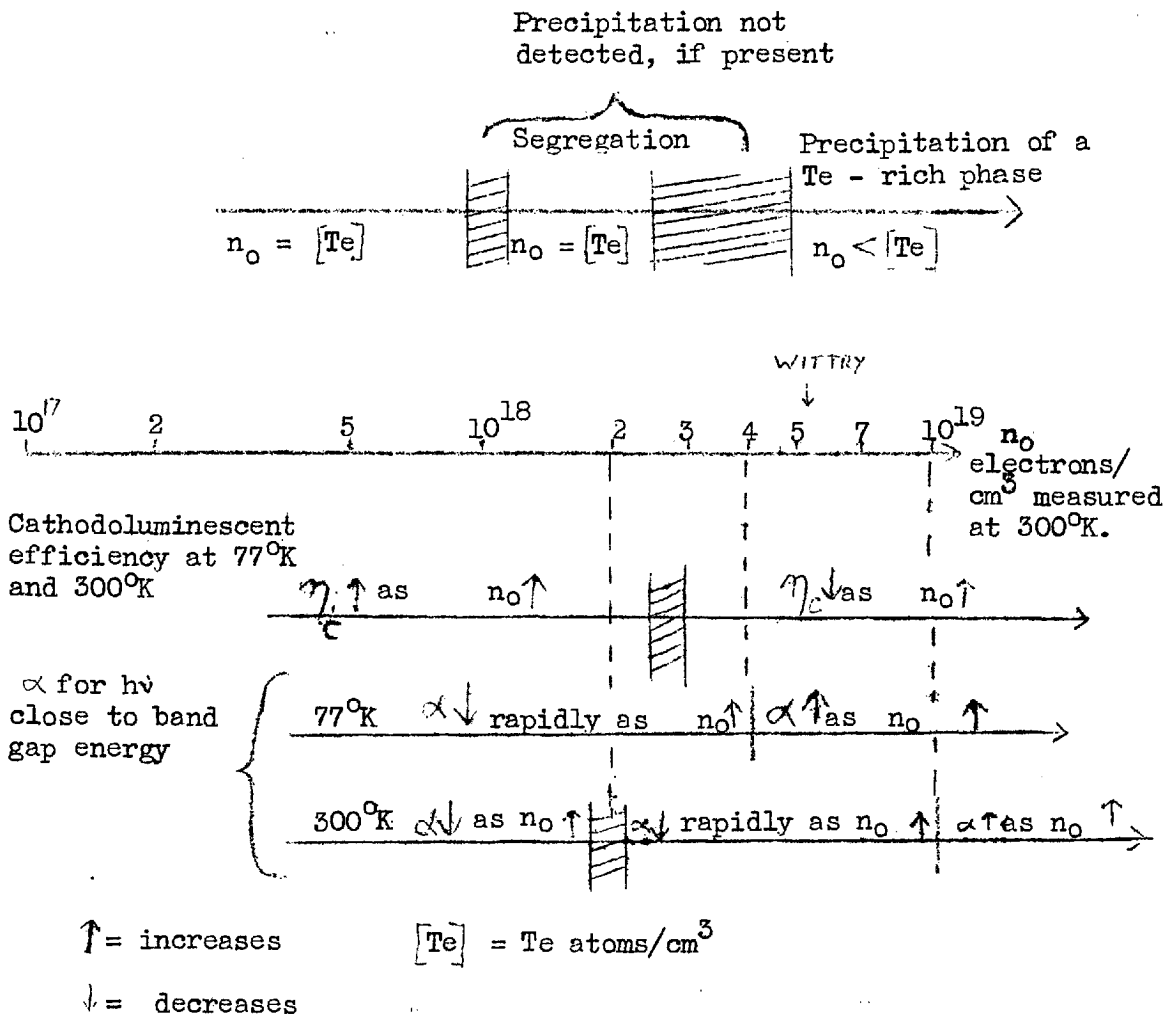

Fig. 5.2. A summary of the proposed behaviour of Te in GaAs with increasing n_o, and the resultant way in which cathodoluminescent efficiency η_c and absorption coefficient α vary. The values at which the changes occur which are not well defined are indicated by shaded regions. By following a vertical line in the diagram, the behaviour of η_c and α of a specimen doped to any n_o is described. The information on α came from the absorption data of Turner and Reese (1964) and Hill (1964) (see also fig. 5.1.) ~~and fig. A.5 of the Appendix)~~ and on η_c from the work of Cusano (1964).

are indicated by shaded boundaries. The position of Wittry's sample is shown.

The transmission samples studied here had concentrations of Te below the proposed level at which precipitation occurs. This was confirmed by the lack of precipitates in the transmission electron micrographs of the n side of two of the Te - doped diodes. The bands of high transmission were therefore bands of high n_o, (see fig. 5.2). This fact will be used in the discussion of the threshold current equation (section 5.2.)

Holt and Chase (1968) using the SEBECC technique and Shaw (1967) using the SEBERR method both found evidence of Te interaction with defects in diodes having the same Te concentrations as those used in this work, i.e. below the level for onset of precipitation. Both techniques produced images having dark centres with bright haloes outlining them. Holt and Chase suggested that the dark regions were due to increased Te concentration and the haloes were due to denuded zones from which some Te had diffused. In the optical transmission micrograph of fig. 4.4.(a), internal crystal defects other than the striations can be seen. These are in the form of short straight lines and randomly oriented lines and dots. This type of detail was seen in all the Te doped diodes but not in Se or Si doped ones. Shaw, and Holt and Chase also found evidence of impurity interaction with defects only in Te doped diodes. Shaw pointed out that the "misfit" of Te on As sites in GaAs was considerably greater than the misfit of Se on As sites or Si on either

site. Because of this, Te is more likely to segregate at defects than atoms having a lesser misfit. Thus it is proposed that the lines and dots observed in Te doped diodes were dislocations or other crystal defects to which Te had segregated. However, the degree of segregation may be very small and is below the level at which precipitation occurs, i.e. n_o as well as Te concentration increases at the defects. This is supported by the fact that the transmitted intensity at these defects is increased and is surrounded, in some cases, by narrow dark areas. This is consistent with increased n_o and decreased α at the centre, and vice versa in the surrounding volume. The density of these defects is very small and would not be detected by transmission electron microscopy.

Casey(1967) attempted to make a semiquantitative interpretation of his SEBERR results on Te doped GaAs at 300°K. From the the lack of spectral shape change he concluded that n_o variations across the striations and the dark dots with haloes, were $< 10\%$. To explain the contrast, he assumed that Te was present in an unionised form at electron concentrations as low as $1 \times 10^{18}/cm^3$, but this is inconsistent with the optical transmission results discussed above. It is possible that precipitation of a Te-rich phase does not occur until about 3×10^{18} Te atoms/cm^3 (see fig. 5.2). However, a completely consistent explanation of the contrast occurring in cathodoluminescence of Te doped GaAs is yet to be found.

Se is known to be present in an unionised form in GaAs at electron concentrations as low as $4 \times 10^{17}/cm^3$ (Vieland and Kudman (1963)). Precipitates, probably of Ga_2Se_3 were found by

transmission electron microscopy by Abrahams, Buiocchi and Tietjen (1966) at electron concentrations above 2 X $10^{18}/cm^3$. The Se diodes examined here appeared very uniform by optical transmission microscopy and no sign of precipitation of the type found by Abrahams et al was seen by transmission electron microscopy. The Si doped diodes also showed no precipitates although they did show large scale inhomogeneities in optical transmission and by chemical etching (fig. 4.12.). Table 5.1. gives a summary of the results found by optical transmission in the diodes.

It is concluded from this discussion that the Te doped diodes studied here were doped to a level below that at which precipitation begins, although segregation of Te was occurring round crystal defects and in the striations. The Te variation due to this segregation was probably less than 10% but optical transmission using wavelengths close to the absorption edge was sensitive to these small variations.

5.1.2. Effect of Zinc Diffusion on Donor Distribution

The presence of the dark and bright bands seen by optical transmission just ahead of the diffusion front in several of the laser diodes is discussed in this section. Column V of table 5.1 refers to the presence or absence of these bands. They were most pronounced in Si doped diodes, less so in Te doped (2659) diodes and not visible in Se doped diodes. Larrabee and Osborne (1966) and Peart et al (1966) using the radio - tracer technique found fluctuations of up to 40% in the distribution of the amphoteric

substrate dopants Cu and Mn in the region of Zn diffusion fronts in GaAs. The explanation given for these distributions was that the potential field in the junction region caused preferential diffusion of some of the donor atoms away from the junction. From the results obtained in this work it is suggested that the same effect occurs to some extent in the cases of Te and Si in GaAs. Variations of less than 10% in the donor concentration could cause the observed effect. The effect of acceptor diffusion on Te, Se and Si distributions does not appear to have been studied. All three of these elements have at least one isotope each, suitable for the radio - tracer work that is necessary to confirm the proposed explanation of the dark and bright bands.

Table 5.1 shows that all the diodes which had dark and bright bands ahead of the junction were diffused at 1100°C with no extra As present in the diffusion tube, and those that showed no bands were diffused at 850°C with added As. Thus two mechanisms may be playing a part in the effect:diffusion temperature and As vapour pressure. At the higher diffusion temperature the mobility of the impurity atoms will be greater than at the lower temperature. The As vapour pressure controls the number of As vacancies (McCaldin and Harada (1966)) and thus also affects the diffusion of Te and Se which occupy As sites when acting as donors. The effect of As pressure should be most pronounced in Si doped material. As Si is a group IV element, it may occupy group III or V sites in the sphalerite structure. When occupying Ga sites it acts as a donor,

and Si doped GaAs is generally n - type. When an increasing fraction of Si atoms occupy As sites the material becomes compensated and eventually p - type. The fact that in diode 2613/7 the bright band was not straight, was due to the non - uniform distribution of Si in the substrate crystal. This was clearly seen throughout the n side of the diode and was revealed by etching (fig. 4.12.)

Unfortunately there is very little data available on diffusion of donors in GaAs. Also, the extent to which the junction field affects the diffusion process is unknown. Te has the greatest lattice misfit of the three donors considered, and may be expected to diffuse more readily than Se and Si. However, the amphoteric properties of Si may explain its increased diffusion ahead of the junction.

5.1.3. P - type GaAs

The laser diodes were examined in the p side by chemical etching and transmission electron microscopy (T.E.M.). Optical transmission techniques could not easily be applied to p - type material because the absorption coefficient was at least an order of magnitude greater than that for the n - type material. The results of T.E.M. applied to p - type GaAs, given in figs. 4.17 - 4.19, all show conclusive evidence for precipitation of what must be a Zn rich phase. Fig. 4.18. shows the p side of diode 2659/7 at a distance of about 10 μ from the p - n junction. Apart from the fairly uniform distribution of precipitates there are many dislocations

present. Since the n side of two diodes from the same diffusion run and same substrate crystal showed no dislocations or precipitates (see fig. 4.15), both the precipitates and dislocations must have been diffusion induced. Many of the dislocations are pinned at precipitates with sections which have bowed out between the precipitates as if stress induced glide had occurred after formation of the precipitates. This means that the precipitates were formed before the dislocations stopped moving and were therefore present during the diffusion process. Fig. 4.19 shows an area about 5 μ beneath a diffusion surface. The precipitates are very much smaller and there is no sign of a dislocation density comparable with that shown in fig. 4.18. Fig.4.17 was taken under two beam diffraction conditions in the electron microscope and shows the characteristic lobe contrast of spherically symmetric coherency strain surrounding the precipitates. This was also seen in some of the larger precipitates of fig.4.19. The line of no contrast is perpendicular to the operating reciprocal lattice vector $\underline{g}$ as is found for small spherical, tetrahedral or cuboid precipitates. There is some evidence in figs. 4.18(b) and 4.19 that the precipitates have a square cross-section. Nothing was detected in the diffraction patterns which could be attributed to the precipitated phase, but a thorough search was not carried out.

An order of magnitude calculation of the precipitate densities assuming a specimen thickness of 5,000$\mathring{A}$ gives $\sim 2 \times 10^{13}$ precipitates/cm^3 in fig.4.18 and $\sim 5 \times 10^{15}$/cm^3 in fig.4.19. Etched surfaces in p - type material always appeared heavily mottled (figs. 4.10 & 4.11). This is to be expected on the assumption that

the precipitates seen by T.E.M. etched preferentially. The density of etch pits counted on etched p - type surfaces agreed to within an order of magnitude with that seen by T.E.M. Accurate comparison cannot be made unless the thickness of the T.E.M. specimens and the depth over which the etchant has an effect are known.

Black and Jungbluth (1967a) found precipitates due to Zn diffusion in GaAs, but were uncertain of their origin, and Black (1967) subsequently showed that some of the precipitates, at least, were Zn rich. As mentioned by Black and Jungbluth, the methods of determining Zn concentrations in GaAs have an accuracy of only 30%. Hence it is possible that the diodes examined here (1×10^{20} Zn atoms/cm^3 by electron probe) had up to 3×10^{19} Zn atoms/cm^3 in an unionised form. From the densities of precipitates mentioned above this gives approximately 10^6 and 5×10^3 Zn atoms per precipitate in figs. 4.18 and 4.19 respectively. The sizes of the precipitates seen in these figures are not inconsistent with these numbers of atoms per precipitate. These precipitates are relatively small and it is possible that they may adopt the sphalerite structure of the host matrix and would therefore be coherent.

Some possible compositions of the precipitates are Zn_3As_2, $ZnAs_2$ and pure Zn. $ZnAs_2$ has a triclinic structure and Zn a hexagonal structure with large c/a ratio, so that neither of these is likely to form coherent precipitates in the sphalerite structure. Zn_3As_2 has a tetragonal space group and a pseudo - body - centred - cubic structure. The arrangement of the Zn and As atoms in this

structure is uncertain, but it is likely that coherent precipitates could be formed with the sphalerite structure. Panish (1966), in studying the Ga - As - Zn system found precipitation of Zn_3As_2 over a considerable range of Zn concentrations. Chase (1968) using electron probe microanalysis has also found large precipitates of Zn_3As_2 at the diffusion surfaces of GaAs slices diffused under identical conditions to the diodes studied here.

Figs.4.17. and 4.18 both show areas close to where the diffusion profile approaches the steep diffusion front and the dislocations seen here might be associated with this diffusion front. Many segments of dislocations run along the $[1\ 1\ 0]$ and $[1\ \bar{1}\ 0]$ directions as is expected if they are the pure edge dislocations which relieve the "misfit" strain at the diffusion front (see the following section).

Direct evidence of precipitation during diffusion of Zn into GaAs has been found by transmission electron microscopy and supported by chemical etching. This confirms the work of Black and Jungbluth (1967 a & b). It has been shown that much information on the diffusion of Zn and on dislocation structures in GaAs can be obtained by transmission electron microscopy and that further systematic work is required.

5.1.4. The Junction Region

Chemical etching revealed lines along $\langle 1\ 1\ 0 \rangle$ directions in the junction regions of all the diodes having (0 0 1) junction

planes. Very little detail of these lines could be seen except in the thin region at the junction where most of the mottling had vanished. Fig.4.9. is an etched surface in this narrow region and shows the rows of etch pits (R) in the $[1\ \bar{1}\ 0]$ direction and grooves (G) in the $[1\ 1\ 0]$ direction. The average distance between these etched lines was about 20μ. In the (0 0 1) plane, misfit dislocations are expected to lie along $<1\ 1\ 0>$ directions and the spacing between them was given by Holt (1966) as

$$p = \frac{\lambda_1 \lambda_2}{\sqrt{2}(\lambda_1 - \lambda_2)} \qquad (5.1.)$$

where λ_1 and λ_2 are the mean lattice parameters on the two sides of the junction. From the tetrahedral covalent radii of Ga, As and the added impurities, λ_1 and λ_2 may be calculated. These radii were given by Pauling (1960) and are: Ga 1·26Å; As 1·18Å; Te 1·32Å; Si 1·17Å; Se 1·14Å and Zn 1·31Å. The expected spacing p, of the misfit dislocations for the doping levels of the diode of fig. 4.9 is calculated here. In the n side of the junction the Te concentration was 2 X 10^{18}atoms/cm^3. In GaAs there are 2·2 X 10^{22} As sites/cm^3 and assuming all the Te atoms occupy As sites this means that 1 in 10^4 As sites are occupied by Te atoms. Assuming that Vegard's Law applies, the average atomic radius of As sites is increased by 10^{-4}(1.32 - 1·18) Å throughout the crystal. If there are 1 x 10^{19} Zn atoms/cm^3 in the p - type region all of them occupying Ga sites and all ionised, then the average atomic radius of Ga sites is increased by 5 X 10^{-4}(1·31 - 1·26) Å. The lattice parameter λ

is given by $\lambda = {}^{4d}/_{\sqrt{3}}$ where d is the bond length between two atoms and is the sum of the two covalent radii. Using equ. (5.1) gives the calculated spacing of the misfit dislocations for the Te doped diodes studied here. A Zn concentration of $10^{19}/cm^3$ gives a dislocation spacing, p, of 40$\mu$and 2 X 10^{19} Zn atoms/cm^3 gives p = 20μ. The value of the Zn concentration to be used in this calculation is that at the knee of the diffusion front, just before the steep Zn concentration gradient (fig.2.6.) However, since a significant proportion of the Zn has been shown to be in the form of precipitates and consequently cannot contribute to the hole concentration, the exact value of Zn concentration to be used is uncertain. The calculated spacing p is probably between 10 and 100$\mu$and agrees well with the value of about 20 μ seen in fig.4.9. The spacing calculated assumed that all the dislocations were in one atomic plane. In diffused junctions this is not so, but the etch will leave an effect due to dislocations over a depth of several microns after the dislocation has been removed. Therefore a picture of all the dislocations in the junction region may be obtained. Transmission electron microscopy examines too thin a layer at too high a magnification to do this. Hence arrays of misfit dislocations were not detected by this technique. However at distances of a few microns from the junction in the p - type material, transmission electron microscopy did reveal apparently random arrays of dislocations which could not be detected by etching.

There is an apparent difference in the etching behaviour of dislocations in the $[1\ 1\ 0]$ and $[1\ \bar{1}\ 0]$ directions. In the $[1\ 1\ 0]$ direction the dislocations etched as continuous grooves over lengths of several hundred microns and in the $[1\ \bar{1}\ 0]$ direction they appeared as rows of approximately equally spaced dots. A difference in these etching properties was noticed by Abrahams and Buiocchi (1966) in epitaxial junctions, and they suggested an explanation based on the difference in core structure of dislocations in the two $[1\ 1\ 0]$ directions.

Fig. 5.3. shows drawings of the (1 1 0) and (1 $\bar{1}$ 0) planes perpendicular to the (0 0 1) junction plane between two GaAs structures having different lattice parameters. This model is a greatly simplified representation of the interface and is a closer approximation to an epitaxial junction than a diffused one. Five atoms above the interface (J - J) correspond to four atoms below. A misfit dislocation in each of the $\langle 1\ 1\ 0 \rangle$ directions in the (0 0 1) plane is seen, as described by Holt (1966). Fig. 5.3.(a) is the view looking along the $[1\ 1\ 0]$ direction which is normal to the plane of the diagram. A pure edge dislocation is present in this $[1\ 1\ 0]$ direction and a double row of dangling bonds is shown. The dotted lines are projections of the $(1\ \bar{1}\ 0)$ planes on the (1 1 0) plane. They show the distortion round the dislocation core and the two half planes which terminate at the dislocation. Fig. 5.3.(b) is the view in the $[1\ \bar{1}\ 0]$ direction perpendicular to the (0 0 1) interface and perpendicular to the

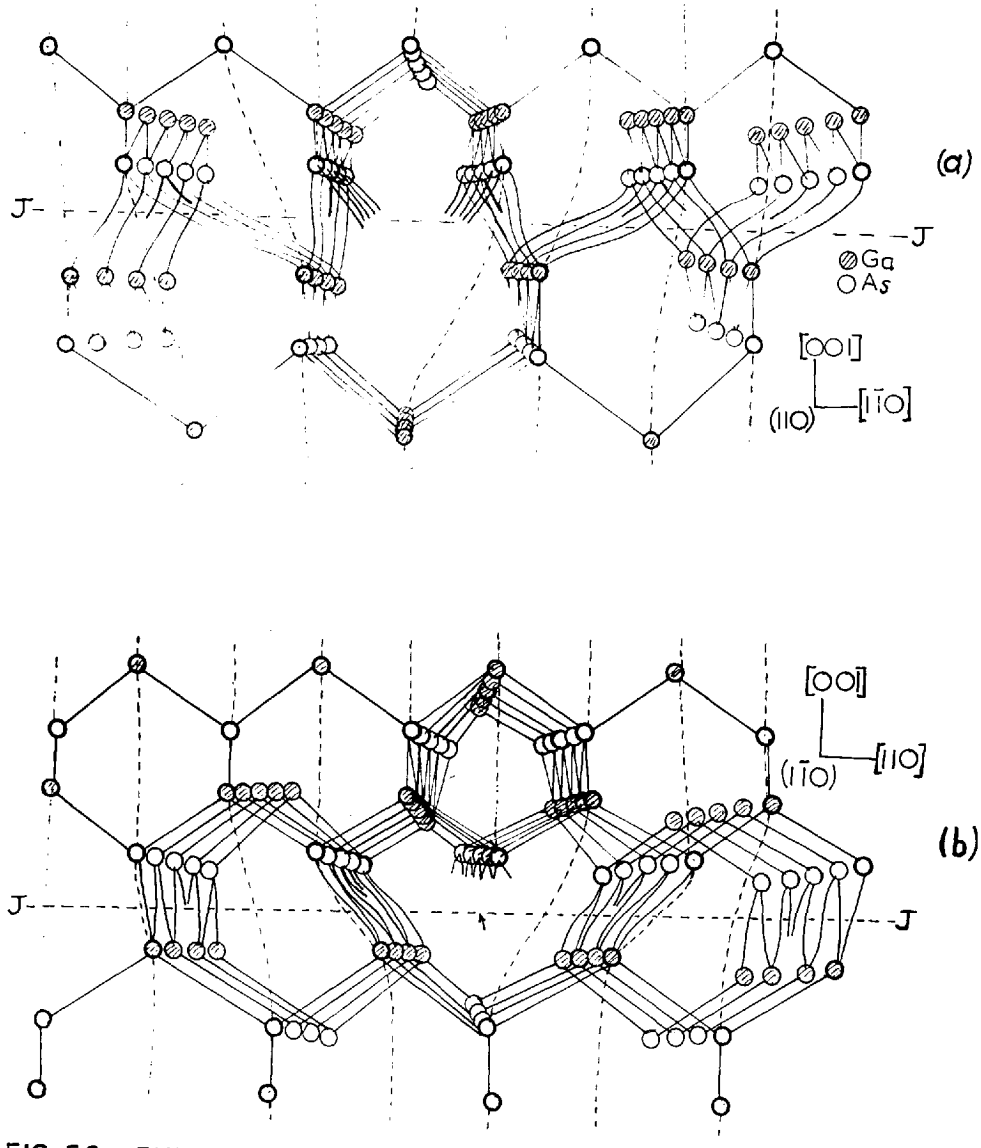

FIG. 5.3 END-ON VIEWS OF MISFIT DISLOCATIONS IN THE (001) INTERFACE ALONG (a) THE [110] & (b) THE [1$\bar{1}$0] DIRECTIONS. (SEE TEXT)

view of fig.5.3.(a). The interface (J - J), is again shown and the dislocation in the $[1\ \bar{1}\ 0]$ direction now has along its core, a row of As atoms each having two dangling bonds. These bond directions lie in the (1 1 0) plane. If this row of atoms diffuses away, the dislocation is then geometrically similar to that of fig.5.3.(a), except that all the dangling bonds come from Ga atoms instead of As atoms. The dislocation core is also then half a lattice parameter above the junction plane. Abrahams and Buiocchi assumed this central row of atoms was not present and considered the two geometrically similar dislocations. They explained the difference in etching characteristics of the $\langle 1\ 1\ 0 \rangle$ dislocations as being due to preferential Zn decoration of the $[1\ 1\ 0]$ dislocation which has missing Ga atoms at its core. Zn on Ga sites is electrically more favourable than on As sites. The question arises of whether the row of As atoms in the core of the $[1\ \bar{1}\ 0]$ dislocation is present or not. If it is present, then Zn atoms could be electrically satisfied by decorating this row. The only reason to suppose that the row of As atoms does diffuse away, is that each As atom has only two satisfied bonds, whereas when the As atoms have gone, the remaining atoms in the dislocation core all have at least three satisfied bonds each.

If the proposal of Abrahams and Buiocchi applies, then Zn decoration on $[1\ 1\ 0]$ dislocations will begin more easily than on $[1\ \bar{1}\ 0]$ dislocations. The etching results obtained here can be explained if the arrays of dislocations revealed were misfit

dislocations. Those in $[1\ 1\ 0]$ direction were heavily Zn decorated and those in $[1\ \bar{1}\ 0]$ direction less so, but still to some extent.

Although decorated misfit dislocations were detected in most diodes they did not correlate with laser emission patterns even when the dislocations were parallel to the laser active filaments. This was contrary to the results of Abrahams and Buiocchi who found the filaments coincided with the misfit dislocations. Therefore another defect was playing the major part in determining the emission patterns in the diodes examined here.

By considering only the (0 0 1) planes of atoms adjacent to the interface in fig. 5.3. it is seen that there is maximum strain between the planes when one atom on the upper plane is immediately above one on the lower plane. Holt (1966), in fig.7. of his paper, showed a view of two (0 0 1) planes of different lattice parameters at a junction viewed from the [0 0 1] direction. However, the dislocations were drawn at the regions of minimum lattice strain instead of at the regions of maximum strain.

5.2. The Threshold Equation

In this section the results are discussed with reference to the equation for the current density at laser threshold which was derived in section 2.3.3. The equation is

$$j_t = \frac{8\pi e \bar{n}^2 \nu^2 \Delta\nu \; d}{\eta c^2} \left[\frac{1}{\ell} \ln \frac{1}{R} + \alpha\right] \qquad (5.2.)$$

$$= \frac{1}{\beta} \left[\frac{1}{\ell} \ln \frac{1}{R} + \alpha\right] \qquad (5.3.)$$

where

e	=	the electronic charge
$\overline{n}$	=	refractive index
ν	=	frequency of laser emission
$\Delta\nu$	=	spontaneous emission linewidth
d	=	active region thickness
η	=	external quantum efficiency
c	=	velocity of light in vacuo
ℓ	=	diode length
R	=	reflectivity
α	=	absorption coefficient in the active region

Spatial variations of these factors inside each diode are considered.

5.2.1. Temperature

Although the temperature does not enter explicity into equ. (5.2.) it is an extremely important factor in determining the threshold current density. Equ. (5.2) was derived assuming an electron distribution corresponding to $T = 0^{o}K$, but the functional form of the equation is obeyed experimentally up to $300^{o}K$. The temperature dependence arises almost entirely from that of the gain factor β (Pilkuhn, Rupprecht and Blum (1964)). All the diodes examined here were operated under identical conditions of temperature and pressure in the cryostat. However the effect of diode heating during operation was noticed in several ways. When a diode was switched on at a current above threshold, the light output detected by the Si cell decreased for about two seconds until thermal equilibrium in the diode was reached. It was also noted that the threshold current increased by up to 5% when the pulse repitition rate was increased by an order of magnitude. Because of this the diodes were all operated at pulse frequencies of about 20 per second. At high current densities, well above threshold the pulse shape was as

shown in fig. 3.4.(b). The quenching effect due to heating during the pulse is seen. Broom et al (1963) used a similar cryostat to that used here, and estimated the diode temperature to be about 100°K. During operation, the mean temperature in the diodes studied here was probably about the same.

5.2.2. Absorption Coefficent, α.

The behaviour of the absorption coefficent, α with inhomogeneities in the n - type material was discussed in section 5.1.1. However the problem here is to determine the behaviour of α in the compensated region just on the p side of the junction where laser action occurs. In this region the Zn concentration varies very rapidly. This is shown in fig.5.4. where a 25% change in Zn concentration occurs over a distance of about $\frac{1}{4}\mu$. This means that α which is highly dopant dependent near band - gap energies, is subject to large changes over short distances. Any substrate inhomogeneities in this junction region must be expected to have a large influence on the absorption coefficent. The results of Hill (1964) and Turner and Reese (1964) for compensated p - type material show that α variations with dopant changes are sufficient to explain the effect on threshold current. Direct correlation of α with emitted intensity was also found (fig.4.7).

Variations in donor concentration may be seen to affect α through the variation of the position of the quasi - Fermi level F_c. The position of F_c drops as donor doping level decreases. If $F_c - F_v$ is then not greater than $h\nu$, absorption instead of gain occurs in the active region. This may also be seen as a Burstein shift of the absorption edge to lower energies which causes α at the laser frequency to increase.

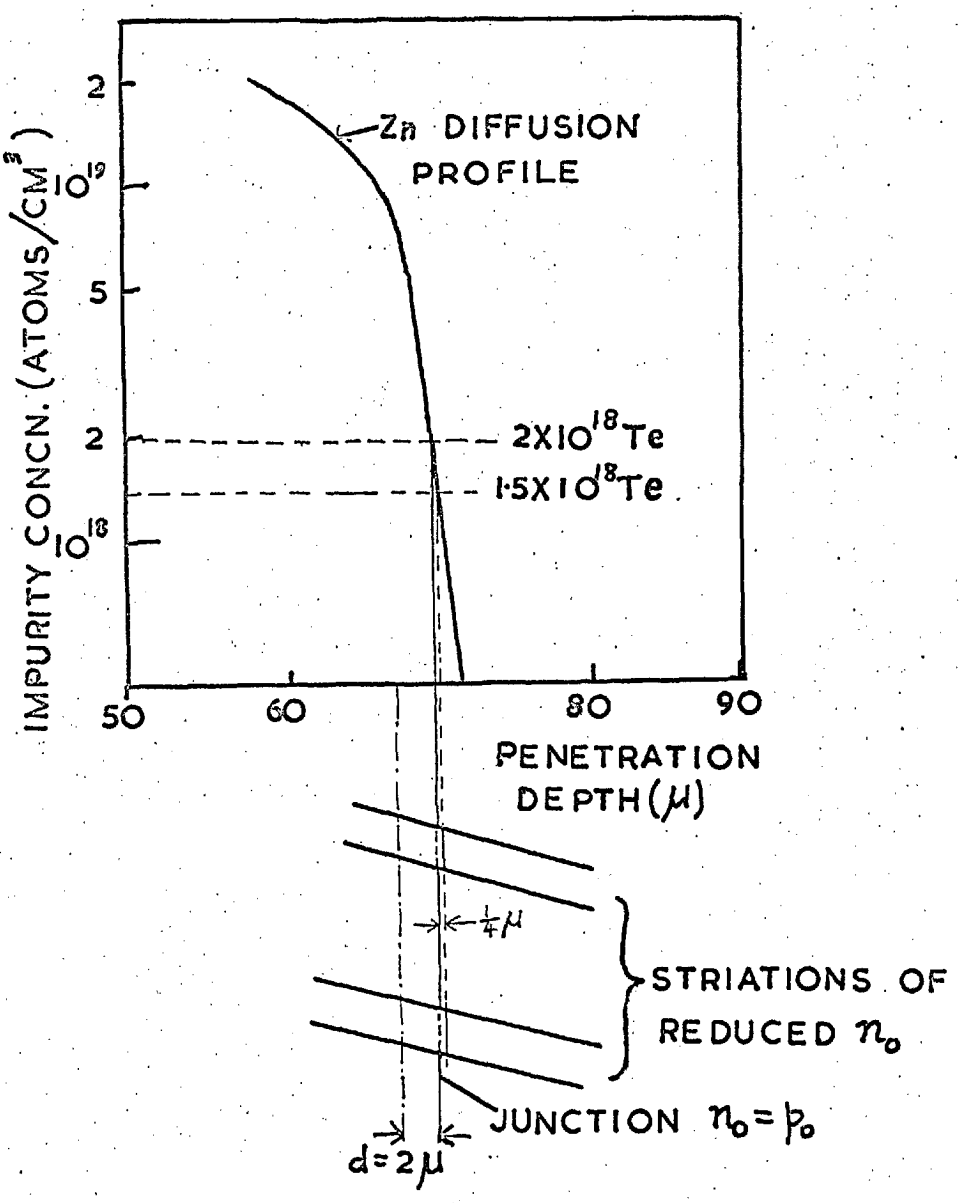

FIG. 5.4 SHOWING THE SMALL EFFECT OF SUBSTRATE DOPING VARIATIONS ON JUNCTION PLANARITY.

The gain factor β for T = 0°K was calculated using the following values for the variables: d = 2μ ; $h\nu$ = 1·46eV; $\Delta h\nu$ = ·02eV; η = 0·5; $\bar{\pi}$ = 3·63. This leads to β = 0·065cm/amp compared with the experimentally determined value of about 0·013cm/amp at 100°K by Pilkuhn, Rupprecht and Blum (1964). Agreement is not expected since β was derived at 0°K and there are also uncertainties in d, η and $\Delta\nu$. Assuming this experimental value 0·013 cm/amp, α in the active region may be estimated. The lowest threshold current density of the diodes examined was 1700 amps/cm^2 which gives α = 13 cm^{-1} if R = 0·32 and ℓ = 0·2 cm. The worst diode had $j_t \simeq$ 5000 amps/cm^2 and α = 44 cm^{-1}. These values of α are within the range of values found by many workers including Nathan, Fowler and Burns (1963) and Pilkuhn and Rupprecht (1963). To explain the rather low values of α the wave - guiding mechanism mentioned in section 2.3.5. is necessary. This would reduce the losses due to scattering from the active region.

5.2.5. Recombination Efficiency, η

Cusano (1964) examined the radiative recombination efficiency η_c of electrons injected into p - type GaAs. His results show that at the doping levels expected in the active region just on the p side of the junction, η_c increases as hole concentration p_o increases. If it is assumed that η for electrons injected across the p - n junction into the active region of the laser diodes varies in the same way as η_c then η increases as hole concentration p_o increases. As electron concentration n_o in the substrate decreases due to in-

homogeneities, the hole concentration p_o must increase if the Zn concentration profile is independent of donor concentration. It is known that n_o decreases in the dark striations in the Te doped diodes and hence p_o increases where these striations pass through the active region. This means η increases and j_t decreases at the dark striations, which is contrary to the observed effect.

5.2.4. Refractive Index $\bar{n}$

Marple (1964) used prisms of GaAs to determine the refractive index at two doping levels for photon energies of 0·7eV up to the band gap energy. The two doping levels were 6 X 10^{16} and 5·5 X 10^{17} donors/cm^3 and the difference in values of $\bar{n}$ between the samples was not more than 0·1%. Weiser and Stern (1964) in successfully predicting the far - field emission pattern from diodes having a p - p^o - n structure, with p^o about 8μ wide, used values of $\bar{n}$ for the various dielectric layers, which ranged from 3·63 to 3·58. Thus variations of less than 2% occur over a wide range of doping levels. It was also shown by Stern (1964) that doping has little effect on $\bar{n}$. The spread of photon energies emitted by GaAs laser diodes is about 20 meV and from Marples' results this spread corresponds to a change of $< 1\%$ in $\bar{n}$. Although refractive index appears as $\bar{n}^2$ in the threshold current equation it cannot explain the large variation of j_t found experimentally.

5.2.5. Spectral Properties, ν and $\Delta\nu$.

The laser emission spectra were not examined in this work. However, Raab, Bachert and Kaiper (1967) examined the spectra of individual spots in the emission patterns of Te doped striated diodes. They found the maximum difference in emitted photon energies was about 15 meV, and Braunstein, Pankove and Nelson (1963) found a similar difference for an order of magnitude change in doping concentration. Lamorte, Gonda and Junker (1966) found a 20 meV photon energy spread in a set of epitaxial diodes prepared from the same GaAs wafer. As $h\nu \simeq 1{\cdot}46$ eV this represents a 1% change which could not directly explain the observed variation of j_t. From the absorption results of Turner and Reese (1964) on compensated p - type GaAs the effect of a 20 meV change in $h\nu$ causes a large change in α. Therefore $h\nu$ variations may affect j_t indirectly through their control of α.

Braunstein, Pankove and Nelson found that $\Delta\nu$ for p - n junction electroluminescence increased with increasing n_o of the substrate. Casey and Kaiser (1967) found the same effect for cathodoluminescence. This behaviour of $\Delta\nu$ would lead to decreased j_t in the regions of low n_o which was contrary to the observed effect. Thus $\Delta\nu$ is eliminated as a cause of j_t variations.

5.2.6. Active Region Thickness, d.

It was shown in section 2.3.5. that d is probably between 1 and 3 μ. Fig.5.4. shows the effect of inhomogeneities in the donor distribution, on d. Part of a typical diffusion profile from Cunnell and Gooch (1960) is shown in the upper part of the figure

and below, two striations with 25% reduction of n_o are shown. It is clear that even such large variations of electron concentration cause a very small variation in the junction position. In this case it is about $\frac{1}{4}\mu$. Variations of this order in d are insufficient to explain the variations in j_t. The small perturbation of the junction plane shows why non-planarities due to substrate inhomogeneities were not revealed by emission photography, etching or scanning electron beam techniques.

Variations of π with donor inhomogeneities might cause variations in d through changes in the degree of wave guiding. This mechanism cannot be eliminated, but the direct effect of α variations through donor variations were shown in section 5.2.3. to be sufficient to explain the observed variations in j_t.

5.2.7 Diode Length ℓ and Reflectivity of Diode Faces, R.

The diodes examined in this work were all 2 mm long which is very large by semiconductor laser standards. With R = 0·32 for a GaAs/air interface the transmission loss $\left[\frac{1}{\ell} \ln \frac{1}{R}\right]$ in equ. (5.1.) equals 5·6 cm^{-1}. α has been shown to be $\gtrsim$ 13 cm^{-1} in these diodes (section 5.2.2.) and so the effect of variations of ℓ and R are small compared with α variations. Variations in R were shown to be $<1\%$, and from interference contrast micrographs of the diode faces it is seen there are no ℓ variations greater than a few hundred Angstroms. Thus variation of ℓ and R are eliminated as being too small to affect the threshold current density j_t.

Any defect which is to influence the emission pattern must be effective over a large fraction of the diode length. The only defects which can fulfil this requirement are planar defects (impurity striations and grain boundaries), or linear defects (dislocations) which are parallel to the diode length. Grain boundaries were shown by Shaw et al (1966) using scanning electron beam techniques, to cause large irregularities in the Zn diffusion front and to greatly reduce the laser efficiency. Defects of this type were not found in the diodes used here. Abrahams and Biliocchi showed that in short epitaxial diodes decorated misfit dislocations running parallel to the diode length correlated with emission spots. In diffused diodes inhomogeneities in the substrate crystal affect the p side properties near the junction. In epitaxial diodes this is not so and substrate inhomogeneities have less effect on the emission pattern. Abrahams, and Pankove (1966) found that dislocations which were not decorated did not cause filamentary laser action in epitaxial diodes. This is to be expected since the capture cross - section of an undecorated dislocation is small compared with the cross - section of laser active filaments.

5.2.8. Current Channelling

Channelling of the current flow in the GaAs throughout the diode, can affect the near - field emission pattern at the junction. This was seen in diodes which had non - uniform contacts, when only some parts of the junctions emitted spontaneously and usually none of them coherently. However in all the diodes examined in detail, ~~the~~

the spontaneous emission intensity showed no non - uniformities when operated well below threshold. Thus non - uniform contacts are eliminated.

Fenner (1966) divided the p side diode contacts, and varied the voltages to each part of the contact in such a way that the laser active regions should have scanned uniformly across the junction from side to side of the diode. He found that the filament jumped across the diode occupying only certain sites, and he showed that this was due to inhomogeneous material parameters in the junction region rather than due to the current distribution.

Conductivity variations due to doping variations may assist the increase in emitted intensity at the bright regions seen in transmission. In the striated diodes, where bright regions in transmission correspond to increased n_o and therefore increased conductivity, channelling of the current by the striations would increase the emission in the bright regions. But the variation of absorption coefficent α with doping is much greater than the variation of conductivity with doping and therefore channelling causes a lesser effect on j_t than does α.

Jonscher and Boyle (1966) and Nannichi (1966) proposed mechanisms which would tend to limit the spread of laser filaments. However, inhomogeneous carrier distributions in the junction region are required to establish the filaments of laser action before these mechanisms can be effective. It is also probable that in the large diodes studied here, the overall uniformity of material parameters

at the junction region is not sufficient for these mechanisms to be noticeable.

Therefore current channelling in any form is probably not occurring and it is the parameters in the junction region which cause the varying emission efficiency. The main factor in this is the absorption coefficient α with possibly the active region thickness d also having some effect.

5.3. Summary and Conclusion.

Several techniques have been used to make a survey of the defects present in GaAs laser diodes, and several types of defects were shown to be present.

Optical transmission using a narrow band of wavelengths close to the absorption edge of GaAs was shown to be a sensitive method for revealing inhomogeneities in the donor distribution. This method should be capable of wider application to the examination of semiconductor materials. Regular striations of varying Te concentration were found as well as probable segregation of Te at dislocations. This segregation occurs in GaAs at concentrations about 1 to 4 X $10^{18}/cm^3$ and before the onset of precipitation which occurs at about 5 X $10^{18}/cm^3$. Considerable irregular variations of Si distribution were shown, but Se doped material showed only very slight inhomogeneities. Optical transmission also revealed an effect of Zn diffusion on the donor distribution. The field of the junction is thought to sweep some of the donor impurity atoms

ahead of the junction as it diffuses in.

Chemical etching revealed some of the same inhomogeneities of donor distribution in the n side as optical transmission did. Precipitates in the p side and the predicted "misfit" dislocations in the junction region were also shown to be present.

A reliable method for preparing transmission electron microscopy specimens from bulk GaAs was developed. Transmission electron microscopy did not show precipitates in the n side of the diodes although some possible evidence for segregation in the Te striations was found. In Zn diffused p - type GaAs considerable precipitation of what must be a Zn rich phase was clearly shown and the presence of diffusion - induced dislocations revealed. A systematic study of Zn diffusion in GaAs is required to explain in detail the prel - iminary results obtained. Transmission electron microscopy has too high a magnification to be suitable for direct correlation of results with electroluminescent emission patterns.

From laser emission and transmission micrographs it was shown that in the diffused diodes examined here the dominant defect causing non-uniform emission was non-uniform distribution of donors in the substrate crystal. This was effective mainly through the variation of the optical absorption coefficient with donor density. The active region thickness, d, and emitted photon energy $h\nu$ are affected by donor variations in such a way that they may contribute to a small extent to the observed variations of threshold current density. Variations in refractive index, reflectivity and diode length were shown to be unimportant and variations of recombination

efficiency and emission linewidth to be of the wrong type to explain the results.

In these high power diodes of large dimensions, substrate inhomogeneities were shown to have a considerable effect on the emission patterns. With the high doping concentrations necessary for laser action it is difficult to produce material that is uniform over big enough volumes for these large diodes to be homogeneous. The application of a transverse magnetic field during crystal growth might reduce the inhomogeneities as was shown by Chedzey and Hurle (1966) for InSb. If donor density variations were completely removed, the effect of decorated misfit dislocations may become dominant, in determining the laser emission patterns. The removal of misfit dislocations may not be possible, because of the large impurity gradients necessary in the junction region. The effect of donor concentration variations on the emission pattern may be less in epitaxial diodes where the p side is not compensated, than in diffused diodes.

5.4. Future Work

As mentioned in the previous section, the preliminary results of the transmission electron microscopy study of the GaAs diodes showed that further investigation is required to elucidate the behaviour of large concentrations of Zn diffusing into GaAs. A systematic study of the effects of temperature, time, arsenic pressure and donor impurity on the crystal structure has been planned in conjunction with S.E.R.L.

Work at S.E.R.L. is now concentrated on GaP. Consequently it is intended to apply the techniques which were used here on GaAs lasers, to study the electroluminescent properties of GaP lamps with relation to crystal defects. This will entail some development work on chemical etching and on a chemical polish for jet thinning of electron microscope specimens. This work will be carried out in conjunction with B.D. Chase who will be using scanning electron beam techniques and X - ray diffraction.

APPENDIX 1

In this Appendix, the electronic circuits constructed for this work are given and described briefly. The circuits of sections A.1.1., A.1.2., and A.1.3. for the laser operation were supplied by S.E.R.L.

A.1.1. Pulse Generator

The circuit diagram is shown in fig. A.1. A full-wave rectifying bridge provided the 20v, 25mA supply. The pulse was produced by transistors 4 and 5, then passed through two stages of amplification to produce a pulse with a sharp leading edge of greater than 5 volts amplitude. The construction of transformers Tr 1 and Tr 2 was critical in determining the pulse shape. These transformers were wound on Mullard Ferrite cores No. FX 1593/A4. In each transformer the primary was 24 turns of 32 s.w.g. enamelled copper wire, secondary 1 was 8 turns of the same wire and secondary 2 was 8 turns of P.T.F.E. - covered 7/·0048 wire. The output of secondary 2 of Tr 1 was used to trigger the oscilloscope. The output of secondary 2 of Tr 2 was the output to the pulse forming line and was electrically isolated from the pulse generator circuit.

A.1.2. Pulse Forming Line Circuit

Fig. A.2. shows the circuit. The silicon controlled rectifier was a Transitron type no. TCR 5020. The power during the pulse was provided by the 0-500 V.D.C. supply. The pulse shape was determined by the pulse forming line which consisted of eight 1 μH inductances, with nine capacitors connected in parallel. These

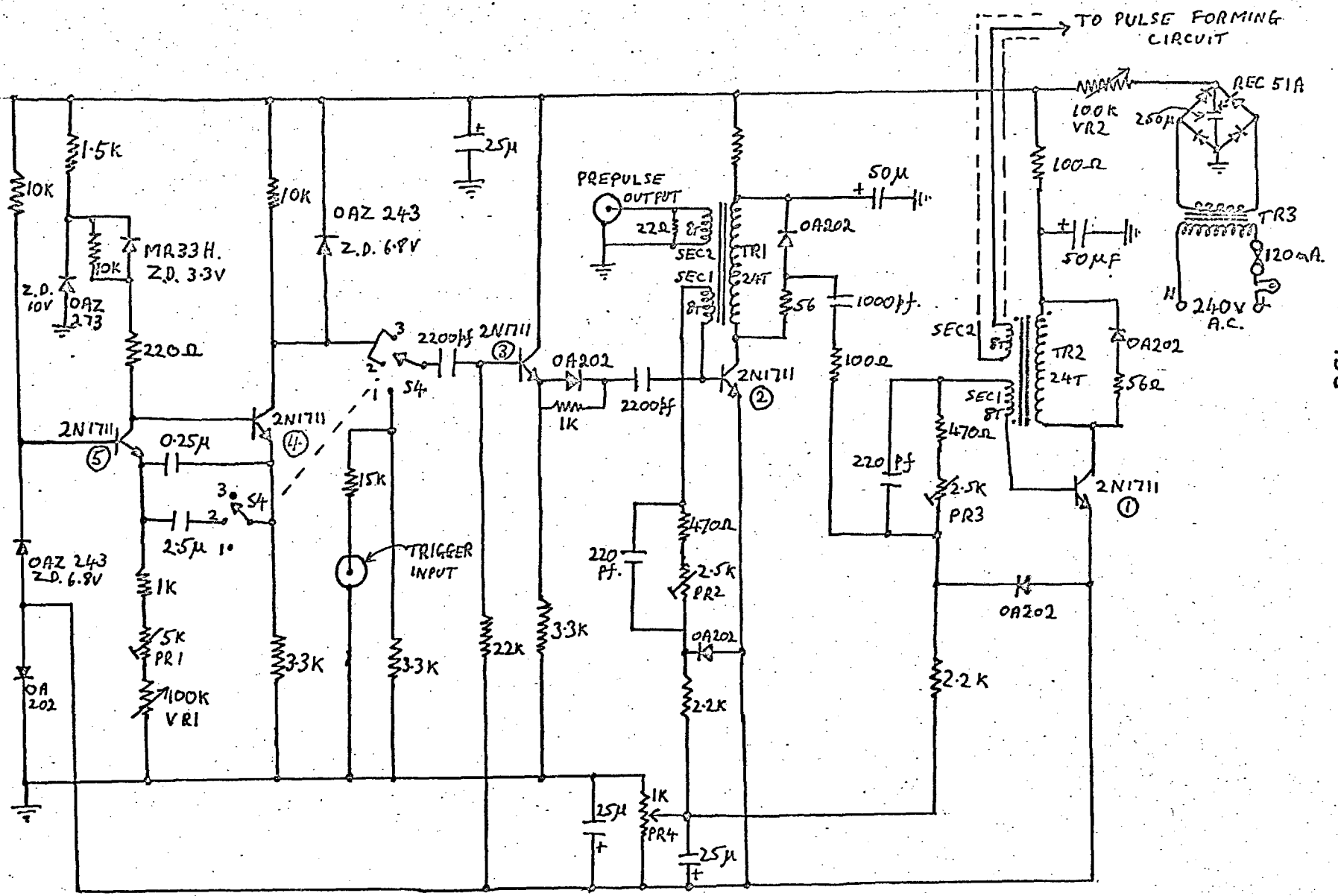

FIG. A.I PULSE GENERATOR CIRCUIT.

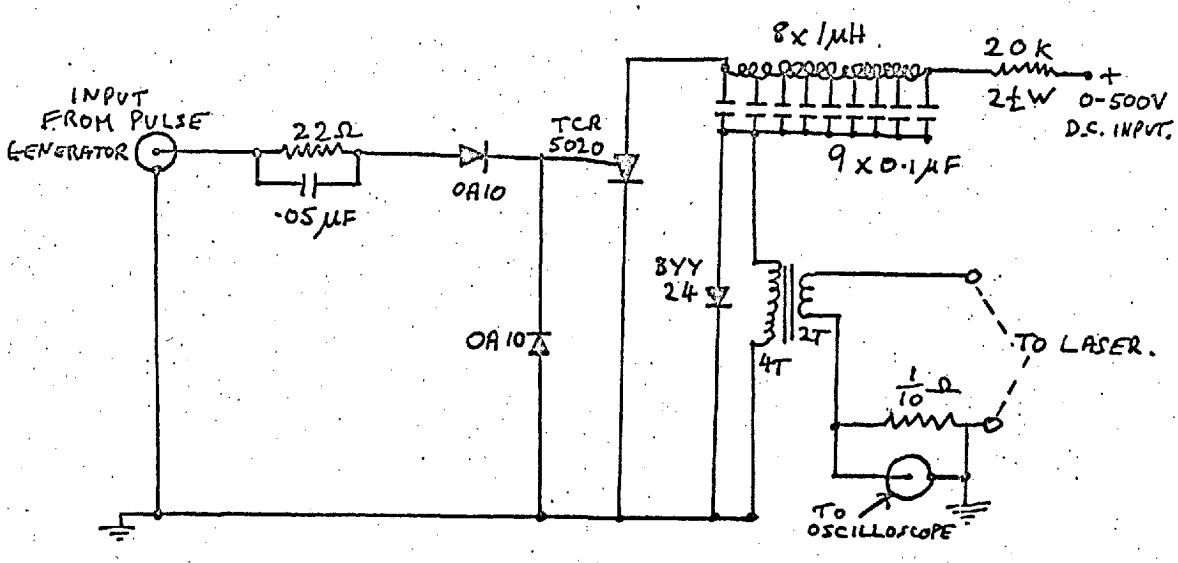

FIG. A.2 PULSE FORMING LINE CIRCUIT.

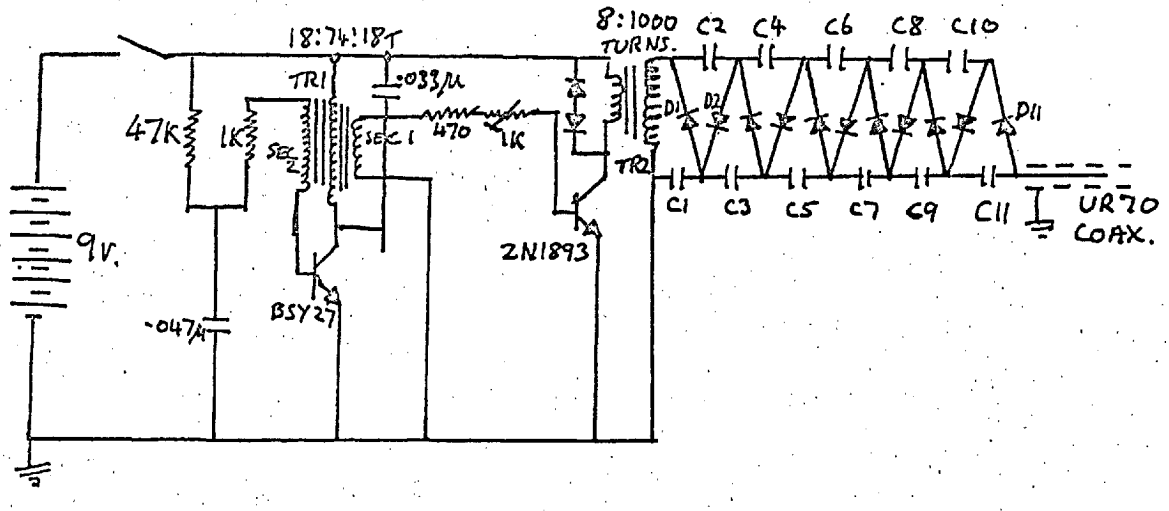

FIG. A.3 10KV. IMAGE CONVERTER SUPPLY.

inductances were each made by winding four turns of 22 s.w.g. enamelled copper wire on to a $\frac{3}{4}$" o.d. tufnol former. The 0·1Ω resistor for monitoring the laser current was inserted immediately before the output to the laser.

A.1.3. Image Converter H.T. Supply

The circuit is given in fig. A.3. By adjusting the primary of transformer Tr 1, the oscillator was tuned to 20 KC/S to match the impedance of the primary of Tr 2. The output from the secondary of Tr 2 was fed to the Cockroft - Walton voltage multiplication ladder which increased the voltage to about 10Kv.

A.1.4. Photomultiplier Amplifier

The amplifier circuit used in the jet thinner is given in fig. A.4. Basically it consists of two long tailed pair amplifiers which were analysed by Grigson (1964), joined in series. The ACY 19 transistor was added to increase the output power, because the S.C.R. drew about 1 mA from the amplifier. The transistors of the first two long tailed pairs had their cans enclosed in an aluminium block to reduce temperature fluctuations. The resistance and capacitance shown with the S.C.R. were found to be necessary to filter out fast random pulses which occasionally triggered the S.C.R.

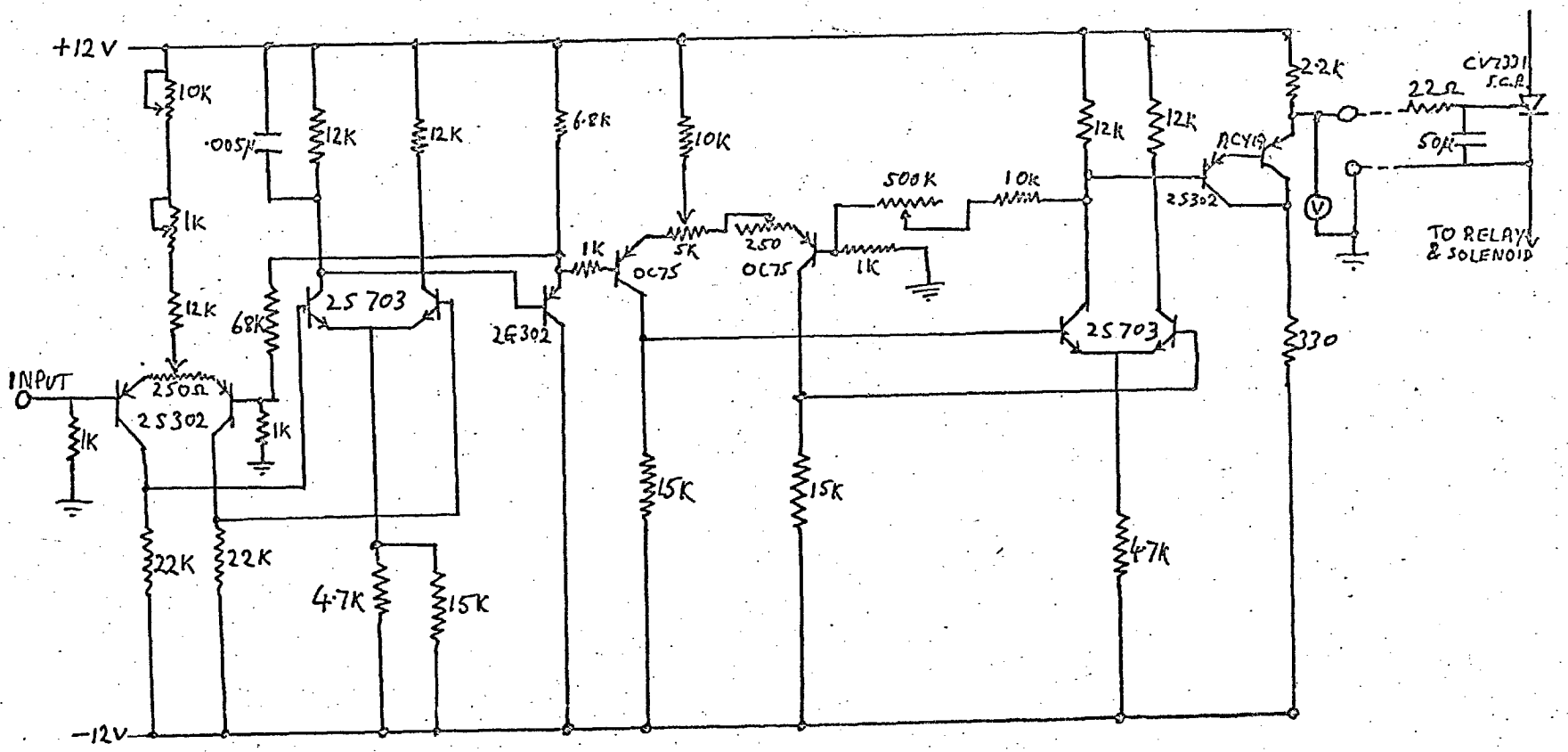

FIG A.4 AMPLIFIER FOR THE PHOTOMULTIPLIER.

LIST OF REFERENCES

Abrahams M.S. & Buiocchi C.J. (1965) J. Appl. Phys. 36 2855

(1966) J. Appl. Phys 37 1973

(1967) J.Phys.Chem.Sol. 28 927

Abrahams M.S., Buiocchi C.J. & Tietjen J.J. (1967) J. Appl. Phvs 38 760

Abrahams M.S. & Pankove J.I. (1966) J. Appl.Phys. 37 2596

Anderson W.W. (1965) I.E.E.E. J. Quantum El. QE-1 228

Aukerman L.W., Millea M.F. & McColl (1967) J. Appl. Phys. 38 685

Bagaev V.S., Berozashvili Yu.N., Vul B.M., Zavaritskaya E.I., Keldysh L.V. & Shotov A.P. (1964) Sov.Phys. Sol.St. 6 1093

Barber H.D. & Heasell E.L. (1965) J. Phys. Chem. Sol. 26 1561

Basov N.G., Krokhin O.N. & Popov Y.M. (1960) Sov. Phys. Uspekhi 3 702
(1961) Sov Phys. JETP 13 1320

Bell R.L., Latkowski R. & Willoughby A.F.W. (1965) J. Matls. Sci. 1 66

Bernard M.G.A. & Duraffourg G. (1961) Phys. Stat. Sol. 1 699

Biedermann E. & Brack K. (1966) J. Electrochem.Soc. 113 108

Black J.F. (1967) J. Electrochem. Soc. 114 1292

Black J.F. & Jungbluth E.D. (1967a) J. Electrochem. Soc. 114 181

(1967b) ibid 114 188

Black J.F. & Lublin P. (1964) J. Appl. Phys. 35 2462

Booker G.R. & Stickler R. (1962) Br. J. Appl. Phys. 13 446

Braunstein R., Pankove J.I. & Nelson (1963) Appl. Phys. Letts. 3 31

Broom R.F., Gooch C.H., Hilsum C., & Oliver D.J. (1963) Nature 198 368

Broudy R.M. (1963) Advances in Physics 12 135

Burns G. & Nathan M.I. (1964) Proc. I.E.E.E. 52 770

Burton J.A. Kolb E.D., Slichter W.P. & Struthers J.D. (1953 b) J. Chem. Phys. 21 1991

Burton J.A. Prim R.C. & Slichter W.P. (1953 a) J. Chem. Phys. 21 1987

Camp P.R. (1954) J. Appl. Phys. 25 459

Carr W.N. & Biard J.R.(1964) J.Appl.Phys. 35 2777

Casey H.C. (1965) Bull. Am. Phys. Soc. 10 1199

Casey H.C. (1967) J. Electrochem. Soc. 114 153

Casey H.C., Archer R.J., Kaiser R.H. & Sarace J.C. (1966) J. Appl. Phys. 37 893

Casey H.C. & Kaiser R.H. J. Electrochem. Soc. (1967) 114 149

Chang L.L. & Pearson G.L. (1964) J. Appl Phys. 35 1960

Chase B.D. (1968) Private Communication.

Chedzey H.A. & Hurle D.T.J. (1966) Nature 210 933

Chynoweth A.G. & Pearson G.L. (1958) J. Appl. Phys. 29 1103

Cunnell F.A. & Gooch C.H. (1960) J. Phys. Chem. Sol. 15 127

Cusano D.A. (1964) Sol. State Commun. 2 353

Dash,W.C. (1965) J. Appl. Phys. 27 1193

Drougard M.E. (1966) J. Appl. Phys. 37 1858

Dumke W.P. (1962) Phys. Rev. 127 1559

Faust J.W. (1962) in "Compound Semiconductors Vol I: Preparation of III - V Compounds" Eds. Willardson & Goering. 445

Fenner G.E. (1966) J. Appl. Phys. 37 4991

Fenner G.E. & Kingsley J.D. (1963) J. Appl. Phys. 34 3204

Fowler A.B. & Walker E.J. (1964) J. Appl. Phys. 35 727

Frank H. & Azim S.A. (1967) Sol. State El. 10 727

Fuller C.S. & Allison H.W. (1962) J. Electrochem. Soc. 109 880

Gatos H.C., Strauss A.J., Lavine M.C. & Harman T.C. (1961) J. Appl. Phys. 32 2057

Gippius A.A. & Vavilov (1963) Sov. Phys. Sol. St. 4 1777

(1965) Sov. Phys. Sol. St. 6 1873

Goldstein B. (1960) Phys. Rev. 118 1024

Gordon J.P., Zeiger H.J. & Townes C.H. (1955) Phys. Rev. 99 1264

Grigson C.W.B. (1964) Electronic Eng. 36 454

Haasen P. (1957) Acta Met. 5 598

Hall R.N. (1963) Sol. State El. 6 405

Hall, R.N. Fenner G.E., Kingsley J.D., Soltys T.J. & Carlson R.O. (1962) Phys. Rev. Letts. 9 366

Heine V. (1966) Phys. Rev. 146 568

Hill D.E. (1964) Phys. Rev. 133 A 866

Hill M.J., Holt D.B. & Unvala B.A. (1968) J. Sci. Inst. Ser II 1 301

Holt D.B. (1960) J. Appl. Phys. 31 2231

(1962) J. Phys. Chem. Sol. 23 1353

(1966) J. Phys. Chem. Sol. 27 1053

Holt D.B. & Chase B.D. (1968) J. Mat. Sci. 3 178

Holt D.B., Porter R. & Unvala B.A. (1966) J. Sci. Inst. 43 371

Hornstra J. (1958) J. Phys. Chem. Sol. 5 129

Hurle D.T.J. (1966) Phil. Mag. 13 305

Hurle D.T.J., Gillman J. & Harp E.J. (1966) Phil. Mag. 14 205

Jonscher A.K. & Boyle M.H. (1966) in "Gallium Arsenide: 1966 Symposium Proceedings" Inst. Phys. & Phys Soc. London 1967 78

Jungbluth, E.D. (1965) J. Electrochem. Soc. 112 580

Keyes R.W. (1963) Proc. I.E.E.E. 51 602

Keyes R.W. & Quist T.M. (1962) Proc. I.R.E. 50 1822

Lamorte, M.F.,Gonda T & Junker H. (1966) Sol. State El. 9 1075

Lang A.R. (1959) J. Appl. Phys. 30 1748

Larrabee G.B. & Osborne J.F. (1966) J. Electrochem. Soc. 113 564

Lasher G.J. (1963)I.B.M. J.Res. & Dev. 7 58

Lasher G.J. & Stern F. (1964) Phys. Rev. 133 A553

Lavine M.C., Gatos H.C. & Finn M.C. (1961) J. Electrochem.Soc. 108 974

Lemay, C.Z. (1963) J. Appl. Phys 34439

Lengyel, B.A. (1962) "Lasers Generation of Light by Stimulated Emission" New York, John Wiley

Levene S.H. (1966) M.Sc. Thesis, Imperial College, London

Logan R.A., Chynoweth A.G.& Cohen B.G. (1962) Phys. Rev. 128 2518

Longini R.L. (1962) Sol. State El. 5 127

Ludman J.E. & Hergenrother K.M. (1966) Sol. State El. 9 863

Maiman T.H. (1960) Nature 187 493

Marinace J.C. (1963) J. Electrochem. Soc. 110 1153

Marple D.T.F. (1964) J. Appl. Phys. 35 1241

McCaldin J.O. & Harada R. (1960) J. Appl. Phys. 31 2065

McWhorter A.L. (1963) Sol. State El. 6 417

Meieran E.S. (1965) J. Appl. Phys. 36 2544

Michel A.E., Nathan M.I. & Marinace J.C. J. Appl. Phys. 35 3543

Michel A.E. & Walker E.J. (1964) J. Appl. Phys. 35 3285

Michel A.E., Walker E.J. & Nathan M.I. (1963) I.B.M.J. Res. & Dev. 7 70

Morizane K., Witt A.F. & Gatos H.C. (1966) J.Electrochem.Soc. 113 51

Müller Von A. & Wilhelm M. (1964) Z.Naturforschg. 19a 254

Nannichi Y. (1966) J. Appl. Phys. 37 3009

Nasledov D.N. (1961) J. Appl. Phys. 32 2140

Nathan M.I., Dumke W.P., Burns G., Dill F.H. & Lasher G.J. (1962) Appl. Phys. Letts. 1 62

Nathan M.I., Fowler A.B. & Burns G (1963) Phys. Rev. Letts. 11 152

Panish M.B. (1966) J. Phys. Chem. Sol. 27 291

Panish M.B. & Casey H.C. (1967) J. Phys. Chem. Sol. 28 1673

Pankove J. I. (1962) Phys. Rev. Letts. 9 283

Pauling L. (1960) "The Nature of the Chemical Bond" Oxford Univ. Press. 246

Peart R.F., Weiser K., Woodall J. & Fern R. (1966) Appl. Phys. Letts. 9 200

Pilkuhn M.H. & Rupprecht H. (1963) Proc. I.E.E.E. 51 1243

(1964) Trans. Met. Soc. A.I.M.E. 230 296

(1967) J. Appl. Phys. 38 5

Pilkuhn M.H., Rupprecht H. & Blum S.E. (1964) Sol. State El. 7 905

Quist T.M. Rediker R.H., Keyes R.J. Krag W.E. Lax B., McWhorter A.L. & Zeiger H.J. (1962) Appl. Phys. Letts. 1 91

Raab S., Bachert H. & Kaiper A. (1967) Phys. Stat. Sol. 19 K59

Salow H. & Benz K - W. (1965) Z. angew. Phys. 19 157

Schottky G. (1966) J. Phys. Chem. Sol. 27 1721

Schwuttke G.H. (1965) J. Appl. Phys. 36 2712

Schwuttke G.H. & Queisser (1962) J. Appl. Phys. 33 1541

Schwuttke, G.H. & Rupprecht H. (1966) J. Appl. Phys. 37 167

Shaw, D.A., Hughes K.A., Neve N.F.B., Sulway, D.V., Thornton P.R., & Gooch C.H. (1966) Sol. State El. 9 664

Shaw D.A. (1967) M.Sc. Thesis U.C.N.W. Bangor

Sorokin P.P., Axe J.D & Lankard J.R. (1963) J. Appl. Phys 34 2553

Steinemann A. & Zimmerli U. (1967) Proc. Int. Conf. on Crystal Growth. Ed. Peiser H.S. New York. 81.

Stern F. (1964) Phys Rev. 133 A 1653

(1966) Phys. Rev. 148 186

Thornton P.R. (1963) Sol. State El. 6 673

(1967) "The Physics of Electroluminescent Devices" E.&F.N. Spon. London pp 215 - 264

Thornton P.R., Culpin M.J. & Drummond I.W. (1963) Sol. State El. 6 532

Turner W.J. & Reese W.E. (1964) J.Appl. Phys. 35 350

Vieland L.J. & Kudman I. (1963) J. Phys. Chem. Sol. 24 437

Vilms J. & Spicer W.E. (1965) J. Appl. Phys. 36 2815

Washburn J., Thomas G., & Queisser H.J. (1964) J. Appl. Phys 35 1909

Weisberg L.R., & Blanc J. (1963) Phys. Rev. 131 1548

Weiser K. (1963) J. Appl. Phys. 34 3387

Weiser K. & Stern F. (1964) Appl. Phys. Letts. 5 115

Weiser K. & Woods J.F. (1965) Appl. Phys. Letts. 7 225

Whitaker J. & Bolger D.E. (1966) Sol. State Commun. 4 181

Willoughby A.F.W. (1965) Ph.D. Thesis London Univ.

Wittry D.B. (1966) Appl. Phys. Letts. 8 142

Yariv A.& Leite R.C.C. (1963) Appl. Phys Letts. 2 55

Ziegler G & Henkel H - J. (1965) Z. angew. Phys. 19 401

ACKNOWLEDGEMENTS

The author would like to thank Dr. D. B. Holt for his constant advice and interest during the course of this work, and for the many valuable discussions. The author is grateful to Professor J. G. Ball for provision of laboratory facilities; to Mr. C. H. Gooch and Services Electronic Research Laboratories for supplying the laser diodes and much helpful information; to the Ministry of Defence (Navy Department) for financial support; to Dr. B. A. Unvala and Mr. R. Porter for helpful advice on experimental details and to all his colleagues for many useful discussions.

Finally the author would like to thank Miss Monica Rowsell for the typing.